The CAS protein and Ca^{2+} signaling in the chloroplast of *Arabidopsis thaliana*

Dissertation

zur Erlangung des Doktorgrades (Dr. rer. nat.)

der

Mathematisch-Naturwissenschaftlichen Fakultät

der

Rheinischen Friedrich-Wilhelms-Universität Bonn

vorgelegt von

Niloufar Pirayesh

aus

Tehran, Iran

Bonn, 2022

Angefertigt mit Genehmigung der Mathematisch-Naturwissenschaftlichen Fakultät der Rheinischen Friedrich-Wilhelms-Universität Bonn

Gutachterin 1: Prof. Dr. Ute C. Vothknecht

Gutachter 2: prof. Dr. František Baluška

Gutachter 3: Prof. Dr. Raoul-Martin Memmesheimer

Gutachter 4: Prof. Dr. Thorsten Lang

Tag der Promotion: 21. November 2022

Erscheinungsjahr: 2023

Table of Contents

Abbreviations

Abbreviation	Definition
$[Ca^{2+}]_{cyt}$	Cytosolic Ca^{2+} concentration
$[Ca^{2+}]_{F}$	Free calcium concentration
$[Ca^{2+}]_{m}$	Mitochondrial Ca^{2+} concentration
$[Ca^{2+}]_{str}$	Stromal Ca^{2+} concentration
$[Ca^{2+}]_{thl}$	Thylakoid lumen Ca^{2+} concentration
$^{\circ}C$	Degree Celsius
A. thaliana	*Arabidopsis thaliana*
AAs	Amino acids
ACAs	Autoinhibited Ca^{2+}-ATPases
AEQ	Aequorin
ATP	Adenosine triphosphate
BICAT1	Bivalent cation transporter 1
BN	Blue native
Ca^{2+}	Calcium Ion
CaMs	Calmodulins
CAS	Calcium sensing receptor
casko	CAS knockout
CBLs	Calcineurin B-like proteins
CBPs	Calcium binding proteins
CDPKs	Calcium dependent protein kinase
CEF	Cyclic electron flow
CMLs	Calmodulin like proteins
CNGCs	Cyclic nucleotide-gated channels
CPK	Calcium dependent protein kinase

CT	C-Terminal domain
CYT*b6/f*	Cytochrome b6f subunit
ECAs	ER-type Ca^{2+}-ATPases
EF	Elongation factor
EGTA	Ethylene glycol tetraacetic acid
ER	Endoplasmic reticulum
Fd	Ferredoxin
FHA	Fork head associated domain
FNR	Ferrodoxin $NADP^{+}$ reductase
GECIs	Genetically encoded Ca^{2+} indicators
GFP	Green fluorescence protein
H_2O_2	Hydrogen peroxide
InsP3	Inositol 1,4,5-trisphosphate
Kb	Kilo base
KDa	Kilo Dalton
$LaCl_3$	Lanthanum chloride
LHC	Light harvesting complex
M	Molar
MS channels	Mechanosensitive channels
MS medium	Murashige-Skoog-Medium
MS/MS	Tandem mass spectrometry
NaCl	Sodium chloride
NT	N-Terminal domain
OSCA1	Reduced hyperosmolality-induced $[Ca^{2+}]_i$ increase1
PAGE	Poly acrylamide gel electrophoresis
PGR5	Proton Gradient Regulator 5
PLC	phosphoinositide signaling pathway
PSI	Photosystem I

PSII	Photosystem II
RLUs	Relative Luminescence Units
ROS	Reactive oxygen species
RuBisCo	Ribulose 1,5 bisphosphate carboxylase/oxygenase
saGFP	Self-assembly GFP
SDS	Sodium dodecyl sulfate
SE	Standard error
SOD	Superoxide dismutase
SOS	Salt Overly Sensitive pathway
ssuRuBisCo	Small subunit of RuBisCo
STN7	State Transition Kinase 7
STN8	State Transition Kinase 8
T-DNA	Transfer DNA used for insertional mutagenesis
TPCs	Two pore channels
WT	Wild type
YFP	Yellow fluorescence protein
µ	Micro

List of figures

List of tables

1 Introduction

1.1 Ca^{2+}: a universal biological secondary messenger

In eukaryotic cells, calcium plays an essential role in regulating a wide variety of cellular processes by acting as a secondary messenger (Berridge, et al., 2000). In plants, calcium is an integral element in the plant's life cycle. In its cation form (Ca^{2+}), it strengthens the cell wall and membranes of plants, helping plants to grow and develop (Wenjuan, et al., 2009; Knight, et al., 1997). Moreover, plants depend on Ca^{2+} for photosynthesis (Brand & Becker, 1984) and to survive pathogenic attacks (Vadassery & Oelmüller, 2009). Ca^{2+} also plays an essential role as a secondary messenger in cells, transmitting a wide range of different stress signals to maintain plants health and growth (Kudla, et al., 2010; Thor, 2019). Under non-stress conditions, the concentration of Ca^{2+} in the cytoplasm ($[Ca^{2+}]_{cyt}$) is usually within the range of 100-200nM (Bush, 1995; Knight, 1999; White, 2000).

Upon exposure to internal or external stimuli, free $[Ca^{2+}]_{cyt}$ increases temporarily (McAinsh & Hetherington, 1998). This increase is sensed by a group of Ca^{2+} binding proteins known as Ca^{2+} sensors (**Figure 1**). The Ca^{2+} sensor proteins react directly to the changes in $[Ca^{2+}]_{cyt}$, by activating various responses such as plant growth, cell division, and the formation of organs (Zhang, et al., 2014).

Most Ca^{2+} sensors contain Ca^{2+} binding domains called EF-hand-motifs (Kawasaki, et al., 1998). In *Arabidopsis thaliana* (*A. thaliana*), the presence of approximately 250 EF-hand-containing proteins counts as evidence of the importance of the Ca^{2+} signaling pathway in plants (Day, et al., 2002). The leading group of Ca^{2+} sensor proteins in all eukaryotic organisms are the calmodulins (CaMs) (**Figure 1**). The Plants also have a unique set of calmodulin-like proteins (CMLs) and two additional Ca^{2+} sensors, calcium-dependent protein kinases (CDPK) and calcineurin B-like proteins (CBL) (Tuteja & Mahajan, 2007). Depending on their intracellular localization and compatibility with Ca^{2+}, these sensors carry out a variety of roles in the Ca^{2+} signaling pathway.

The Ca^{2+} signaling response to a stimulus can be divided into three significant steps: Ca^{2+} influx, efflux, and decoding (Edel, et al., 2017). The combined effects of Ca^{2+} influx through Ca^{2+} channels and active energy-dependent Ca^{2+} efflux via Ca^{2+} transporters generate stimulus-specific Ca^{2+} signatures, decoded by the Ca^{2+} sensors to imply the corresponding cellular responses. In *A. thaliana*, five families of Ca^{2+}-permeable channels have been identified: cyclic nucleotide-gated channels (CNGCs), plant glutamate receptors (GLRs) (Price, et al., 2012), two-pore channels (TPCs) (Morgan & Galione, 2014), mechanosensitive (MS) channels (Kurusu, et al., 2013) and the reduced hyperosmolality-induced $[Ca^{2+}]_i$ increase1 (OSCA1) (Yuan, et al., 2014). These channels, responsible for the influx of Ca^{2+}, are

counterbalanced by at least four families of Ca^{2+} transporters that extrude Ca^{2+} in order to return to its basal levels and maintain Ca^{2+} homeostasis: autoinhibited Ca^{2+}-ATPases (ACAs), ER-type Ca^{2+}-ATPases (ECAs), P1-ATPases (heavy metal ATPase 1) and Ca^{2+}/H^{+} exchangers (Manohar, et al., 2011; Bonza & Michelis, 2011). However, the exact function, regulation, and localization of most members of these Ca^{2+} influx and efflux systems remain largely a mystery.

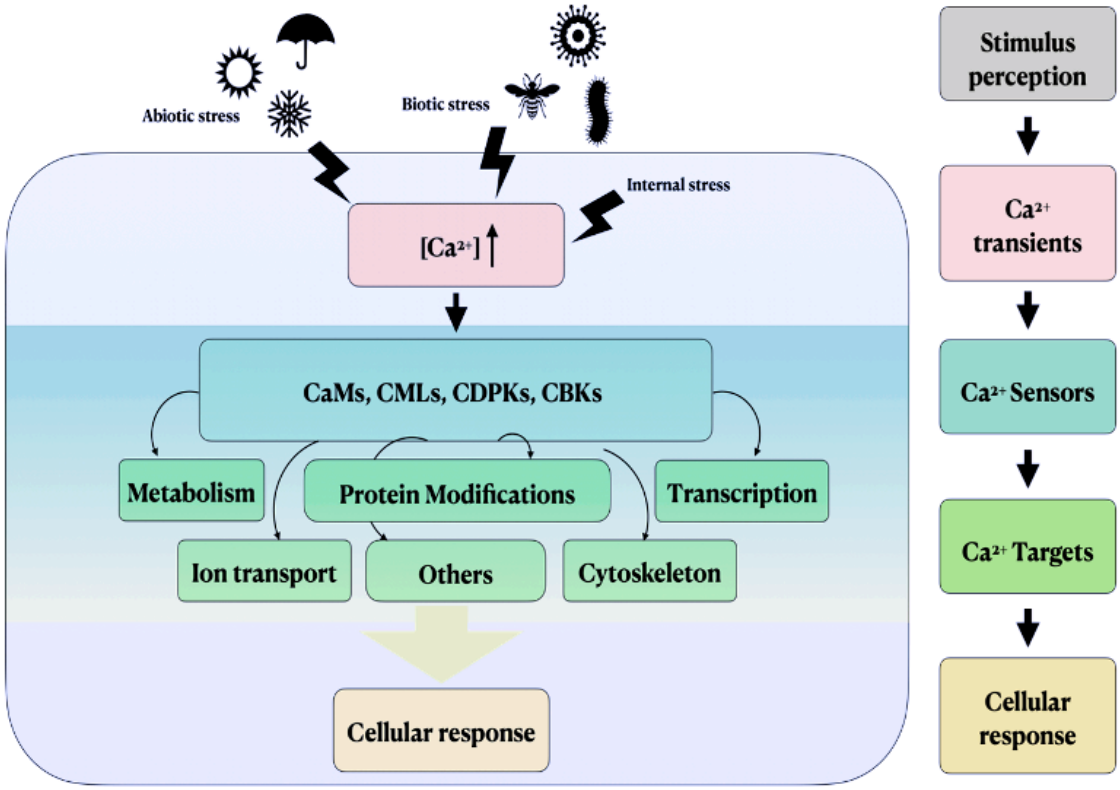

Figure 1. Ca^{2+} signaling network in plant cells. An increase in $[Ca^{2+}]$ is induced by abiotic and biotic stress as well as by internal stimuli, which is then sensed by Ca^{2+} sensors such as calmodulins (CaMs), calmodulin-like proteins (CMLs), Ca^{2+}-dependent protein kinases (CDPKs) and Calcineurin-B-like proteins (CBLs). As a result, these sensors activate a variety of downstream processes, which then produce an overall cellular response specific to the original stimulus and in connection with information from other signaling pathways.

The "Ca^{2+} signature" principle states the presence of distinct temporal and spatial patterns in Ca^{2+} transients caused by different stimuli. The Ca^{2+} signatures of plants have already been identified in several studies since 1991, including those conducted in *A. thaliana* (Knight, et al., 1991), *Nicotiana tabacum* (Manzoor, et al., 2012), and more recently in *Oryza sativa* (Zhang, et al., 2015). Ca^{2+} signatures are generated by numerous factors such as biotic (injuries, pathogens, etc.) and abiotic (salinity, heat, drought, etc.) stimuli.

1.2 Ca^{2+} measurement in plants subjected to biotic and abiotic stress

Changes in the [Ca^{2+}] can be measured by utilizing non-ratio metric Ca^{2+} dyes such as Fluo-3 and 4, Rhod-2 and 3, and Calcium Green-1, as well as genetically encoded Ca^{2+} sensors such as aequorin (AEQ). In plants, some difficulties have been encountered when using fluorescent dyes (Callaham & Hepler, 1991), such as the dye not being absorbed by the nuclei or the dye fluorescence not increasing after increasing $[Ca^{2+}]_{cyt}$ artificially, suggesting the dye is not measurable within the cytosol (Knight, et al., 1993). By contrast, recombinant AEQ complements these techniques and may provide additional benefits. Natural photoproteins, such as those found in coelenterates (hydroids and jellyfish), produce light in response to Ca^{2+} ions. A jellyfish known as *Aequoreu victoria* synthesizes the AEQ protein under normal conditions, containing a single polypeptide chain (ca. 22 kDa) and three Ca^{2+}-binding EF-hand motif sites (Deng, et al., 2005). Upon binding to Ca^{2+}, AEQ changes its conformation and acts as an oxygenase, converting coelenterazine into its excited form, coelenteramid, which produces a blue light (λ = 469 nm) that can be detected and recorded (**Figure 2**). Finally, calibration curves make it possible to convert the emitted light, expressed as Relative Luminescence Units (RLUs), into [Ca^{2+}] concentrations (Allen & Prendergast, 1977).

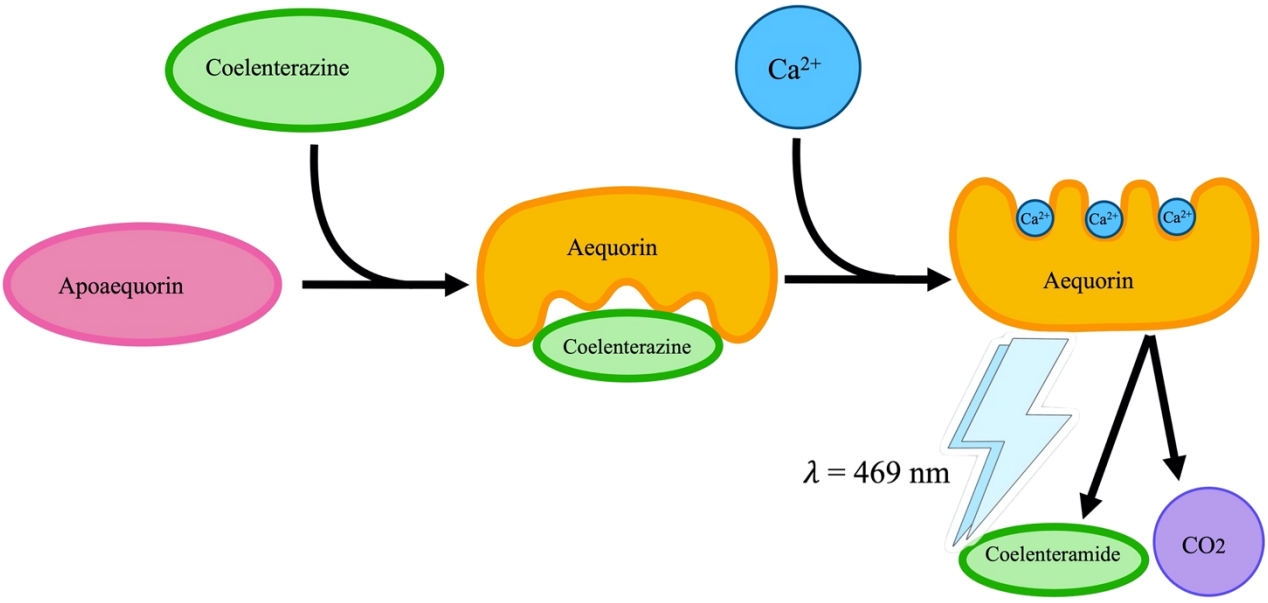

Figure 2. Molecular mechanism of light emission by aequorin upon binding to Ca^{2+}. The Ca^{2+}-binding photoprotein, aequorin, is composed of an apoprotein (apoaequorin) and a prosthetic group known as coelenterazine which is a luciferin molecule. The functional holoprotein aequorin is reconstituted spontaneously in presence of oxygen. The protein contains three EF-hand Ca^{2+}-binding sites. Upon occupying these sites with Ca^{2+}, aequorin undergoes a conformational change and behaves as an oxygenase which converts coelenterazine into excited coelenteramide, which is released along with carbon dioxide. The excited coelenteramide relaxes to the ground state, causing the emission of blue light (λ = 469 nm) which can be detected by a luminometer.

In plants, through the introduction of AEQ into plants targeted to the cytosol or different organelles (Knight, et al., 1991; Knight, et al., 1996) and cell types such as guard cells (Dodd, et al., 2006), the monitoring of $[Ca^{2+}]$ changes have been possible. To date, using AEQ, the changes in the $[Ca^{2+}]_{cyt}$ of plant cells were measured in response to various abiotic stresses such as salt and drought (Knight, et al., 1998; Ranf, et al., 2008), oxidative stress (Evans, et al., 2005), cold stress (Knight, et al., 1991; Knight, et al., 1996), as well as hormones (Zhu, et al., 2013) and pathogen elicitors (Lecourieux, et al., 2006).

1.2.1 Ca^{2+} signaling in response to salt and drought stress

Throughout the world, soil salinity remains one of the most severe environmental problems related to agriculture, hindering food production. Salinity inhibits the growth and development of plants, such as seed germination (Ungar, 1996; Dash & Panda, 2001) and seedling growth (Katembe, et al., 1998). Salt stress leads to the impairment of all the major activities carried out by plants, including photosynthesis energy, lipid metabolism, and protein synthesis (Anuradha & Rao , 2001; Babu, et al.,

2012). The presence of salt causes membrane leakage, ion imbalances, and increased reactive oxygen species (ROS) production (Roychoudhury, et al., 2008).

Salt stress commonly affects plants in three ways: osmotic stress (water stress), ionic stress, and oxidative stress (Munns & Tester, 2008). Tolerating these stresses requires plants to accumulate osmolytes and osmoprotectants. Additionally, the expression of antioxidants enzymatically and non-enzymatically is another mechanism to cope with salt stress. In general, salt has two adverse effects on the ability of plants to acquire minerals. In the first place, the ionic strength of the substrate influences nutrient uptake and translocation. Alternatively, by introducing a competitive environment with ions, such as sodium (Na^+) and chloride (Cl^-), salinity can disrupt the mineral relations between plants and the environment in the substrate (Peuke & Jeschke, 1999). This eventually causes imbalances and nutritional disorders in plants, which may ultimately damage plant cells (Xu, et al., 2010), injure the chlorophyll, and consequently cause loss of photosynthetic activity. This is followed by leaf senescence (De Michele, et al., 2009) and plant growth suppression (Garg & Manchanda, 2009).

Plants can cope with salinity stress through a variety of responses. In recent years, Ca^{2+} has been extensively studied for its role as a signal transducer in response to salt stress. Substantial progress has been made concerning the Salt Overly Sensitive (SOS) pathway, comprised of three components SOS1, SOS2, and SOS3 (Zhu, 2000). A critical step in the SOS signal transduction cascade is the activation of the Ca^{2+} spike, which is caused by a Ca^{2+} flux upon facing salinity stress. This increase in cytosolic [Ca^{2+}] is detected by SOS3, a calcineurin B-like protein, which then interacts with the protein Kinase SOS2. The SOS3-SOS2 complex activates the SOS1 protein (a plasma membrane Na^+/H^+ antiporter) and restores Na^+ homeostasis (Zhu, 2002).

Another abiotic stress that plants face is drought stress. Drought has the same effects on osmotic potential, leading to several modifications, including the stomata closure to prevent further water loss (Davies, et al., 1981), accumulation of proline (Savoure, et al., 1995), and other osmoprotectants (Bartels & Nelson, 1994). Despite studies carried out in *A. thaliana* plants under mannitol treatment, mimicking drought stress (Lu, et al., 2021), the molecular mechanism by which plants distinguish between Ca^{2+} signaling that promotes gene expression under drought and salt stress remains unclear.

1.2.2 Ca^{2+} signaling in response to oxidative stress

In plants, oxidative stress is caused directly by the effects of environmental stress or indirectly by the production and accumulation of ROS. Despite the fact that ROS is necessary for normal plant development and performance, excess amount of ROS causes exhibit growth obstacles, including the

loss of leaves and flowers (Muñoz & Munné-Bosch, 2018; Goldental-Cohen, et al., 2017), gravitropism of roots (Mugnai, et al., 2014), delay in seed germination (Shi, et al., 2014) and finally death.

To protect themselves from the damaging effects of ROS, plant cells have been proposed to incorporate several models for monitoring ROS levels and signaling (Apel & Hirt, 2004; Asada, 2006; Demidchik & Maathuis, 2007; Foyer & Noctor, 2009; Sierla, et al., 2013; Noctor, et al., 2015; Mittler, 2017; Waszczak, et al., 2018). Different potential ROS receptors have been identified: (I) two-component histidine kinases, (II) redox-sensitive transcription factors, such as NPR1 or Heat Shock Factors, (III) ROS-sensitive phosphatases, (IV) redox-regulated ion channels (Apel & Hirt, 2004; Demidchik & Maathuis, 2007; Sierla, et al., 2013; Demidchik, et al., 2014). Also, compounds referred to as antioxidants are considered capable of quenching ROS without undergoing its conversion into a destructive radical (Noctor & Foyer, 1998) (Drög, 2002). Superoxide dismutase (SOD) is one prominent example that can metabolize the superoxide and converts it into H_2O_2, which in turn is neutralized by other antioxidants or translocated to other cells (Asada, 1994; Foyer, et al., 1994). Similarly, nonprotein thiols act as antioxidants by preventing the oxidation of other redox-active molecules (Noctor & Foyer, 1998).

A variety of studies have been carried out on the role of Ca^{2+} signaling in response to oxidative stress in plants. One study showed that low concentrations of H_2O_2 and superoxide cause significant increases in $[Ca^{2+}]_{cyt}$ in guard cells of *Commelina communis* (McAinish, et al., 1996). H_2O_2 has been reported to cause a transient increase in $[Ca^{2+}]_{cyt}$ in tobacco seedlings (Price, et al., 2012). *A. thaliana* whole seedlings exposed to H_2O_2 showed an increase in $[Ca^{2+}]_{cyt}$ with a double peak, where the initial Ca^{2+} peak occurs within the cotyledons, and the delayed peak exclusively occurred within the root system (Rentel & Knight, 2004).

By understanding how plants demonstrate stress responses, we will be able to address fundamental questions regarding how abiotic stress is translated into electrochemical signals and comprehend a few of the vital biological processes that allow plants to grow and develop under stressful conditions.

1.3 Ca^{2+} signaling in plant cell compartments

Due to its tendency to bind to other components and precipitation leading to cellular physiological threads, Ca^{2+} is usually found bound to proteins or stored in various cell organelles (Logan & Knight, 2003). Former studies were mainly concentrated on the role of Ca^{2+} signaling in the cytosol, however, later studies showed that this regulatory pathway is also present in other organelles, such as the nucleus, chloroplast, mitochondria, peroxisomes, and the endomembrane system [recently reviewed in: (Pirayesh, et al., 2021)].

By employing specifically targeted genetically encoded Ca^{2+} indicators (GECIs) to the cytosol and various cell organelles, changes in [Ca^{2+}] in response to biotic and abiotic stimuli were measured (Costa, et al., 2018). In order to protect the cell from Ca^{2+} toxicity, the cell sustains the cytosolic $[Ca^{2+}]_{cyt}$ at a sub-micromolar level of 50 to 100 nM (**Figure 3**) (Logan & Knight, 2003). Similarly, the amount of resting free Ca^{2+} inside the nucleus was estimated at 100 nM (Brini, et al., 1993) (**Figure 3**). In the mitochondria, the resting free $[Ca^{2+}]_m$ measured in the mitochondria was around 200 nM (Logan & Knight, 2003).

Unfortunately, there is only a little information available concerning the storage properties of the endoplasmic reticulum and the peroxisome and their role in the Ca^{2+} signaling network in plant cells. Our understanding of the amount of free [Ca^{2+}] in peroxisomes and the ER is confined to studies in animal cells (**Figure 3**).

In the Ca^{2+} measurement studies, the chloroplast is the most well-studied subcompartment among all organelles. In the chloroplast, the free ($[Ca^{2+}]_{str}$) in the stroma has been determined to be between 100 and 150 nM (Sai & Hirschie Johnson, 2002; Sello, et al., 2016), while in the thylakoid lumen, the $[Ca^{2+}]_{thl}$ concentration was around 200 nM during the day and increased to 500 nM at night (Sello, et al., 2018) (**Figure 3**). In spite of the fact that the molecular mechanism of this light-off response has not been elucidated, it has nevertheless been proposed that the thylakoid lumen might be involved in dispersing the increase in $[Ca^{2+}]_{str}$ that is associated with the light-dark transition (Sai & Hirschie Johnson, 2002; Sello, et al., 2016; Sello, et al., 2018). The purpose of this study is to gain a deeper understanding of calcium signaling in Arabidopsis chloroplasts.

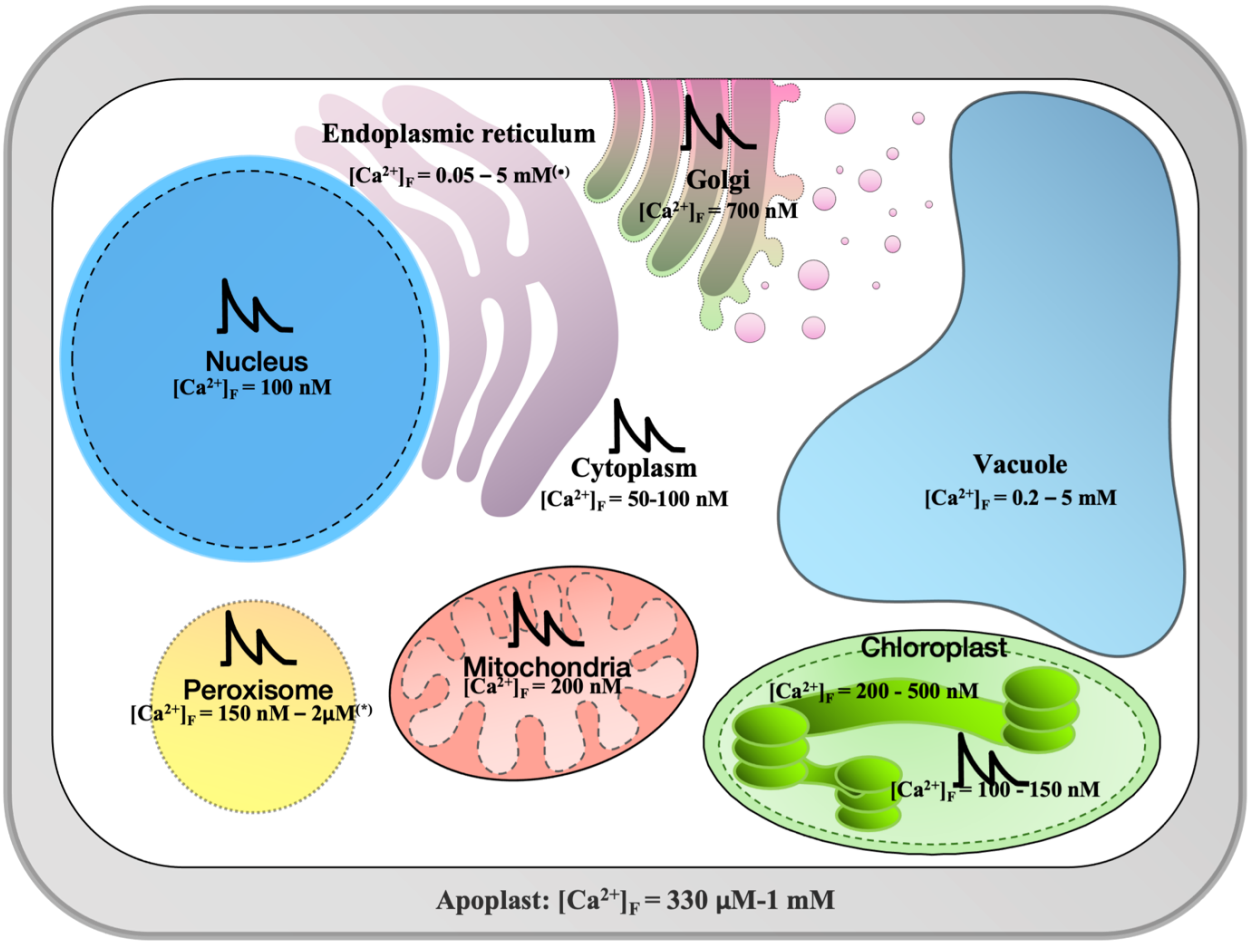

Figure 3. Schematic presentation of free Ca^{2+} concentrations in various plant compartments. A diurnal rhythm seems to be responsible for regulating $[Ca^{2+}]_F$ in the chloroplast stroma and thylakoids. Because plant ER and peroxisome values have not been documented, the given values have been taken from animal data and indicated by an asterisk (*). Two peaks indicate the presence of stimulus induced Ca^{2+} fluxes.

1.4 Ca^{2+} signaling in the chloroplast

It was the pioneering work of Neish in 1939 that suggested the chloroplast as potential Ca^{2+} storage in the plant cell (Neish, 1939). Chloroplasts have a relatively high total Ca^{2+} concentration (higher than 15 mM), with only a small amount of which is in free Ca^{2+} form (Larkum, 1968; O'keefe & Dilley, 1977; Yamagishi, et al., 1981). Most of the Ca^{2+} in chloroplasts is bound to the thylakoid membrane or in a complex with stromal proteins (Hochmal, et al., 2015). Specific intra-chloroplast Ca^{2+} signatures have previously been described using chloroplast sub-localized AEQ and cameleon under stress conditions including salt stress, oxidative stress, flg22, and other biotic and abiotic stressors (Sello, et al., 2016; Nomura, et al., 2012; Loro, et al., 2016; Manzoor, et al., 2015). Even though all

stimuli mentioned above are also detected in the cytosol, a subsequent study revealed that in *A. thaliana*, a destructive heat shock of 25°C - 45°C triggers an independent chloroplastic Ca^{2+} signature that is not detected in the cytosol (Lenzoni & Knight, 2019). Interestingly, prior to this study, it had been reported that in several species, such as *Nicotiana plumbaginifolia*, heat shocks above 45°C generate changes in $[Ca^{2+}]_{cyt}$ but not in the $[Ca^{2+}]_{chl}$ (Gong, et al., 1998; Liao, et al., 2017). This indicates that the chloroplasts are capable of producing independent Ca^{2+} signals.

Chloroplasts contain Ca^{2+}-sensing proteins, which among them several EF-hand containing proteins have been described, such as (p)ppGpp synthetase (Tozawa, et al., 2007). The chloroplasts also contain a Ca^{2+} sensing protein lacking the EF-hand domain, known as CAS (Calcium sensing receptor), which is localized in the thylakoid membrane (Vainonen, et al., 2008; Cutolo, et al., 2019).

On the other hand, a few channels and transporters linked to Ca^{2+} homeostasis in chloroplast have been identified. Two homologs of the bacterial mechanosensitive (MS) like channels, MSL2, and MSL3 are localized in the chloroplast inner envelope of *A. thaliana* (Haswell & Meyerowitz, 2006). Likewise, a more recent study has uncovered a new chloroplastic Ca^{2+} transporter, localized in the thylakoid membrane, called the bivalent cation transporter 1 (BICAT1) (Frank, et al., 2019).

1.4.1 Ca^{2+}-sensing proteins in the chloroplast

Ca^{2+} transients in the chloroplast stroma and thylakoid lumen are assumed to be determined by members of protein families involved in Ca^{2+} transport and sensing (Navazio, et al., 2020). Chloroplast is predicted to contain about 21 Ca^{2+} sensors, although their role in interpreting organellar Ca^{2+} signatures is yet to be determined (Navazio, et al., 2020). Of these 21 predicted proteins, only three have been confirmed to be present in *A. thaliana* so far: CPK20, CPK31, and CAS (Navazio, et al., 2020). Furthermore, several CML and CaM proteins have also been predicted to be localized in the chloroplast, but for now, the localization of none of them has experimentally been confirmed (McCormack & Braam , 2003; Dell'Aglio, et al., 2016).

1.4.1.1 The Calcium sensing receptor (CAS)

CAS is one of the less functionally characterized chloroplast phosphoproteins, with low affinity and high capacity for binding Ca^{2+} (Han, et al., 2003). CAS, a protein of 42 kDa, was revealed to contain a single transmembrane domain (**Figure 4**). Based on in-silico prediction, two major domains have been identified for CAS: N-terminal domain (NT) and C-terminal domain (CT). The CT has been described as a phosphorylation target containing two potential functional sub-domains: a Rhodanese homology domain (amino acids 231-352) which lacks functional characterization, and a region

consisting of amino acids with potential protein-protein interactions with the 'fork-head-associated' (FHA) domain (**Figure 4**) (Vainonen, et al., 2008). Interestingly, it has been anticipated that, unlike CaMs, CAS lacks the high affinity Ca^{2+} binding domain (EF-hand). Nevertheless, it has been predicted that due to its isoelectric point and the presence of acidic amino acids, the N-terminus of CAS (**Figure 4**) might act as a Ca^{2+} binding domain (Wang, et al., 2016).

CAS was initially considered a plasma membrane protein. However, expression of CAS-YFP in tobacco protoplasts and immunoblotting studies have revealed that CAS is a chloroplastic protein localized in the thylakoid membrane with both C- and N-terminus facing the stroma (Nomura, et al., 2008; Cutolo, et al., 2019).

Even though no molecular activity has been determined for the CAS, the protein has been linked to a number of physiological processes such as: 1) regulation of the salicylic acid signaling pathway, providing immunity against *S. sclerotiorum*, a plant pathogen causing white mold via Ca^{2+} signaling (Tang, et al., 2020), 2) dependency of Ca^{2+} signaling of chloroplast triggered by temperature on CAS (Lenzoni & Knight, 2019), 3) regulation of photosynthetic processes by acting on photoacclimation pathways by the state transition kinase 7 and 8 (STN7 and STN8) networks (Cutolo, et al., 2019), 4) activation of ABI4 resulting on LHCB repressing during retrograde signaling (Guo, et al., 2016), and 5) stomatal closure regulation (Wang, et al., 2012; Nomura, et al., 2008; Weinl, et al., 2008).

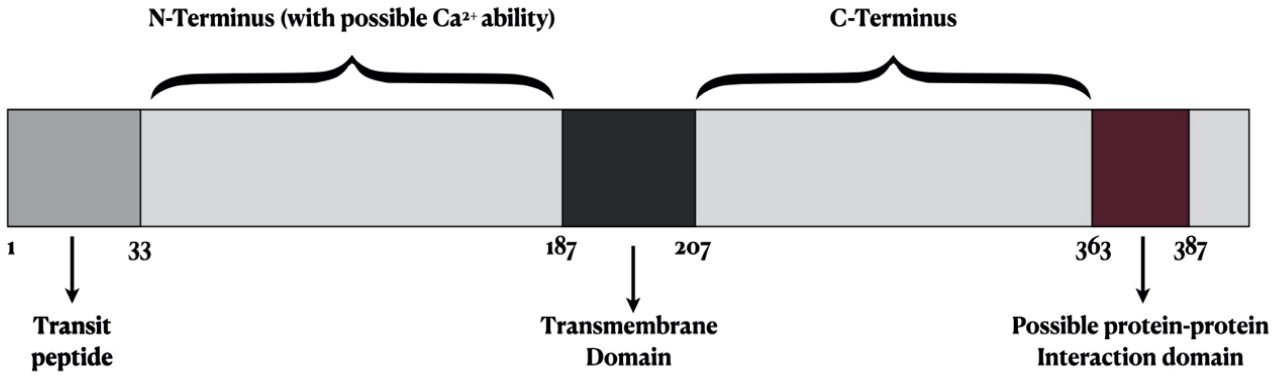

Figure 4. Schematic illustration of CAS protein structure. CAS's N-terminus contains a potential Ca^{2+}-binding domain, while the C-terminus contains a potential protein-protein domain. The 33-amino acid transit peptide determines the location of CAS in the cell. CAS has a single transmembrane domain that acts as an anchor for its localization in the thylakoid membrane.

Based on primary studies on CAS, describing the protein as a phosphoprotein in *A. thaliana*, it has been suggested that CAS, via its phosphorylation, may also be involved in further regulating activities in response to numerous stimuli. It was initially stated that CAS is a possible substrate of STN8 (Vainonen, et al., 2008). However, it was shown later that CAS is not only phosphorylated by STN8 but also by STN7 together with another yet unknown Ca^{2+} dependent kinase(s) (Stael, et al., 2012 a.; Cutolo, et al., 2019).

In Chlamydomonas, the cyclic electron flow (CEF) is mediated by a complex composed of CAS, photosystem I (PSI), cytochrome b6f (CYT*b6/f*), and the proteins PGRL1 and ANR1 (Terashima, et al., 2012). In *A. thaliana*, the CEF occurs specifically around the PSI, leading to an electron transfer from the PSI to Ferredoxin (Fd) and from there to CYT*b6/f*, resulting in ATP synthesis and generating a proton gradient across the thylakoid membrane, without reduction of $NADP^+$ (Terashima, et al., 2012). CEF has been believed to play a role in photoprotection and regulation of photosynthesis of plants, especially under fluctuating light rather than constant light (Yang, et al., 2019). However, the role of CAS in the CEF in *A. thaliana* is not yet described.

1.4.1.2 Calmodulin and Calmodulin-like proteins

CAMs and CMLs are two significant Ca^{2+}-sensing protein groups present in plants. In *A. thaliana*, seven genes encode the CAM proteins, which are very similar and differ only in 4 amino acids at most (Yang & Poovaiah, 2003; McCormack & Braam , 2003). CaMs, with 4 EF-Hands, located at two global ends as a pair, are small and acidic proteins with about 150 amino acids and are present in all eukaryotic organisms (Cyert, 2001; Luan, et al., 2002; McCormack & Braam , 2003; Yang & Poovaiah, 2003; Zielinski, 1998). An EF-hand is composed of a helix-loop-helix structure in which a Ca^{2+} chelating loop joins two α-helixes. The loop consists of 29 amino acids, of which the central 12 are negatively charged and can bind the positively charged Ca^{2+}.

In addition to CaMs, the *A. thaliana* genome encodes 50 different CMLs, each having between 1-6 EF-hands and no other functional domains. They can be more prominent in size than CAMs and can even contain N or C-terminus extensions (Bussemer, et al., 2009; McCormack & Braam , 2003).

2 Aim of this work

In Chlamydomonas, it has been shown that CAS makes a complex with PSI, CYT*b6/f*, and other proteins such as PGRL1 and ANR1 in the chloroplast (Terashima, et al., 2012). However, in *A. thaliana*, such a CAS complex has not been shown yet. Thus, one of the aims of this study was to investigate the ability of CAS to build a protein complex in the chloroplast of *A. thaliana*. To that end, BN-PAGE followed by MS/MS analysis was used. On the other hand, to better understand the role of CAS in *A. thaliana*, growth phenotype and photosynthetic activity were investigated in a cas-knockout (*casko*) *A. thaliana* mutant line compared to wild-type plants (WT).

The second focus of this work was to investigate the role of CAS in the Ca^{2+} signaling pathway in response to salt, mannitol, and oxidative stress. Herein, changes in [Ca^{2+}] were determined in response to these stimuli in WT and *casko* mutant plants expressing the Ca^{2+} reporter AEQ, targeted to the cytosol, stroma, or thylakoid lumen. Additionally, this study focused on discovering the potential source of Ca^{2+} responsible for generating these [Ca^{2+}] changes.

A further objective aimed to discover the correct cellular localization of CML36, one of the 50 CMLs present in the *A. thaliana*. This approach was achieved using the full-length YFP-tag and the self-assembly GFP (saGFP) system in leaf tissue and isolated protoplasts and using laser confocal fluorescence microscopy.

3 Material and Methods

3.1 Material

3.1.1 Chemicals

All chemicals used unless otherwise stated were PA grade or the highest grade available.

Table 1. **List of chemicals used in this study**

Name	Company
1-(4-Hydroxy-3,5-dimethoxyphenyl) ethan-1-one (Acetosyringone)	Sigma-Aldrich GmbH, Germany
Albumin (BSA) Fraction V (pH 7.0)	PanReac Applichem ITW Reagents
ATP (Adenosine-5'-triphosphate)	Roche, Germany
Cellulase "Onozuka R-10" from Trichoderma viride	Serva Electrophoresis GmbH
Coelenterazine	Carl Roth GmbH, Germany
Complete protease inhibitor cocktail, EDTA free	Roche, Germany
Confidor WG 70	Bayer Agrar, Germany
Coomassie® Brilliant blue G	Sigma-Aldrich GmbH, Germany
EDTA	Sigma-Aldrich GmbH, Germany
EGTA	Sigma-Aldrich GmbH, Germany
Ɛ-Aminocapronic acid	Carl Roth GmbH, Germany
IPTG	Duchefa Biochemie, Netherlands
Lanthanum chloride	Sigma-Aldrich GmbH, Germany
Macerozyme R-10 from Rhizopus sp. lyophil	Serva Electrophoresis GmbH
Murashige and Skoog medium (MS) medium	Duchefa Biochemie, Netherlands

n-Dodecyl β-D-maltoside	PanReac Applichem ITW Reagents
Ni-NTA agarose	Qiagen, Germany
Oligonucleotides	Thermo Scientific, USA
Percoll™	Cytiva, Sweden
PhosSTOP™ phosphatase inhibitor	Roche, Mannheim, Germany
Phytagel	Sigma-Aldrich GmbH, Germany
Pierce® protein A plus Agarose	Thermo scientific
Plant potting soil	Flora Guard, Germany
PMSF	Roche, Mannheim, Germany
PVDF membrane	Thermo Scientific, USA
Silver nitrate ≥ 99.9% p.a	Carl Roth GmbH, Germany

3.1.2 Buffers, Enzyms and Kits

Table 2. List of Buffers, enzymes, and kits employed in this study

Name	Company
Buffer G	Thermo Scientific, USA
DNA restriction enzymes	Fermentas, Germany
FastDigest Restriction enzymes	Thermo Scientific, USA
Gel/PCR Fragment extraction kit	Macherey-Nagel (Düren, Germany).
HiYield® Plasmid DNA Kit	HiYield® DNA Isolation SLG
HiYield® Plasmid mini kit	Süd-Laborbedarf GmbH
Native Page 4-16% Bis-Tris gel Native page 3-12% Bis-Tris gel	Invitrogen, USA
NotI, ApaI, SapI	Thermo Scientific, USA

Nucleospin Extract II Kit	Macherey-Nagel, Qiagen, Germany
Phusion Hi-Fidelity polymerase	Thermo Scientific, USA
PstI	Fermentas, Germany
RevertAid First Strand cDNA synthesis Kit	Thermo Scientific, USA
T4 DNA ligase Kit (Buffer and ligase)	Thermo Scientific, USA
Taq polymerase	Genaxxon, Germany

3.1.3 Plasmid DNA vectors and constructs used in this study

Binary vector pBIN19-YFP (supplied by Dr. Norbert Mehlmer) was used in transient tobacco (*Nicotiana benthamiana*) transformation to study the CML36 localization. On the other hand, plasmid vector pET21b (Stratagene, USA) was employed in the in vitro protein expression in *E. coli*. The list of constructs used in this study are presented in the (**Table 3**).

Table 3. List of pBIN19-plasmid and pET21b constructs used in this study

Construct name	AGI code of gene	Plasmid	purpose
AtCML36-saGFP$_{1\text{-}10C}$	At3g10190 CDS	pBIN19-saGFP$_{1\text{-}10C}$	Protein localization
AtCML36-saGFP$_{11C}$	At3g10190 CDS	pBIN19-saGFP$_{11C}$	Protein localization
ssRuBisCo-saGFP$_{1\text{-}10C}$	AT1G67090 CDS	pBIN19-saGFP$_{1\text{-}10C}$	Protein localization
ssRuBisCo-saGFP$_{11C}$	AT1G67090 CDS	pBIN19-saGFP$_{11C}$	Protein localization
CPK17$_{G2A}$-saGFP$_{1\text{-}10C}$	AT5G12180 CDS	pBIN19-saGFP$_{1\text{-}10C}$	Protein localization
CPK17$_{G2A}$-saGFP$_{11C}$	AT5G12180 CDS	pBIN19-saGFP$_{11C}$	Protein localization
OGD-saGFP$_{1\text{-}10C}$	AT3G07880 CDS	pBIN19-saGFP$_{1\text{-}10C}$	Protein localization

OGD- saGFP$_{11C}$	AT3G07880 CDS	pBIN19-saGFP$_{11C}$	Protein localization
MIA-saGFP$_{1-10C}$	AT5G23395.1 CDS	pBIN19-saGFP$_{1-10C}$	Protein localization
MIA-saGFP$_{11C}$	AT5G23395.1 CDS	pBIN19-saGFP$_{11C}$	Protein localization
AtCML36-YFP	AT3G10190 CDS	pBIN19-YFP	Protein localization
CAS-CT	At5g23060.1 CDS (aa 234-387)	pET-21b	Protein overexpression

3.1.4 Primers

All primers used in this study were purchased from Invitrogen by Thermo fishers Scientific. In all naming cases the FW stands for forward primer and Rev stands for revers primer and CDS stands for coding sequence

Table 4. List of primers studied in this study.

Primer Name	Sequence (5'➢3')	Purpose of use
RP_CAS_SALK1	TGGTTGATTGTTTTCTCCACC	CAS specific genotyping
LP_CAS_SALK1	ATGTGTGTTTGCTCGTCTTCC	
RpS15	GATTCCTTGTCCTTGTCCAAGAGGACC	Transketolase specific, Genotyping and DNA quality check
LpS15	TCCAACGGTCATATTTGATCC	
Lba1	TGGTTCACGTAGTGGGCCATCG	T-DNA insertion
CAS_cDNA_FW	CGTCTCCTCTCTCACTGAAGTGGAGAAAA	CAS CDS amplification
CAS_cDNA_REV1	AAACGCAGCACCAGCAGCAAC	
CAS_cDNA_REV2	TTTTCGCCACTATCTTAGCCGAATCCG	
CAS_cln CT_FW	CAAGAATTCATGTACTTGATGGTGGATATA AGATCAG	

CAS_cln CT_Rev	ATAGCGGCCGCGTCGGAGCTAGGAAG	α-CAS_CT antibody design
FW_CAS_amplify	CTTATGGCTATGGCGGAAATG	CAS CDS
Rev_CAS_amplify	CTTGTCGGAGCTAGGAAGG	

3.1.5 Antibodies

The self-designed α-CAS-CT polyclonal antibody in rabbit was produced by David's Biotechnologie GmbH (Regensburg, Germany) from recombinant CAS as antigen. List of other antibodies used in this study is brought in the (**Table 5**).

Table 5. List of Antibodies and their manifactures used in this study

Name of Antibody	Dilution	Organism made in	Source
α-CAS_CT	1:2000	Rabbit	Self-made
α-CAS_NT	1:2000	Rabbit	Supplied by AG. Vothknecht
α-GFP	1:1000	Mouse	Roche, Germany
α-Mouse_Secondary antibody-ALK	1:1000	Mouse	Supplied by AG. Vothknecht
α-Rabbit-Secondary antibody-ALK	1:30000	Rabbit	Sigma Aldrich Chemie
α-TKL1	1:5000	Rabbit	Supplied by AG.Vothknecht

3.1.6 Molecular weight and size markers

Table 6. List of molecular weight and size markers used in this study

Name	Purpose	Company
GenreRuler^{TM} 1Kb plus DNA ladder	DNA size marker for agarose gel electrophoresis	Thermos Scientific, USA
PeqGOLD Protein-Marker IV	Protein size marker for SDS PAGE	VWR Life Science, Germany
PageRuler^{TM} Plus restained protein ladder	Protein size marker for SDS PAGE	Thermo Fisher Scientific, Waltham, MA, USA
NativeMark^{TM} Unastained protein standard	Protein size marker for Blue Native gel	Thermo Fisher Scientific, Waltham, MA, USA

3.1.7 Plant material and growth conditions

In all experiments, *A. thaliana* Columbia 0 (Col-0) was used as the WT control. *CAS-1* (*casko*) (SALK_070416) mutant used in all experiments, were kindly provided by Professor Eva Mari Aro, University of Turku, Finland.

A. thaliana WT plants stably transformed with a 35S:YFP-*APOAEQUORIN* construct targeted to the cytosol, the stroma an the thylakoid lumen, were produced by (Mehlmer, et al., 2012; Sello, et al., 2018). On the other hand, *casko A. thaliana* containing the apoequorine protein targeting the cytosol, stroma, and thylakoid lumen had been previously crossed by Dr. Eduardo Cutolo (Cutolo, Ph.D. 2018). A complete list of *A. thaliana* lines containing Aequorin used in this study is presented in (**Table 7**).

Plants were grown either on soil or on ½ MS media plates, depending on the experiment. The plants were grown in growth-chambers under controlled conditions. Depending on the experiment, plants were grown either in long day condition of 16/ 8 h light/ dark cycle at 20 °C under 100-120 µmol m^{-2} S^{-1} photons illumination (growth light, GL) or short-day condition of 8/16 h light/dark cycle under 100-120 µmol m^{-2} S^{-1} photons illumination (growth light, GL). The growth chambers humidity was set to 65%. For Agrobacterium-mediated infiltration experiments and transit expression for microscopy-based localization, tobacco plants (*Nicotiana benthamiana*) were grown in growth chambers assembled with Philips TLD 18 W

of altering 830/ 840 light color temperature under a long day condition of 16/8 h of light/dark cycle.

Table 7. List of *A. thaliana* lines used in the calcium measurement study.

Line name	Genetic background	Construct	Localization of YFP-AEQ	Zygosity
WT-YFP/AEQ-LUM-C	Col-0	475.1C TLP-YFP-AEQ	Thylakoid Lumen	Homozygote
*casko*YFP/AEQ-LUM-E	*CAS-1* SALK_070416	475.1A TLP-YFP-AEQ	Thylakoid Lumen	Heterozygote
WT-YFP/AEQ-CHL-H	Col-0	286.1 ntThxR-YFPAEQ NTRC-YA	CHL-Stroma	Homozygote
casko-YFP/AEQ-CHL-L	*CAS-1* SALK_070416	286.1 ntThxR-YFPAEQ NTRC-YA	CHL-Stroma	Heterozygote
WT-YFP/AEQ-CYT-AA	Col-0	391.1 CPK17G2A-NES	Cytosol	Homozygote
casko-YFP/AEQ-CYT-P	*CAS-1* SALK_070416	391.1 CPK17G2A-NES	Cytosol	Homozygote

3.1.8 Bacterial strains and growth conditions

Various bacterial strains of *E. coli* and *Agrobacterium tumefaciens (A. tumefaciens)* were used depending on the experiment. Bacteria samples were grown on LB broth medium agar plates or LB broth medium liquid culture containing corresponded antibiotics. As for *E. coli* strains, the samples were grown at 37 ℃ for 16-18 hours, and in case of *A. tumefaciens* samples, bacteria samples were grown at 28 ℃ for 48 hours. (**Table 8**) presents the information of the bacterial strains used in this study.

Table 8. List of bacterial strains used in this study.

Organism	Strain	Usage	Company
E. coli	DH10α DH10β	Cloning, Amplification of DNA plasmid	Stratagene, USA
	RIPL-ER2566	Protein expression	NEB, Germany
A. tumefaciens	GV3101	Stable transformation of *A. thaliana* by floral dipping	Van Larebeke *et al.,* 1974
	LBA1334	Transit transformation of tobacco for localization assays	

3.2 Methods

3.2.1 Bacterial transformation methods

3.2.1.1 *E. coli* transformation using heat shock technique

E. coli samples of desired strain were transformed using the basic molecular biology technique, the heat shock method. This method introduces an external plasmid or ligation product to *E. coli* cells. In this method, 100 µl of selected *E. coli* strain was mixed with 3-5 µl of plasmid DNA on ice. The mixture was then incubated for 15 min on ice. The incubation step was followed by the precisely 45 seconds of heat shock at 42 ℃ before moving back on the ice for 2 min. Next, 800 µl of fresh liquid LB media without antibiotics was added to the mixture. The sample was then incubated for 45 minutes with agitation at 650 rpm at 37 ℃. Finally, the grown bacteria clones were centrifuged at 5000 g for 1 minute. The harvested bacteria cells were resuspended with 100 µl of fresh liquid Luria-Bertani (LB) media before plating on LB plates containing corresponding antibiotics. The *E. coli* cells were then grown at 37 ℃ overnight. The success of the transformation was measured by visualization of colony formation.

3.2.1.2 *Agrobacterium tumefaciens* transformation via electroporation technique

A. tumefaciens was transformed by mixing 25 µl of bacteria cells with 1-3 µl of plasmid DNA and 25 µl of 10% sterile glycerol (v/v). After a gentle mix, the mixture was moved to an electroporation cuvette (Carl Roth, Germany). Next, electroporation was performed using the BioRad electroporation chamber using "Agr" mode. The electroplated mixture was then mixed with 400 µl fresh LB media, transferred in a fresh eppie, and incubated at 28 ℃, 650 rpm for 2 hours. The transformed bacteria cells were then harvested by centrifugation for 1 minute at 5000 g. The pellet was resuspended in 100 µl fresh LB before plating on LB media plates containing Kanamycin (25 µg/ml), Rifampicin, and 1 M $MgCl_2$. The Agrobacterium plates were then incubated at 28 ℃ for 48 hours for successful colony transformation.

3.2.1.3 Protein Expression and purification

Overnight grown 20 ml LB liquid cultures containing the corresponding antibiotic of desired *E. coli* RIPL sample was diluted in 500 ml LB liquid culture with corresponding antibiotics. The OD_{600} was measured continuously up till the OD_{600} reached 0.5-0.8. At this point, 0-hour non-indued samples of 500 µl were taken, and the rest of the culture was incubated for 3 hours with IPTG. Next, a 500 µl induced sample was taken from the induced culture and was pelleted down. Then using the IMPACT™-TWIN system (New England Biolabs, Frankfurt, Germany), following the manufacturer's instructions, purification was performed under native conditions.

3.2.2 Plant methods

3.2.2.1 Chloroplast isolation

Intact chloroplast was isolated from 4-weeks-old *A. thaliana* plants, as previously mentioned by (Seigneurin-Berny, et al., 2008). The plants were grown in short-day conditions, of 8/16 h light/dark cycle, and leaves were harvested 2 hours after the beginning of the light cycle. Growth light samples were kept for the mentioned 2 hours under normal light conditions of 120 µmol m^{-2} s^{-1} photons illumination. The intact chloroplast samples were kept at -80 ℃ as 50 µl aliquots after direct freezing using liquid nitrogen.

Chlorophyll concentration was ascertained by mixing 5 µl of the sample with 5 ml 80% Acetone (v/v), as previously described by (Porra, et al., 1989), and measured as below:

$$[(OD_{663}\text{-}OD_{750}) \times 8.2] + [(OD_{645}\text{-}OD_{750}) \times 20.2] = X\ \mu g/\mu l$$

3.2.2.2 Chloroplast fractionation

In order to separate the thylakoids from the stroma, 50 µl of intact chloroplasts sample was treated for 15 minutes with 200 µl lysis buffer (20 mM Tricine pH 7.6, 10% (v/v) glycerol, 1 mM DTT, completeTM, EDTA-free protease inhibitor), on ice. Membrane proteins were then separated from soluble fractions by centrifugation at 20000 g for 10 minutes at 4 °C. The pellet containing membranal proteins (thylakoid enriched) was then washed 2-3 times with 200 µl of cold lysis buffer to remove excess stromal contamination. All described previously by (Rocha, et al., 2014).

3.2.2.3 Total leaf protein isolation

Total leaf protein was isolated by grinding 100 mg of 3-week-old plant leaves in 150 µl of extraction buffer (100 mM NaCl, 50 mM Tris-HCl pH 7.5, 0.5 M Triton x-100, 100 mM beta-mercaptoethanol, 1 mM PMSF). The extract was then centrifuged at 13000 g for 5 minutes at room temperature. The supernatant containing proteins of interest was mixed 1:1 with sample buffer [125 mM Tris-HCl pH 6.8, 5% (w/v) SDS, 10% glycerol (v/v), 5% beta-mercapto-ethanol (v/v)]. The mixture was heated for 5 minutes at 95 °C before loading on gel. All described before by (Rensink, et al., 1998).

3.2.2.4 Transit transformation of tobacco plants using Agrobacterium infiltration in contemplation of CML36 localization

Agrobacterium-mediated transit transformation is an efficient technique as it is not affected by chromosomal positional effects (Fischer, et al., 1999). Overnight *A. tumefaciens* cells grown in 5 ml LB liquid culture supplied with 50 mg/ml Kanamycin were harvested by 5 minutes centrifugation at 4000 g. The harvested cells were resuspended in 1 ml cold Infiltration buffer [20 mM Citric acid (monohydrate), 2% (v/w) sucrose pH 5.2 using NaOH 5 M] and autoclaved prior to use supplemented with 200 µM acetosyringone. Next, OD_{600} was measured for samples by diluting 1:1 of the sample using Infiltration media mixed with acetosyringone. The OD_{600} was adjusted to 0.1-0.3 (samples with higher OD_{600} were diluted using the Infiltration media

mix). The samples were incubated for 2 hours at RT while rotating at dark prior to infiltration of 3–4-week-old tobacco leaves. Transit transformation expression signal peaks at 48-60 hours after infiltration therefore, the infiltrated leaves were controlled using a confocal microscope after 48-60 hours of dark incubation post infiltration.

3.2.2.5 Protoplast isolation from transit transformed tobacco leaves

Transformed tobacco leaves were cut into 0.5-1 mm pieces and submerged in enzyme solution [1-1.5% (v/w) cellulase R10, 0.2-0.4% (v/w) macerozyme R10, 0.4 M mannitol, 20 mM KCl, 20 mM MES pH 5.7]. Afterward, the solution mixture was heated at 55°C for 10 minutes and mixed with 10 mM CaCl2 after it had been cooled down to room temperature. The mixture was then passed through a 0.45 µm filter. Using a vacuum, for 30 minutes, the filtered mixture turns dark green, representing the protoplast release.

Since the protoplasts are very fragile, the samples need to be carried under extra caution from this step. The vacuumed mixture was then placed on a shaker rotating at 40 rpm in dark conditions for 90 minutes, followed by a 5 minute faster shake of 80 rpm. The samples were filtered through 100 µm nylon mesh to isolate protoplast from leaf strips, and the protoplast mixture was centrifuged at 100 g for 10 minutes at RT while the break was off. The supernatant containing broken protoplast was removed, and the pellet was washed with W5 buffer (154 mM NaCl, 125 mM $CaCl_2$, 5 mM KCl, 2 mM MES pH 5.7). The washed protoplasts were centrifuged at 100 g for 10 minutes at RT with no break. A major part of the supernatant was removed, and the pellet was dissolved in the rest of the supernatant, by gently shaking prior to confocal laser scanning.

3.2.2.6 Floral dipping method using *Agrobacterium tumefaciens*

(Zhang, et al., 2006) method was employed to make transformed seeds in *A. thaliana*. 500 ml LB mixture of desired transformed bacteria and appropriate antibiotic was incubated overnight at 28 ℃. The transformed cells were harvested by centrifugation the following day for 10 minutes at 4000 g at 4 ℃. The pellet was resuspended in 500 ml sucrose solution [5% (w/v) sucrose, 200 µl 0.5 M acetosyringone, 200 µl 100% Tween20). The *A. thaliana* plants were kept in the dark overnight after dipping and moved to the growth chamber the day after. The dipping was repeated one additional time to increase the transformation.

3.2.2.7 Self-assembly GFP (saGFP) assay

Transient transformation of tobacco was done using a modified pBIN19 binary vector carrying C-terminally the sequence coding either for $saGFP_{1-10}$ or $saGFP_{11}$ (Bevan, 1984). The genes of interest harboring an ApaI overhang or NotI overhang were cloned in the pBIN19 vector expressing either the $saGFP_{11}$ or $saGFP_{1-10}$ tags. The cloned vector was then introduced into agrobacteria (described in material and methods 3.2.1.2). Co-infiltration of leaves of 3-4 weeks old tobacco plants (*Nicotiana benthaminana*) was then performed (as described in 3.2.2.4). Subcellular localization of the proteins was analyzed by confocal laser scanning microscopy using the Olympus FluoView FV1000 confocal laser scanning microscope, and the images were processed with the FV10- ASW Viewer software.

3.2.3 Nucleic acid methods and cloning

3.2.3.1 Genomic DNA isolation from leaf samples

Genomic DNA isolation was done using 3 to 4-weeks-old leaf samples. Single leaf tissue was grounded using a metal bead and 400 µl extraction buffer (200 mM Tris-HCl pH 7.5, 250 mM NaCl, 25 mM EDTA). The grounded sample was centrifuged at 13000 g for 10 minutes. In this step, the genomic DNA is released into the supernatant. 285 µl of supernatant containing genomic DNA was mixed with 715 µl of 70% Ethanol. The mixture was centrifuged after vertexing at 13000 g for 10 minutes. The clear pellet after centrifugation contains the genomic DNA and was dried at 50 ℃ for 2 hours before resuspending in 50 µl Tris-HCl pH 8.5. DNA samples were kept at -20 ℃ until further desired experiments.

3.2.3.2 Isolation of plasmid DNA

According to the manufacturer's descriptions, plasmid DNA from transformed *E. Coli* cells was isolated in all studies using a HiYield® Plasmid mini kit (Süd-Laborbedarf GmbH).

3.2.3.3 Polymerase chain reaction (PCR)

In order to amplify genomic DNA or plasmid DNA fragments for genotyping, cloning, and other analytical purposes, the PCR technique was employed. According to the manufacturer’s instructions, either GoTaq DNA polymerase (Promega, USA) or Phusion Hi-Fidelity polymerase (Thermo Scientific, USA) were used. The standard components of a PCR reaction are presented in **Table 9**.

Table 9. Standard components of PCR reaction

Components	Taq polymerase reaction mix	Phusion polymerase reaction mix
5x Buffer	5.0 µl	5.0 µl
DNA template (10-50 ng/µl)	1.0 µl	1.0 µl
dNTPs (200 µM)	0.5 µl	0.25 µl
H_2O	17.3 µl	16.8 µl
$MgCl_2$ (25 mM)	0.0 µl	1.25 µl
Polymerase	0.2 µl	0.2 µl
Primer 1 (1 µM)	0.5 µl	0.25 µl
Primer 2 (1 µM)	0.5 µl	0.25 µl
Total	25 µl	25 µl

According to the expected amplicon size and the calculated annealing temperature of the primers used in the reaction, the elongation time and the annealing temperatures were adjusted explicitly. **Table 10** presents the optimized PCR settings used in this study.

Table 10. Optimized PCR settings performed on a thermocycler

PCR Steps	GoTaq Polymerase Temperature (°C) – Time (S)	Phusion polymerase Temperature (°C) – Time (S)	Number of cycles
Initial denaturation	95 °C - 120 s	98 °C - 30 s	x1
Denaturation	95 °C - 120 s	98 °C - 10 s	x35
Annealing	✻ - 60 s	✻ - 30 s	
Elongation	72 °C - 60 s /kb	72 °C - 30 s /kb	
Final elongation	72 °C - 300 s	72 °C - 300 s	x1
Hold	4 °C - ∞		

3.2.4 Protein methods

3.2.4.1 SDS PAGE analysis

Protein samples were prepared for SDS-polyacrylamide gel electrophoresis (SDS-PAGE) by mixing the isolated protein, with 4X SDS solubilisation buffer [40% (v/v) Glycerol, 240 mM Tris-HCl pH 6.8, 8% (w/v) SDS, 0.04% (w/v) bromophenol blue, 5% (v/v) beta-mercaptoethanol]. The mixture was then heated at 96 ℃ for 5 minutes and loaded on 10% or 12% SDS gel after cooling down, based on the sample size. **Table 11** and **Table 12** present the gel compositions for the running and the stacking gel.

Table 11. Composition of SDS PAGE Running gel

Components	10% SDS gel	12% SDS gel
H_2O	4.0 ml	3.3 ml
30% (v/v) Acrylamide mix	3.3 ml	4.0 ml
1.5M Tris (pH 8.8)	2.5 ml	2.5 ml
10% SDS	0.1 ml	0.1 ml
10% APS	0.1 ml	0.1 ml
TEMED	0.004 ml	0.004 ml

Table 12. Composition of SDS PAGE Stacking gel

Components	5 ml
H_2O	3.4 ml
30% (v/v) Acrylamide mix	0.83 ml
1.0 M Tris (pH 8.8)	0.63 ml
10% (w/v) SDS	0.05 ml
10% APS	0.05 ml
TEMED	0.005 ml

3.2.4.2 Blue native gel electrophoresis

The preferred chlorophyll amount to be loaded on Blue native gels, in the case of this study unless mentioned, has been determined to be 20 mg. Chloroplast was diluted to the corresponding concentration and brought to a final volume of 45 µl using ACA buffer (750 mM Ɛ-Aminocapronic acid, 50 mM BisTris pH 7.0, 0.5 mM EDTA). The mixture of chloroplast/ACA was incubated on ice for 15 min while kept dark before mixing with 5 µl 10% *n*-Dodecyl β-D-maltoside, a non-ionic detergent, used in membrane studies. The mixture was then vortexed and incubated on ice for 30 min while kept dark. The mixture was subsequently centrifuged at 21000 g for 10 min at 4 °C. The supernatant in this step, which is light green, is separated and is mixed with 5 µl of 5% serve blue G (750 mM ACA, 5% (w/v) Coomassie® Brilliant blue G) and incubated for 5 min on ice before loading on gel. The empty pockets of the gel were filled with a mixture of 1:1 ACA buffer and 5% serve blue G. The gels ran for 1 hour with 1x cathode buffer with Coomassie® Brilliant blue G (**Table 14**) and 1x Anode buffer (**Table 14**) at 100 v, 2 mA for one big gel and 2 hours at 150 V for small blue native gels from Invitrogen (Native page 3-12% Bis-Tris gel, Native Page 4-16% Bis-Tris Gel). The cathode buffer was then changed to 1x cathode buffer without Coomassie® Brilliant blue G in the dark. The composition of the different percentages of blue native gels is brought in **Table 13** Buffers used for running the gel are mentioned in **Table 14** (all buffers must be stored at 4 °C).

Table 13. Components of different percentage gel used in Blue native gel

Chemicals	Running gel 6% (8 ml)	Running gel 14% (8 ml)	Stacking gel (5ml)
30% Acrylamide mix	1.6 ml	2.67 ml	0.66 ml
6x Gel buffer	1.33 ml	1.33 ml	0.83 ml
Glycerol	0 ml	1.6 gr	0 ml
H_2O	5.07 ml	2.82 ml	3.5 ml
TEMED	3.8 µl	3.8 µl	5 µl
APS	15.2 µl	15.2 µl	50 µl

Table 14. Buffers used in running blue native gels.

Buffer name	Reagents and Concentrations
5x Cathode buffer with **Coomassie**® Brilliant blue G	250 mM Tricine, 75 mM Bis-Tris, 0.1% (w/v) Coomassie 250G (pH 7.0 using HCl)
5x Cathode buffer without **Coomassie**® Brilliant blue G	250 mM Tricine, 75 mM Bis-Tris (pH 7.0 using HCl)
6x Anode buffer	300 mM Bis-Tris (pH 7.0 using HCl)
6x Gel buffer	1.5 M Amino caproic Acid, 150 mM Bis-Tris (pH 7.0 using HCl)

3.2.5 Aequorin reconstitution and luminescence measurements

To study Ca^{2+} transients, *A. thaliana* seedlings of WT and *casko*, carrying the apoaequorin protein targeted to the cytosol, stroma, and the thylakoid lumen were grown on ½ MS media supplemented with sugar and vitamin for eight days under long-day conditions (120 mol). The

whole seedlings were reconstituted in a 5 M coelenterazine solution (Carl Roth, Karlsruhe, Germany) for 16 hours prior to the measurements. For treatments with inhibitors, seedlings were incubated for one hour in 1 mM lanthanum chloride ($LaCl_3$) or 1 mM EGTA after reconstitution. A plate luminometer (Multimode ReaderTriStar² LB 942, Berthold Technologies) was used to measure all measurements in a 96-well plate (Lumitrac 600, Greiner Bio-One, Kremsmünster, Austria). To measure the baseline prior to injecting a 2-fold concentrated solution of $CaCl_2$, H_2O_2, NaCl, and mannitol, Luminescence measurements were made for 120 seconds with a 1 second integration time. Luminescence was measured for another 600 seconds following injection. The luminescence signal was detected for another 300 seconds with the same integration time following injection of the discharge solution (1 M $CaCl_2$ in 10% ethanol). In calculating $[Ca^{2+}]$, the background correction was derived from measurements of empty wells in the same conditions for all cell comparisons. For calculating $\Delta[Ca^{2+}]$, the mean $[Ca^{2+}]$ from 10 seconds of baseline preceding treatment was subtracted from the maximum $[Ca^{2+}]$ after injection.

4 Results

4.1 Characterization of CAS protein

CAS has been identified as a Ca^{2+}-sensing protein localized in the thylakoid membrane of the chloroplast (Nomura, et al., 2008). CAS is nuclear-encoded and post-translationally transported into the chloroplast with the help of a 33 amino-acid transit peptide (**Figure 4**). After transport into the chloroplast, the transit peptide is cleaved to produce the mature form of CAS with a molecular weight of 34 kDa (Nomura, et al., 2008). In Chlamydomonas, it has been shown that CAS makes a supercomplex with the complexes PSI, CYT*b6/f* complex, as well as with the proteins PGRL1 and ANR1 in the chloroplast (Terashima, et al., 2012). In *A. thaliana*, however, such a CAS supercomplex has not been shown yet. Thus, one of the aims of this thesis was to investigate the ability of CAS to build a protein complex in the chloroplast of *A. thaliana*. On the other hand, to better understand the role of CAS in *A. thaliana*, phenotypic investigations and measurements of photosynthetic activity were performed by comparing WT (Col-0) with a *casko* mutant line.

4.1.1 Blue native PAGE analysis

Blue native (BN) PAGE assays were performed using intact chloroplasts isolated from *A. thaliana* WT and *casko* lines (SALK_070416) (**see 3.2.4.2**) to determine whether the absence of CAS affects the protein complex composition of the chloroplast. Indeed, differences in the protein complex patterns on the BN-gel were observed between the WT and *casko* chloroplasts (**Figure 5**). The most differences were observed between 556 kDa and 292 kDa, with at least four bands (B, C, D, and E) which are absent in *casko* chloroplasts. One additional band (A) with a molecular weight higher than 556 kDa was also detected only in the WT chloroplast. The other known major complexes of the photosynthesis reaction in the thylakoid membrane were not affected, except the LHC trimer, which was less abundant in the *casko* chloroplast (**Figure 5, trimeric LHC**). By contrast, the LHC monomer was more dominant in the *casko* chloroplasts compared to the WT (**Figure 5, LHC monomer**).

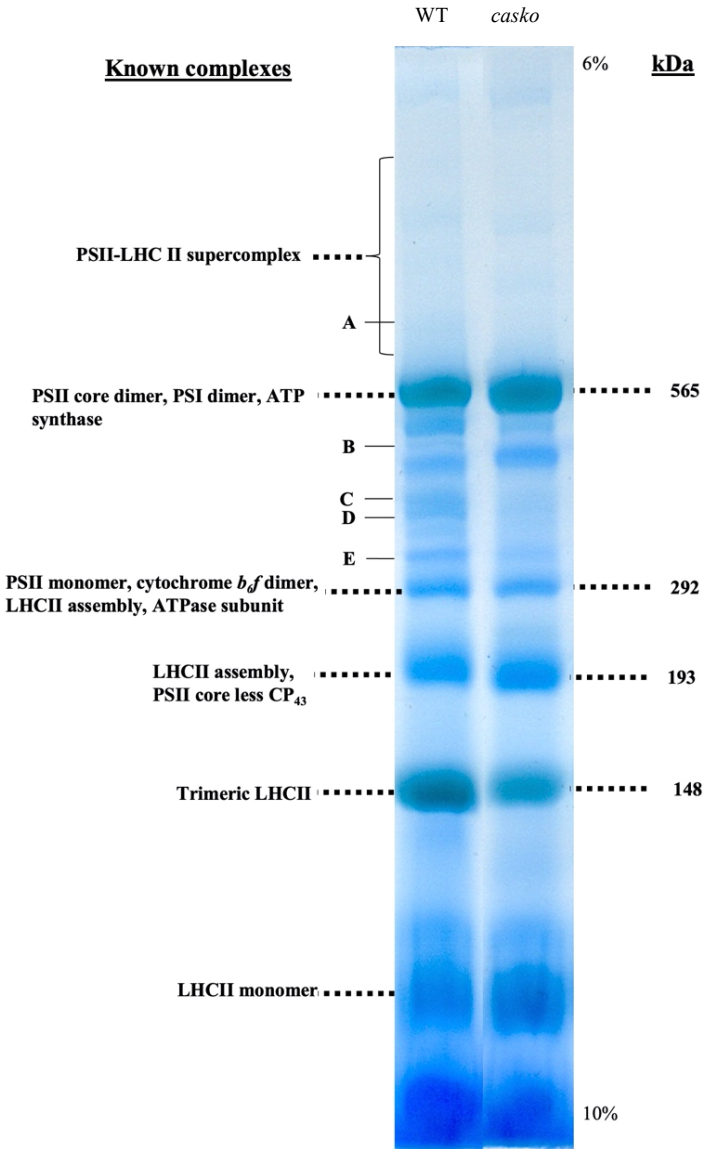

Figure 5. BN-PAGE of WT and *casko A. thaliana* intact chloroplast. The figure presents the known chloroplastic complexes and their size on a (6-10%) BN-gel. Letters marked on the gel (A, B, C, D, and E) indicate the differences observed between the WT and *casko* chloroplast.

To determine the protein composition of each band showing differences between WT and *casko* chloroplasts, the corresponding areas were cut from the gel and analysed by MS/MS. The results showed that bands A, B, C, D, and E contain CAS protein in different amounts. The bands A, B, and D contain a very elevated amount of CAS, indicating a high probability that CAS is a subunit of three different complexes.

Table 15. CAS protein iBAQ values obtained from MS/MS analysis of the protein complexes showing differences between WT and *casko* chloroplasts on BN-gels.

	Band A	Band B	Band D	Band C	Band E
CAS (Calcium sensing receptor)	1196200	1085900	906240	615790	610230

Since bands A, B, and D, showed the highest amount of CAS protein, further detailed analyses were performed only with them to identify the nature of their protein compositions. MS/MS analysis showed that the three bands contain different subunits of the complexes PSI, PSII, LHCs, CYT*b6/f*, and ATP-synthase (**Tables 16, 17, and 18**). One main difference concerned the isoforms of the ferredoxin-$NADP^+$ reductase 1 and 2 (FNR1 and FNR2), which could be detected only in bands B and D, but not in A. Interestingly, the LHC proteins also showed a differential distribution within these bands. Band A contains different LHCA and LHCB proteins which are known to interact with PSI and PSII, respectively (**Table 16**). However, in band B, mostly LHCA proteins were present (**Table 17**), while in band D, only LHCB proteins could be detected (**Table 18**). Additionally, all the bands contain PGR5-like A (PGRL1) protein. In Chlamydomonas, it has been shown that CAS is interacting with a supercomplex composed of (PSI-LHCI), (PSII-LHCII), CYT*b6/f*, in addition to FNR and the thylakoid protein PGR5-like1 (Iwai, et al., 2010; Petroutsos, et al., 2009). The bands A, B, and D have quite similar protein compositions to the Chlamydomonas supercomplex, suggesting that the bands A, B, and D might also correspond to supercomplexes in *A. thaliana.* For further analysis, the bands were called supercomplex A, B, and D. Supercomplex A is composed of the complexes PSI-LHCA, PSII-LHCB, CYT*b6/f*, ATP-synthase, and the proteins CAS and PGR5-like A (PGRL1). Supercomplex B is composed of the complexes PSI-LHCA, PSII, CYT*b6/f*, ATP-synthase, and the proteins CAS, PGR5-like A (PGRL1) and FNR1/FNR2, while supercomplex D contains the complexes PSI, PSII-LHCB, CYT*b6/f*, ATP-synthase and the proteins CAS, PGR5-like A (PGRL1), and FNR1/FNR2. In *A. thaliana*, CAS is an essential component for the formation of these supercomplexes, since in its absence, in *casko* mutant chloroplasts, they could not be detected anymore (**Figure 5**).

Table 16. Protein composition of supercomplex A. Protein composition of band A from the BN-gel shown in Figure 5 is determined by MS/MS analysis. The proteins are divided into PSI (light green), PSII (dark green), CYT*b6/f* (orange), LHC (pink), ATP synthesis (light blue), and PGR (red) groups.

Predicted protein	iBAQ
CAS calcium sensing receptor	1196200
PSAF photosystem I subunit F	18823000
PSAD-2, PSAD-1 photosystem I subunit D-1, D-2	16061000
PSAB Photosystem I, PsaA/PsaB protein	14739000
PSAL photosystem I subunit l	12406000
PSAE-1 Photosystem I reaction centre subunit IV / PsaE protein	11035000
PSAH2, PSAH-2, PSI-H photosystem I subunit H2	10548000
PSAA Photosystem I, PsaA/PsaB protein	10116000
PSAG photosystem I subunit G	5471700
PSAK photosystem I subunit K	3895900
PSAC iron-sulfur cluster binding	3576600
PSAJ PSAJ	965330
PSAH-1 photosystem I subunit H-1	191010
PSAE-2 photosystem I subunit E-2	161560
PSBB photosystem II reaction center protein B	8276200
PSBD photosystem II reaction center protein D	8136600
PSBC photosystem II reaction center protein C	5507900
PSBA photosystem II reaction center protein A	3922000
PSBE photosystem II reaction center protein E	3705200
PSBL photosystem II reaction center protein L	905550
PETB photosynthetic electron transfer B	1009500
PETA photosynthetic electron transfer A	878630
PETG	462200
PETC photosynthetic electron transfer	323930
LHCA3 photosystem I light harvesting complex gene 3	70269000
LHCA4, CAB4 light-harvesting chlorophyll-protein complex I subunit A4	13068000
LHCA2 photosystem I light harvesting complex gene 2	7779700
LHCA1 photosystem I light harvesting complex gene 1	6376700
LHCB1.3 chlorophyll A/B binding protein	2159900
LHCB2 photosystem II light harvesting complex gene	681340
LHCB6, CP24 light harvesting complex photosystem II subunit 6	466540
LHCB4.2 light harvesting complex photosystem II	375540
LHCB4.1 light harvesting complex photosystem II	326190
ATPH ATP synthase subunit C family protein	8878900
ATP synthase subunit (ATP alpha)	1212400
ATP synthase subunit (ATPF)	1202300
ATP synthase alpha/beta family protein	894200
Beta subunit of ATP synthase	801340
ATP synthase subunit (ATP alpha)	454120
ATP synthase subunit 1	330970
PGR1 photosynthetic electron transfer	323930
PGR5-LIKE A	244270

Table 17. Protein composition of supercomplex B. Protein composition of band B from the BN-gel shown in Figure 5 is determined by MS/MS analysis. The proteins are divided into PSI (light green), PSII (dark green), CYT*b6/f* (orange), FNR (dark blue), LHC (pink), ATP synthesis (light blue), and PGR (red) groups.

Predicted protein	iBAQ
CAS calcium sensing receptor	1085900
PSAF photosystem I subunit F	49419000
PSAB Photosystem I, PsaA/PsaB protein	30823000
PSAL photosystem I subunit l	30820000
PSAD-2, PSAD-1 photosystem I subunit D-1, D-2	30223000
PSAE-1 Photosystem I reaction centre subunit IV / PsaE protein	29427000
PSAH2, PSAH-2, PSI-H photosystem I subunit H2	26538000
PSAA Photosystem I, PsaA/PsaB protein	24846000
PSAG photosystem I subunit G	12405000
PSAC iron-sulfur cluster binding	10961000
PSAJ	3545600
PSAE-2 photosystem I subunit E-2	1697800
PSAK photosystem I subunit K	1447100
PSAP, PSI-P photosystem I P subunit	122110
PSBB photosystem II reaction center protein B	26393000
PSBD photosystem II reaction center protein D	25407000
PSBE photosystem II reaction center protein E	21259000
PSBA photosystem II reaction center protein A	13116000
PSBC photosystem II reaction center protein C	4508400
PSBL photosystem II reaction center protein L	2818700
PSBH photosystem II reaction center protein H	634500
PETA photosynthetic electron transfer A	2097600
PETB photosynthetic electron transfer B	974380
PETC photosynthetic electron transfer C	694990
PETG	484210
ATLFNR1, FNR1 ferredoxin-NADP(+)-oxidoreductase 1	523380
ATLFNR2 ferredoxin-NADP(+)-oxidoreductase 2	406840
LHCA4, CAB4 light-harvesting chlorophyll-protein complex I subunit A4	32032000
LHCA1 photosystem I light harvesting complex gene 1	16285000
LHCA3 photosystem I light harvesting complex gene 3	10201000
LHCA2 photosystem I light harvesting complex gene 2	508230
LHCB1.3 chlorophyll A/B binding protein	492500

ATP synthase subunit (ATP alpha)	7406900
Beta subunit of ATP synthase	5179900
ATP synthase subunit (ATPF)	2938300
ATPH ATP synthase subunit C family protein	2327000
ATP synthase subunit (ATP gamma1)	1297300
ATP synthase subunit (ATPG)	915470
ATP synthase subunit (ATP epsilon)	482420
PGR1 photosynthetic electron transfer C	694990
PGR5-LIKE A	131140

Table 18. Protein composition of supercomplex D. Protein composition of band D from the BN-gel shown in Figure 5 is determined by MS/MS analysis. The proteins are divided into PSI (light green), PSII (dark green), CYT*b6/f* (orange), FNR (dark blue), LHC (pink), ATP synthesis (light blue), and PGR (red) groups.

Predicted protein	iBAQ
CAS calcium sensing receptor	906240
PSAD-2, PSAD-1 photosystem I subunit D-1, D-2	59308000
PSAE-1 Photosystem I reaction centre subunit IV / PsaE protein	55848000
PSAL photosystem I subunit l	45834000
PSAH2, PSAH-2, PSI-H photosystem I subunit H2	44273000
PSAB Photosystem I, PsaA/PsaB protein	38604000
PSAA Photosystem I, PsaA/PsaB protein	38424000
PSAG photosystem I subunit G	21289000
PSAC iron-sulfur cluster binding	20967000
PSAF photosystem I subunit F	13687000
PSAE-2 photosystem I subunit E-2	8530000
PSBE photosystem II reaction center protein E	6062900
PSBB photosystem II reaction center protein B	5393900
PSBD photosystem II reaction center protein D	4537200
PSBA photosystem II reaction center protein A	1470600
PSBC photosystem II reaction center protein C	1319400
PSBH photosystem II reaction center protein H	342110
PSBL photosystem II reaction center protein L	314970
PETA photosynthetic electron transfer A	5037800
PETB photosynthetic electron transfer B	3878000
PETG	922850
PETC photosynthetic electron transfer C	887890
PETD photosynthetic electron transfer D	318970
ATLFNR1, FNR1 ferredoxin-NADP(+)-oxidoreductase 1	950190
ATLFNR2 ferredoxin-NADP(+)-oxidoreductase 2	579090
LHCB1.3 chlorophyll A/B binding protein	510350
LHCB4.2 light harvesting complex photosystem II	497480
LHCB4.1 light harvesting complex photosystem II	210310

LHCB6, CP24 light harvesting complex photosystem II subunit 6	193450
LHCB5 light harvesting complex of photosystem II 5	159640
ATP synthase subunit (ATP alpha)	20861000
Beta subunit of ATP synthase	18453000
ATP synthase subunit (ATPF)	6050200
ATP synthase subunit (ATP gamma1)	4058500
ATPH ATP synthase subunit C family protein	3745800
ATP synthase subunit (ATP epsilon)	3411800
ATP synthase subunit (ATPG)	2844000
ATP synthase subunit (ATP alpha)	785340
ATP synthase subunit (ATP beta)	396720
PGR1 photosynthetic electron transfer C	887890
PGR5-LIKE A	70650

4.1.2 In-silico protein-protein network prediction of CAS

Bioinformatic molecular interaction predictions are useful for interpreting experimental data as they allow one to get a broad picture of how proteins can interact with one another. In this work, a mass spring conserved entropy-based networking model along with a co-expression network was constructed using the available STRING database (https://string-db.org/) connected using the R-based Bioconductor package (**Figure 6**). STRING networks are usually constructed based on confidence scores of interaction predictions. Higher confidence interaction modules (based on either co-expression or gene neighborhood) would usually be placed in close proximity and vice-versa. As evident from (**Figure 6)**, after the construction of the network with the sequenced proteins from MS/MS, CAS could be placed closely with the proteins FNR1 and FNR2. These proteins are known to facilitate the last step of electron transfer from ferredoxin to NADPH, catalyzing the final step of electron flow, thereby facilitating carbon fixation, along with the canonical PETC (PGR1) protein, proposed to be a part of the CYT*b6/f* complex involved in cyclic electron flow (Nikkanen, et al., 2018; Yamamoto & Shikanai, 2019). Also, other significant proteins like LHCA3, a component of the light-harvesting complex, and PSAf, a subunit of PSI, were closely placed to CAS, thereby

signifying a high degree of predicted association between them. This also corresponds to the results of the BN gel electrophoresis and MS/MS analysis, where CAS was co-localized with the complex CYT*b6/f* along with FNR1/FNR2. To closer scrutiny, these results obtained with MS/MS sequencing and in-silico predictions in *A. thaliana* also tallies with the observations made in Chlamydomonas where, using immunoblotting with extracted thylakoid fractions, CAS was shown to be a component involved in cyclic electron flow along with other approved proteins involved in the cyclic electron flow like FNR and PGRL1 (Terashima, et al., 2012; Leister & Shikanai, 2013).

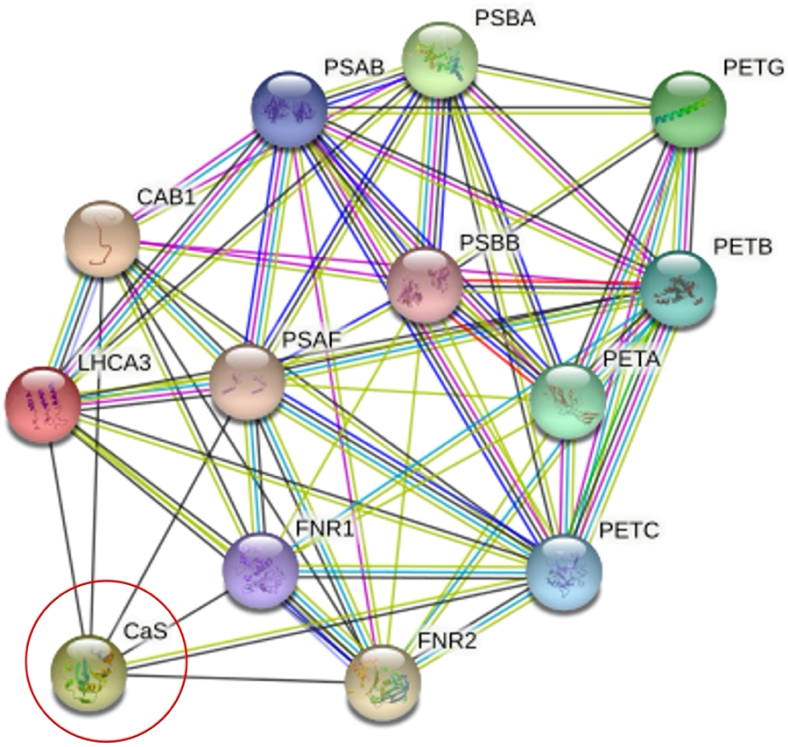

Figure 6. Functional association network of CAS with chloroplastic proteins and the observed Co-expression in *A. thaliana*. Interacting network of CAS. The edges represent protein-protein associations. In the diagram, light blue lines indicate known interactions (from the curated database) and pink lines indicate experimentally determined interactions. Predicted interactions on the other hand are shown in dark green (gene neighborhood), red (gene fusions) and dark blue (gene co-occurrence). The co-expression genes are connected by black lines, while the light green bands represent the previous publications. The edges represent protein-protein interactions. The concepts of associations and binding ought to be specific and meaningful. For instance, proteins collaborate to perform a joint function rather than physically interacting.

4.1.3 In vivo analysis of CAS function in *A. thaliana*

Using the BN-PAGE analysis, it was shown that CAS might be a part of three different supercomplexes composed of at least the complexes PSI, PSII, and CYT*b6/f*. These complexes are known to be essential for photosynthesis and hence for the growth of plants. Consequently, in further investigation, we addressed whether the absence of CAS affects the photosynthetic activity and the growth of the plants. For this purpose, the *casko* mutant line was used in comparison to WT.

Under normal growth conditions, no alterations could be observed in the phenotype of *casko* plants compared to WT plants (**Figure 7A, upper panel**). In addition, the efficiency of photosynthesis (PSII Yield) is not affected (**Figures 7B and C**). These results indicated that the CAS protein is not essential for plant growth and photosynthesis activity under normal growth conditions. However, when the plants were challenged with stress conditions such as salt (NaCl) and oxidative stress (H_2O_2), they showed different photosynthetic activity (**Figures 7B and C**). In the case of salt, both WT and *casko* plants showed a decrease in the activity to nearly the same extent (**Figures 7B and C**). By contrast, in the case of H_2O_2, a decrease in the activity was observed only in the WT (**Figure 7B**), while in the *casko* mutant, it remained unchanged (**Figure 7C**). These results indicated that plants might cope better with the H_2O_2 stress in the absence of CAS and suggested that CAS might be involved in the cellular response process to H_2O_2.

Previous studies have suggested that CAS regulates stomatal physiology and thus water use efficiency (Han, et al., 2003; Nomura, et al., 2008; Weinl, et al., 2008; Vainonen, et al., 2008). This also corresponds to our results, which showed the stomata in the WT leaves have 30% less aperture opening compared to the *casko* leaves (**Figures 7D and E**). However, these differences have no effect on the phenotype of both plant lines even when the plants were grown under drought stress conditions (**Figure 7A**).

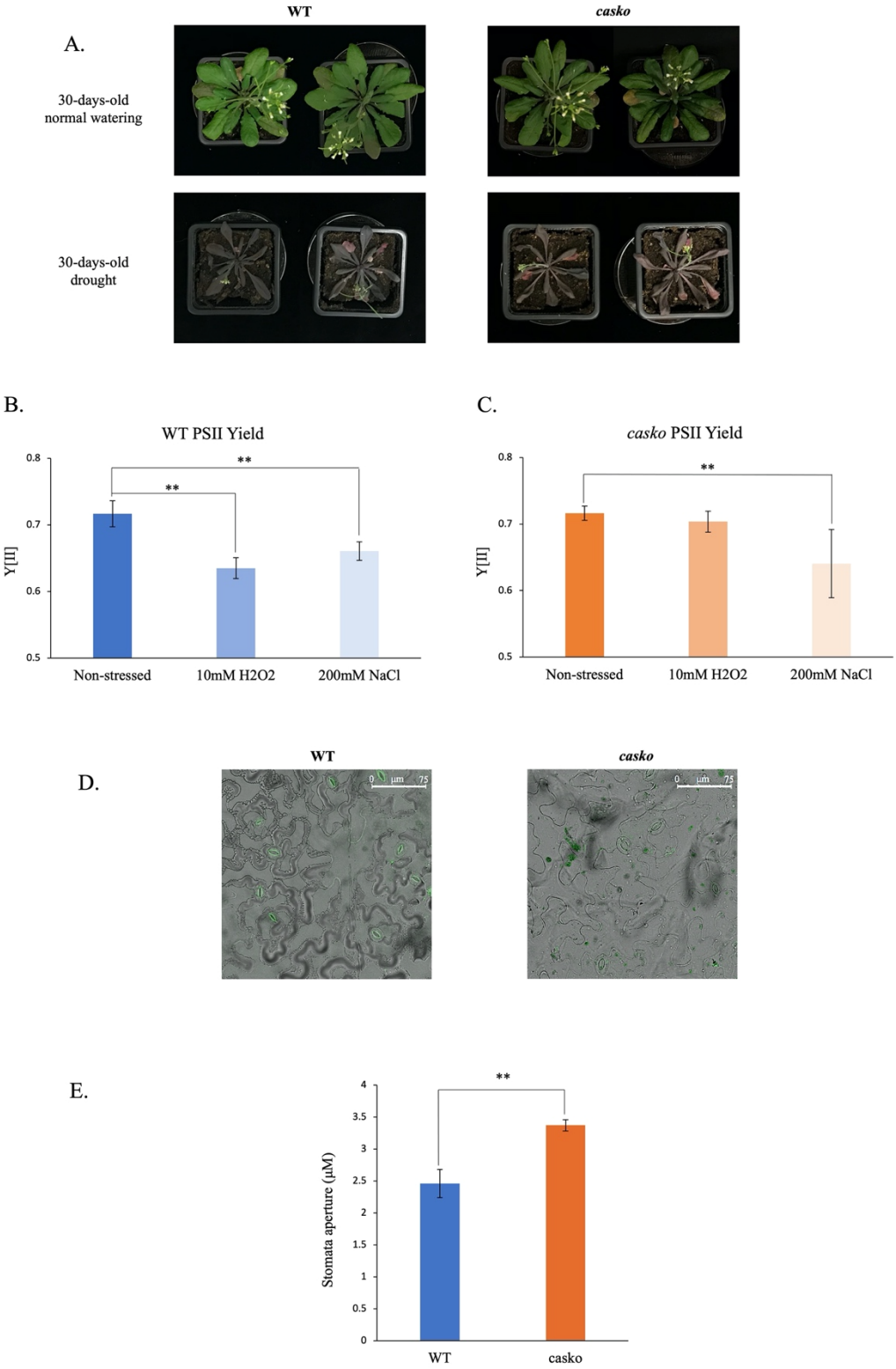

Figure 7. Characterization of *casko* compared to WT plants. (A.) No phenotypical differences were observed between WT and *casko* neither under normal nor under drought stress conditions. (B, C.) photosystem II yield Y[II] analysis of WT and *casko* 15-days-old *A. thaliana* under non-stress conditions *vs* exposed to salt and H_2O_2 stress. (D, E) *casko* lines show a bigger stomata aperture compared to the WT samples under normal conditions. Values represent means ± SE of ten independent replicates (*P< 0.05 **P<0.01).

4.1.4 Comparison of Ca^{2+} signaling between WT and *casko* mutant *A. thaliana* plants

CAS was initially detected to be localized in the plasma membrane and was suggested to have an extracellular Ca^{2+}-sensing characteristic (Han, et al., 2003; Tang, et al., 2007). However, later biochemical and immunodetection studies proved that CAS has a chloroplastic rather than a plasma membrane localization (Vainonen, et al., 2008; Cutolo, et al., 2019). So far, no specific molecular activity has been described for CAS, but in *A. thaliana*, CAS appears to be involved in a wide range of physiological processes, including the regulation of stomatal closure (Nomura, et al., 2008; Weinl, et al., 2008), modulation of immunity-related gene expression (Nomura, et al., 2012) and activation of retrograde signals (Guo, et al., 2016). Moreover, the ability to bind Ca^{2+} in vitro (Han, et al., 2003) and several experimental pieces of evidences for the involvement of CAS in both chloroplastic and cytosolic [Ca^{2+}] transient oscillations in response to external stimuli (Nomura, et al., 2012; Nomura, et al., 2008; Weinl, et al., 2008) suggested a crucial role of CAS in Ca^{2+} signaling in both the chloroplast and the cytosol. In this work, the effect of CAS on the [Ca^{2+}] dynamics in response to H_2O_2, NaCl, and mannitol stress in the cytosol as well as in two sub-compartments of the chloroplast, the stroma, and the thylakoid lumen have been investigated.

4.1.4.1 Characterization of WT and *casko* plants expressing YFP-AEQ

For these experiments, stably transformed *A. thaliana* WT and *casko* (SALK_070416) mutant plants with a 35S::YFP-*APOAEQUORIN* construct (Mehlmer, et al., 2012; Sello, et al., 2018; Cutolo, Ph.D. 2018; Pirayesh, Master thesis 2017) were used. The generated transgenic lines express the apoaequorin, targeted to different cellular compartments: the cytosol (Cyt-AEQ), the stroma (Str-AEQ), and the thylakoid lumen (Thl-AEQ). The successful targeting of AEQ has been confirmed by fluorescence microscopy (**Figure 8**). A clear localization of the YFP signal in the desired (sub)-compartments has been observed for all three lines. Epidermal cells were shown in the case of Cyt-AEQ, and mesophilic cells were shown in the case of the Str-AEQ and the Thl-AEQ (**Figure 8**). Nevertheless, the correctness of the localizations of the lines by a more thorough fluorescence microscopy analysis was also verified previously (Mehlmer, et al., 2012).

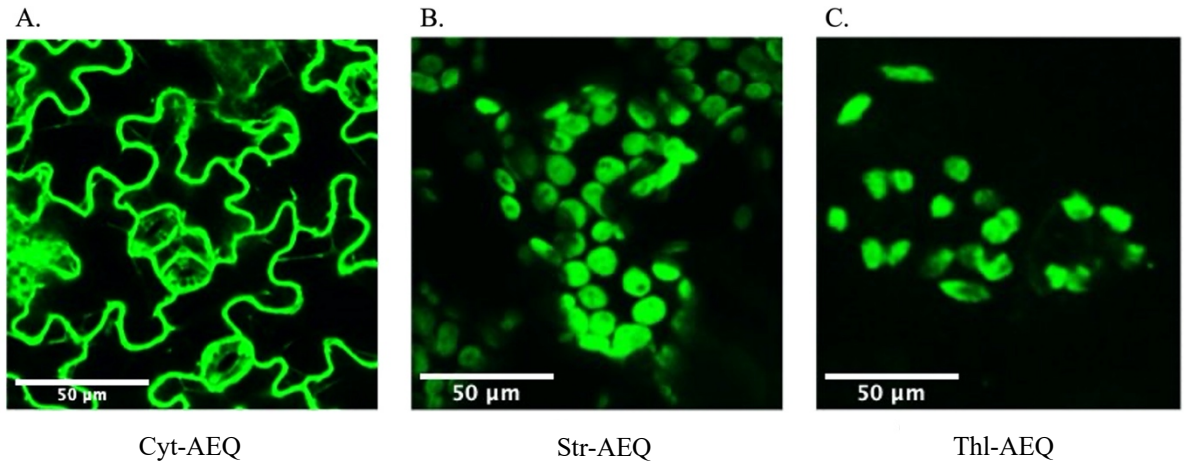

Figure 8. In vivo localization of YFP-aequorin targeted to different cellular sub-compartments in *A. thaliana* leaves. *A. thaliana* lines stably transformed by YFP fused AEQ targeted to (A) the cytosol (Cyt-AEQ), (B) the stroma (Str-AEQ), or the (C) thylakoid lumen (Thl-AEQ). The correct localization was confirmed by YFP fluorescence (green) using fluorescence microscopy. The figure presents the results from the WT samples, and similar results were also obtained for the *casko* lines.

In order to exclude that the inserted *APOAEQUORIN* affects the growth of the plants, WT and *casko A. thaliana* seedlings were compared phenotypically with the transgenic plants expressing *APOAEQUORIN* under normal growth conditions. No differences in the apparent phenotype of the plants could be detected, demonstrating that the inserted AEQ does not affect the growth of the transgenic plants (**Figure 9**).

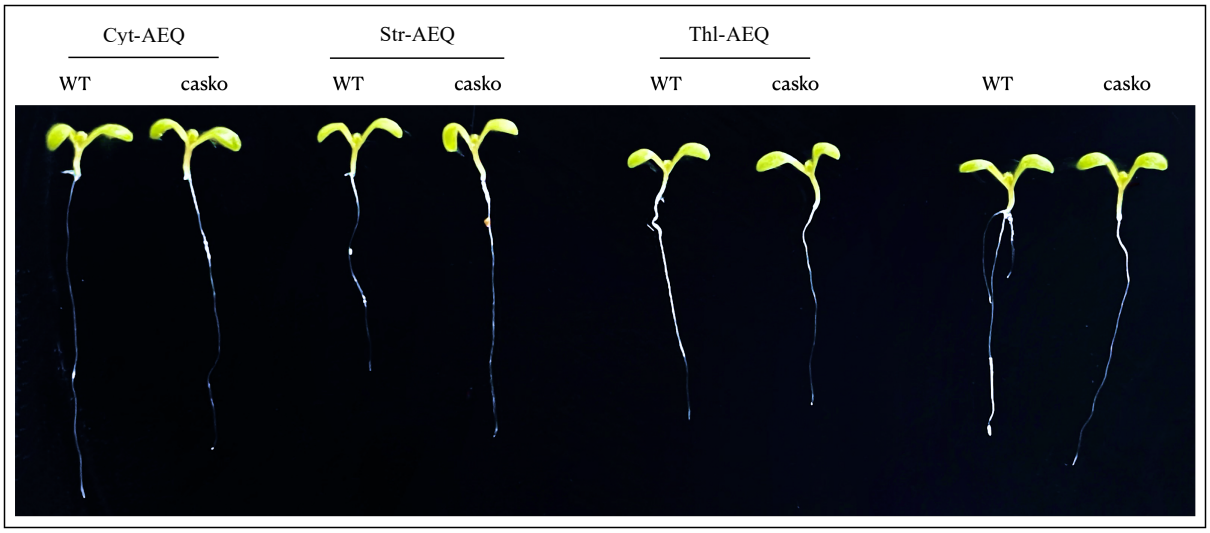

Figure 9. Phenotypic analysis of *A. thaliana* wild type (WT) and *casko* compared to transgenic WT and *casko* plants expressing AEQ. Nine-day-old *A. thaliana* WT and *casko* seedlings grown under normal conditions on ½ MS-media were compared to transgenic plants stably transformed by YFP-*APOAEQUORIN* targeted to the cytosol (Cyt-AEQ), stroma (Str-AEQ), or thylakoid lumen (Thl-AEQ). No visible differences in the phenotypes were observed, indicating that the inserted aequorin has no effect on the growth of transgenic plants.

4.1.4.2 Ca^{2+} responses induced by exogenous Ca^{2+}

In order to check the efficiency of the expressed apoaequorin in reporting changes in the [Ca^{2+}], the different transgenic WT and *casko* plants (Cyt-AEQ, Str-AEQ, and Thl-AEQ) were treated with exogenous Ca^{2+} (10 mM $CaCl_2$) after the reconstitution of AEQ with coelenterazine. The AEQ luminescence was recorded using a plate luminometer. Ca^{2+}-treated seedlings showed a response in the form of an increase in [Ca^{2+}] with the strongest response in the cytosol (Cyt-AEQ) for both lines WT and *casko* (**Figure 10**).

Previous studies have shown that in *A. thaliana*, the free Ca^{2+} resting level is higher in the stroma and thylakoid lumen with ~0.5 and 0.6 µM, respectively, compared to cytosol with ~0.2 µM (Sai & Hirschie Johnson, 2002; Sello, et al., 2018). Comparable values for the Ca^{2+} resting levels (between 0-120 s before injection of the treatment) were obtained in this study in the WT and the *casko* mutant (**Figure 10**). Upon injection of external Ca^{2+}, the [Ca^{2+}] in all tested compartments increased immediately and reached a maximum within 5-7 seconds before declining to basal levels (**Figures 10A, C, and E**). Comparing the amplitude of the peaks (Δ[Ca^{2+}]) (**as explained in 3.2.5**), the cytosol showed a higher increase in WT as well as in *casko* plants with approximately 0.8 and 0.4 µM, respectively (**Figure 10A**). By contrast, the stroma and thylakoid lumen showed a lower increase than in the cytosol, and no significant differences between the WT and *casko* lines could be observed (**Figures 10C and E**).

Taken together, these results demonstrated the functionality of the transgenic lines expressing AEQ in different cellular compartments in reflecting changes in [Ca^{2+}] upon application of a stimulus. The data also showed that the absence of CAS does not affect the basal levels of Ca^{2+} in the cytosol nor the stroma and thylakoids lumen.

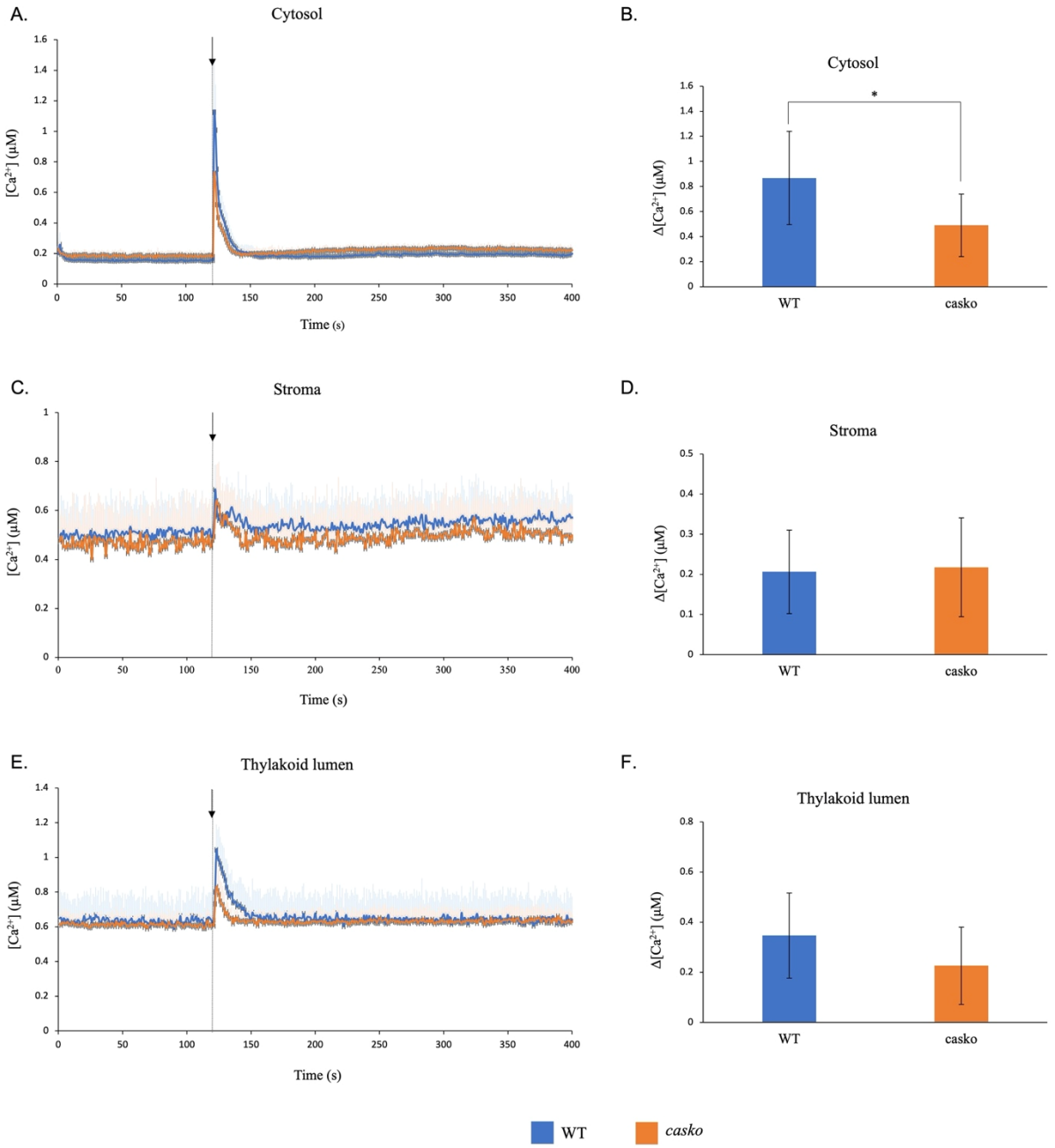

Figure 10. Induction of Ca^{2+} signals in response to application of exogenous Ca^{2+}. [Ca^{2+}] changes in nine-days-old *A. thaliana* WT and *casko* whole seedlings in response to exogenous application of Ca^{2+} (10 mM $CaCl_2$). The [Ca^{2+}] was measured using a luminometer in (A, B) cytosol, (C, D) stroma, and (E, F) thylakoid lumen. WT is presented with blue lines and bars, and the *casko* is shown in orange lines and bars. The time point at which the stimulus was injected is marked with a black arrow (at 120 seconds). Values represent means ± SE of seven independent replicates (*P< 0.05).

4.1.4.3 Ca^{2+} response induced by H_2O_2

In several studies, exogenous H_2O_2 was used as a stimulus to investigate the Ca^{2+}-response to oxidative stress in plants. This study examined the effect of CAS on the Ca^{2+} response induced by H_2O_2 in the cytosol, stroma, and thylakoid lumen. Nine-days-old *A. thaliana* WT and *casko* seedlings expressing AEQ were exposed to 10 mM H_2O_2, and the Ca^{2+} response was recorded using a luminometer. In all three compartments, different responses to H_2O_2 were observed. Both WT and *casko* seedlings showed two [Ca^{2+}] peaks in the cytosol. The first peak appeared immediately upon injection of H_2O_2, followed by a second and much higher peak after 30 seconds of the injection (**Figure 11A**). The same two peaks could be observed in the stroma WT, albeit with much reduced amplitudes (**Figure 11C**). Intriguingly, the stroma of the *casko* seedlings showed only the first peak (**Figure 11C**). By contrast, in the thylakoid lumen, only the first peak could be observed in both the WT and the *casko* plants (**Figure 11E**).

In the cytosol, the Ca^{2+} response dynamics showed a similar pattern in WT and *casko* seedlings, which lasted for about 50 seconds before declining to a new elevated basal level, although differing in the amplitude of the peaks (**Figure 11B**). The first peak had reached a maximum of 0.6 µM and 0.45 µM, and the second peak reached a plateau of 1.3 µM and 1.0 µM in WT and *casko* plants, respectively.

In the case of the thylakoid lumen, both WT and *casko* plants showed quite similar Ca^{2+} dynamics, but the peak was much higher in WT, reaching a plateau of 0.9 µM as *casko* with a peak of 0.4 µM (**Figure 11F**). By contrast, the Ca^{2+} response to H_2O_2 in the stroma showed notably different dynamics between the two plant lines (**Figure 11C**). While in the WT, two peaks could be observed, the *casko* showed only the first peak, and the second peak was utterly absent. For the first peak, both lines showed a comparable $[Ca^{2+}]_{str}$ increase of 0.2 µM (**Figure 11D**). Taken together, the results indicated differences in the H_2O_2 triggered Ca^{2+} signaling between the WT and the *casko* lines, especially at the stroma level.

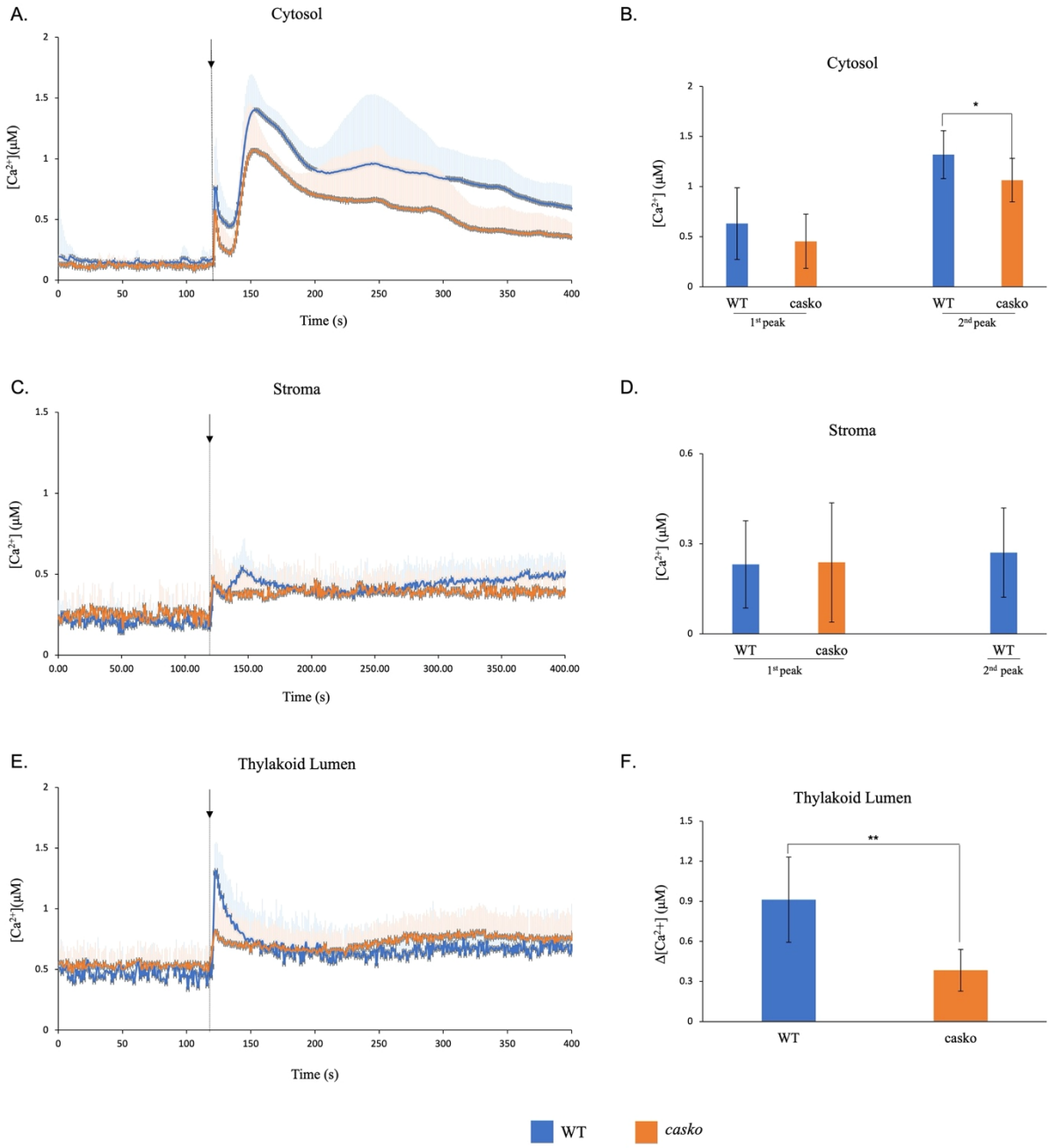

Figure 11. H_2O_2 induced Ca^{2+} response in WT and *casko* plants. [Ca^{2+}] changes in nine-days-old *A. thaliana* WT and *casko* whole seedlings in response to H_2O_2 stress (10 mM H_2O_2). The [Ca^{2+}] was measured using a luminometer in the cytosol (A, B), stroma (C, D), and thylakoid lumen (E, F). WT is presented with blue lines and bars, and the *casko* is shown in orange lines and bars. The time point at which the stimulus was injected is marked with a black arrow (at 120 seconds). Values represent means ± SE of seven independent replicates (*P< 0.05 **P<0.01).

4.1.4.4 Source of Ca^{2+} fluxes in response to H_2O_2 stress

To investigate the potential sources of [Ca^{2+}] elevations in response to H_2O_2, the effect of the lanthanum chloride ($LaCl_3$) and EGTA (β-aminoethyl ether)-*N*,*N*,*N*′,*N*′-tetraacetic acid) on the [Ca^{2+}] transients was tested. A common application of La^{3+} is to inhibit the influx of Ca^{2+} from the apoplast into the cytosol by blocking plasma membrane Ca^{2+} channels (Tracy, et al., 2008). On the other hand, EGTA is a well-known Ca^{2+} chelator (Barr, et al., 1980). The *A. thaliana* WT and *casko* seedlings were incubated for 1 hour with 1 mM $LaCl_3$ or 1 mM EGTA prior to exposure to H_2O_2.

In both the WT and *casko* lines, the two inhibitors lead to a reduction in the Ca^{2+} response in the cytosol to H_2O_2 stress in the cytosol (**Figure 12**). In WT, EGTA and La^{3+} reduced the first Ca^{2+} peak to ∼15% and ∼60% and the second peak to ∼30% and ∼70%, respectively (**Figure 12B**). In *casko*, EGTA and La^{3+} lead to a reduction in the first Ca^{2+} peak in the cytosol to ∼35% and ∼50% and the second Ca^{2+} peak to ∼40% and ∼70%, respectively (**Figure 12D**). In both plant lines, the effect of La^{3+} was stronger than EGTA.

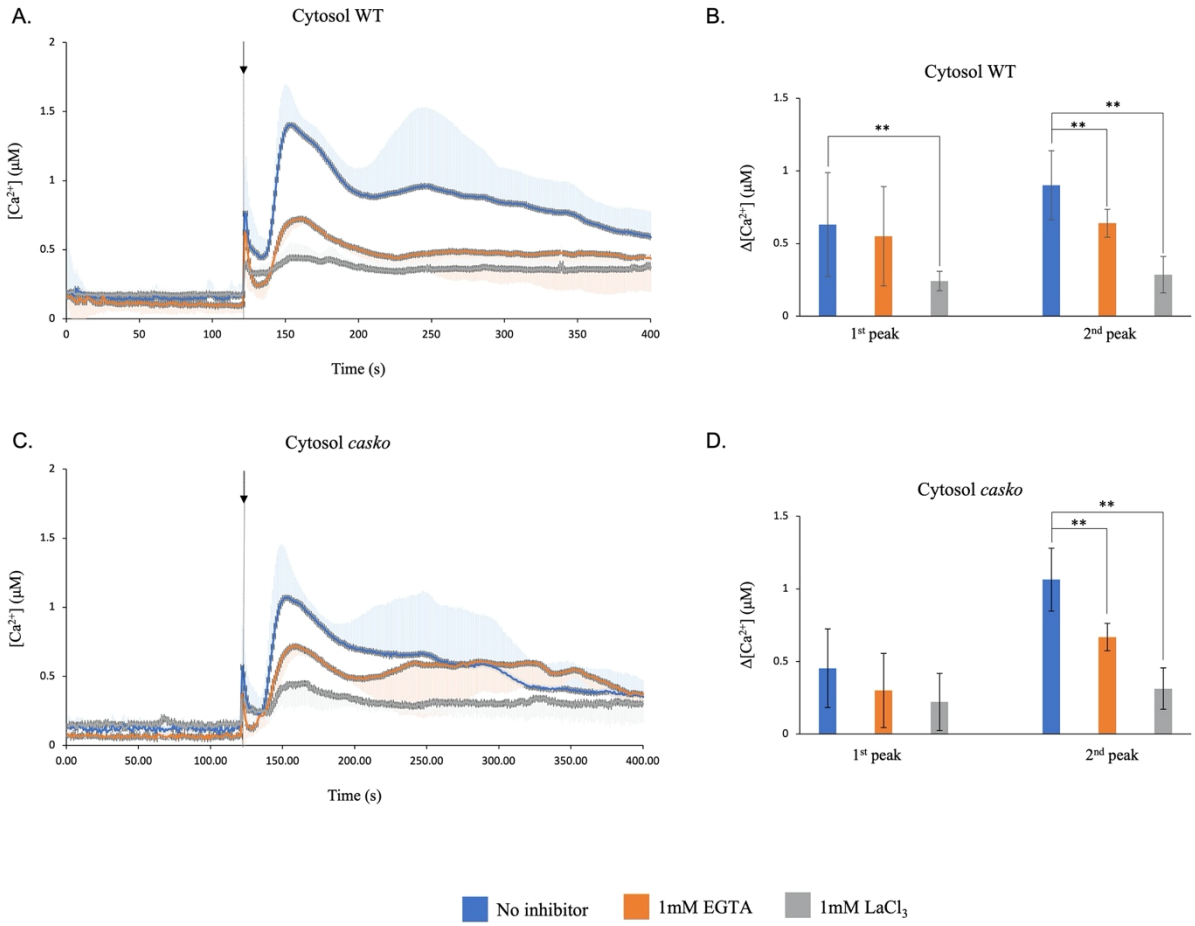

Figure 12. Inhibitory effect of pre-treatment with $LaCl_3$ and EGTA on Ca^{2+} response to H_2O_2 in cytosol of WT and *casko* plants. $[Ca^{2+}]_{cyt}$ changes in nine-days-old *A. thaliana* WT and *casko* seedlings in response to 10 mM H_2O_2 after pre-treatment with 1 mM $LaCl_3$ or 1 mM EGTA. The $[Ca^{2+}]_{Cyt}$ was measured using a luminometer in the WT (A and B) and *casko* (C and D). Non treated samples of both are presented with blue line and bar, samples pre-treated with 1 mM EGTA are presented in orange, and with 1 mM $LaCl_3$ are presented in gray. The time point at which the stimuli was injected is marked with a black arrow (at 120 seconds). Values represent means ± SE of seven independent replicates (*P< 0.05 **P<0.01).

The same experiments were performed in WT and *casko* plants expressing Str-AEQ and Thyl-AEQs. EGTA and La^{3+} effected only the second peak in the WT stroma, while the first peak was unaffected (**Figure 13A**). On the other hand, no significant reduction was observed with either the La^{3+} or the EGTA for the *casko* samples (**Figure 13B**). It appears that the first Ca^{2+} peak in the stroma of both WT and *casko* is not generated by Ca^{2+} influxes from the apoplast, whereas in the case of WT samples, the second peak appears to be generated by the apoplast. In the thylakoid lumen, pre-incubation of samples in EGTA and $LaCl_3$ lead to a significant reduction for $[Ca^{2+}]_{thyl}$ with ~70% in WT (**Figure 14B**) and ~30% and ~65% in *casko* samples, respectively (**Figure 14D**).

Taken together, the results showed the requirement of Ca^{2+} influxes from the extracellular compartment for generating the response to the H_2O_2 in the cytosol and thylakoid lumen in both WT and *casko* mutant plants. The fact that the inhibitors could not completely abolish the Ca^{2+} response to H_2O_2 in either of the samples suggests that internal Ca^{2+} stores may generate the Ca^{2+} response to H_2O_2.

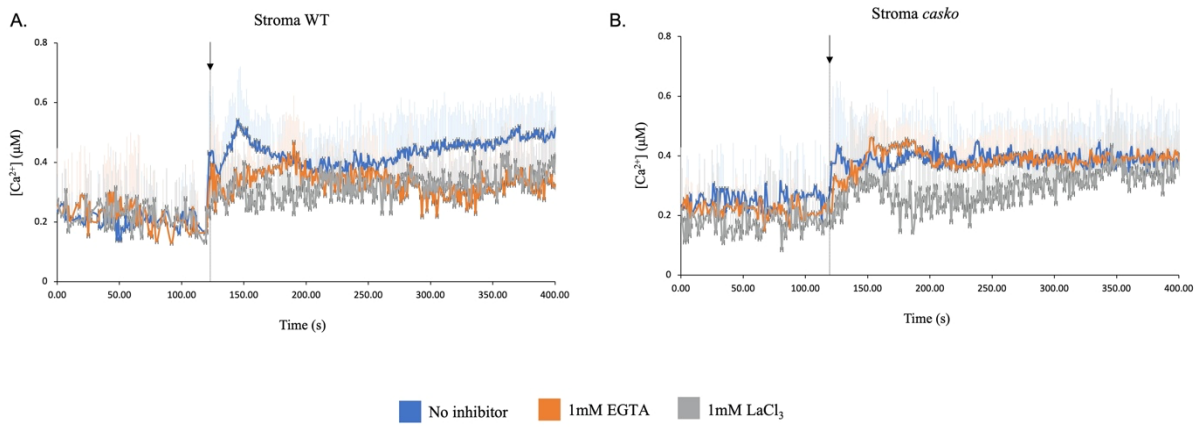

Figure 13. Inhibitory effect of pre-treatment with $LaCl_3$ and EGTA on Ca^{2+} response to H_2O_2 in stroma of WT and *casko* plants. $[Ca^{2+}]_{str}$ changes in nine-days-old *A. thaliana* WT and *casko* seedlings in response to oxidative stress (10 mM H_2O_2) under 1 mM $LaCl_3$ or 1 mM EGTA. The $[Ca^{2+}]_{str}$ was measured using a luminometer in the stroma WT (A) and *casko* (B). Non treated samples of both WT and *casko* are presented with blue line, samples pre-incubated in 1 mM EGTA are presented in orange, and samples pre-incubated in 1 mM $LaCl_3$ are presented in gray. The time point at which the stimuli was injected is marked with a black arrow (at 120 seconds). Values represent means ± SE of seven independent replicates (*P< 0.05 **P<0.01).

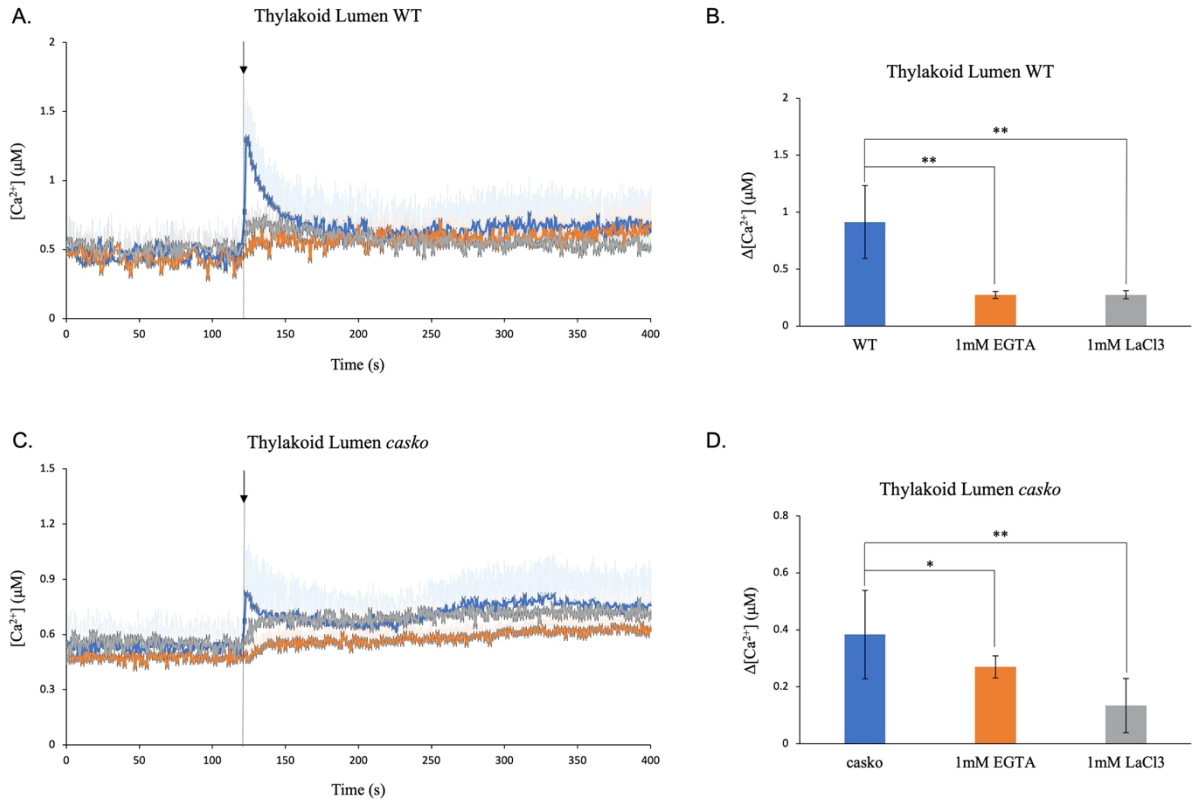

Figure 14. Inhibitory effect of pre-treatment with $LaCl_3$ and EGTA on Ca^{2+} response to H_2O_2 in thylakoid lumen of WT and *casko* plants. $[Ca^{2+}]_{thyl}$ changes in nine-days-old *A. thaliana* WT and *casko* seedlings in response to oxidative stress (10 mM H_2O_2) under 1 mM $LaCl_3$ or 1 mM EGTA. The $[Ca^{2+}]_{thyl}$ was measured using a luminometer in the thylakoid lumen WT (A and B) and *casko* (C and D). Non treated samples of both WT and *casko* are presented with blue line and bar, samples pre-incubated in 1 mM EGTA are presented in orange, and samples pre-incubated in 1 mM $LaCl_3$ are presented in gray. The time point at which the stimuli was injected is marked with a black arrow (at 120 seconds). Values represent means ± SE of seven independent replicates (*P< 0.05 **P<0.01).

4.1.4.5 Ca^{2+} responses induced by NaCl

In order to examine the Ca^{2+} response to salt in *A. thaliana* WT and *casko* mutant, 200 mM NaCl was used since it has previously been established as the optimal concentration to induce Ca^{2+} response in *A. thaliana* (Sello, et al., 2018). In both lines, upon injection of NaCl, a rapid increase in [Ca^{2+}] was observed in the cytosol, the stroma as well as the thylakoid lumen (**Figure 15**). In all the three compartments, a maximum was reached within 5-7 seconds before declining to basal levels. The cytosolic response was the highest in both WT and *casko* mutant, with a peak at 6.1 µM and 3.8 µM, respectively (**Figures 15A and B**). Also, the dynamics of the Ca^{2+} transient showed notable differences in the shape between WT and *casko* mutant (**Figure 15A**). Additionally, several secondary small peaks could be observed in the cytosol of the *casko*, which were absent in the WT.

In the stroma, the differences could be observed only in the shape of the curves but not in the amplitude of the peak between WT and *casko* (**Figures 15C and D**). The amplitude of the peaks was at 1.8 µM and 2.4 µM in WT and *casko*, respectively. By contrast, for the thylakoid lumen, the differences could be observed only in the amplitude of the peaks, while the shape of the curves is quite similar between the WT and *casko* (**Figures 15E and F**). Here, the amplitude of the peaks was at 3.08 µM and 1.8 µM in WT and *casko*, respectively.

The differences in Ca^{2+} response dynamics indicated differences in the Ca^{2+} signaling components involved in response to NaCl between the two plant lines WT and *casko*.

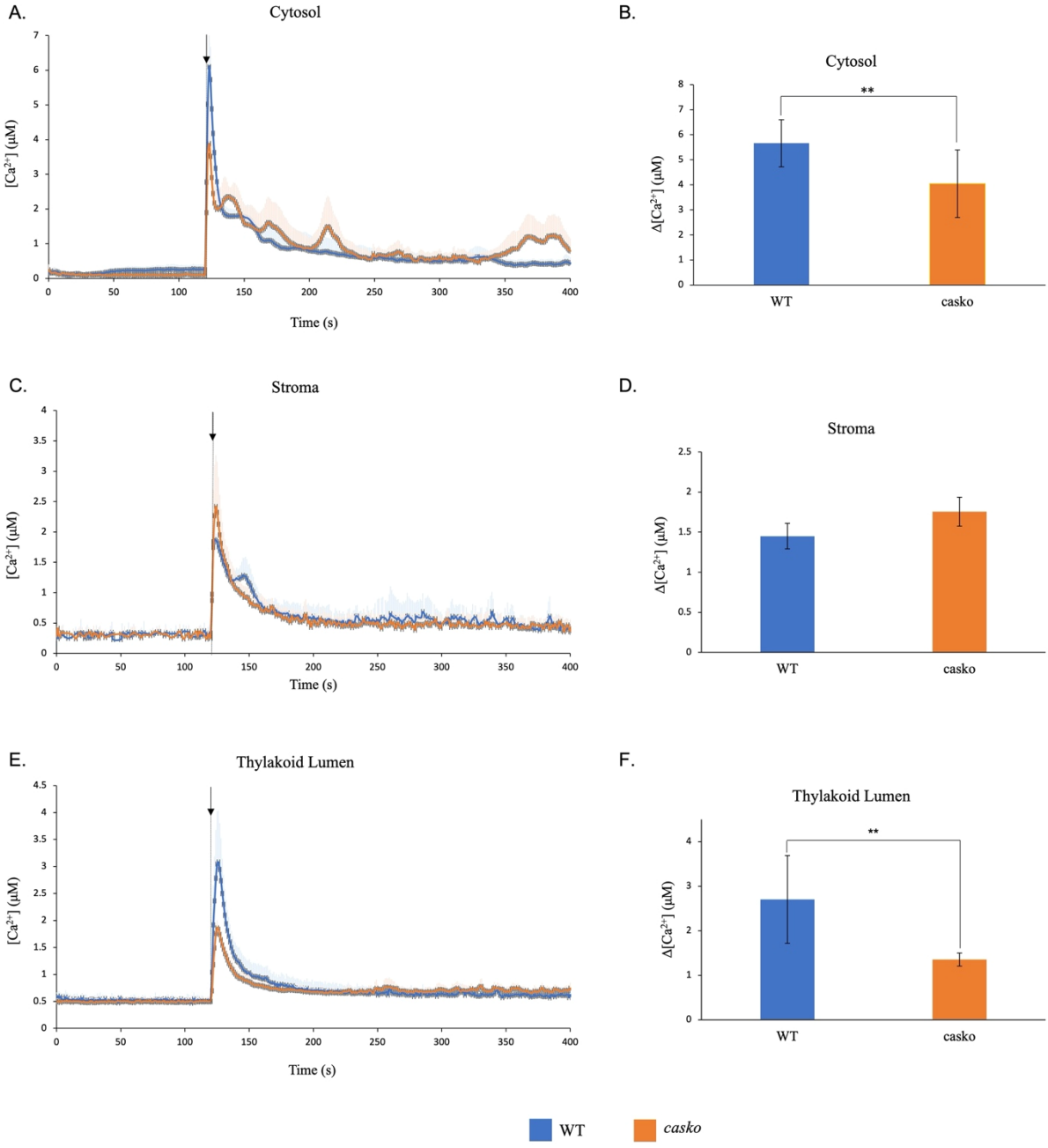

Figure 15. Induction of Ca^{2+} response to NaCl in WT and *casko* plants. [Ca^{2+}] changes in nine-days-old *A. thaliana* WT and *casko* whole seedlings in response to salt stress (200 mM NaCl). The [Ca^{2+}] was measured using a luminometer in the cytosol (A, B), stroma (C, D), and thylakoid lumen (E, F). WT is presented with blue lines and bars, and the *casko* is shown in orange lines and bars. The time point at which the stimulus was injected is marked with a black arrow (at 120 seconds). Values represent means ± SE of seven independent replicates (*P< 0.05, **P<0.01).

4.1.4.6 Source of Ca^{2+} transients in response to salt stress

In order to identify the Ca^{2+} sources involved in the $[Ca^{2+}]$ elevations in response to NaCl, 1 mM $LaCl_3$ and 1 mM EGTA were utilized. WT and *casko* plants expressing Cyt-AEQ, Str-AEQ, and Thyl-AEQs were pre-incubation for 1 hour in 1 mM EGTA and 1 mM $LaCl_3$. Measurements showed that both compounds lead to a reduction of the cytosolic $[Ca^{2+}]$ of WT and *casko* lines (**Figure 16**). In the WT line, EGTA showed less effect than La^{3+}, while in *casko*, both inhibitors showed a similar effect. In WT, EGTA and La^{3+} implied a decrease in the Ca^{2+} signal in the cytosol to ~25% and ~60%, respectively (**Figures 16A and B**). In the *casko* mutant, both EGTA and La^{3+} lead to a ~50% decrease in the $[Ca^{2+}]_{cyt}$ (**Figures 16C and D**).

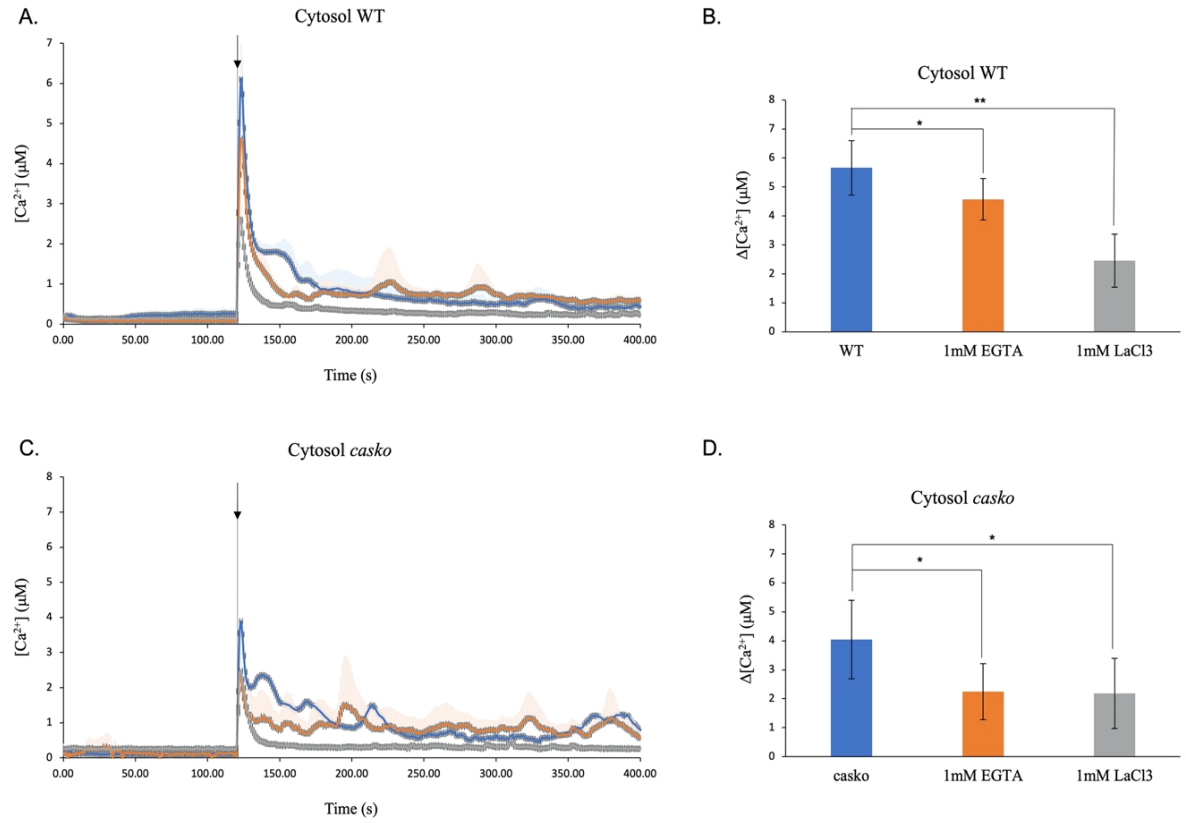

Figure 16. Inhibitory effect of pre-treatment with $LaCl_3$ and EGTA on Ca^{2+} response to NaCl in cytosol of WT and *casko* plants. $[Ca^{2+}]_{cyt}$ changes in nine-days-old *A. thaliana* WT and *casko* seedlings in response to salt stress (200 mM NaCl) under 1 mM $LaCl_3$ or 1 mM EGTA. The $[Ca^{2+}]_{Cyt}$ was measured using a luminometer in the cytosol WT (A and B) and *casko* (C and D). Non treated samples of both WT and *casko* are presented with blue line and bar, samples pre-incubated in 1 mM EGTA are presented in orange, and samples pre-incubated in 1 mM $LaCl_3$ are presented in gray. The time point at which the stimuli was injected is marked with a black arrow (at 120 seconds). Values represent means ± SE of seven independent replicates (*P< 0.05 **P<0.01).

Similar to the cytosolic lines, by pre-incubation of samples for 1 hour in 1 mM EGTA or 1 mM $LaCl_3$, the NaCl-induced $[Ca^{2+}]_{str}$ and $[Ca^{2+}]_{thyl}$ transients implied a significant reduction (**Figures 17 and 18**). In the WT, pre-incubation in EGTA and La^{3+} leads to a ~70% decrease of the $[Ca^{2+}]_{str}$ (**Figure 17B**), while in *casko*, EGTA and La^{3+} lead to a reduction of the increase in $[Ca^{2+}]_{str}$ to ~30% and ~55%, respectively (**Figure 17D**). In the thylakoids, EGTA and La^{3+} inhibit the response to ~50% in WT (**Figure 18B**), whereas the effect is more substantial in *casko* with an implied inhibition of ~80% and ~65% with EGTA and La^{3+}, respectively (**Figure 18D**).

Taken together, the results showed the requirement of Ca^{2+} influxes from the extracellular compartment for generating the response to the NaCl in the cytosol, stroma, and thylakoid

lumen in both WT and *casko* mutant plants. Furthermore, since the inhibitors were unable to abolish the Ca^{2+} response completely, internal Ca^{2+} stores may be involved in the generation of the Ca^{2+} response to NaCl.

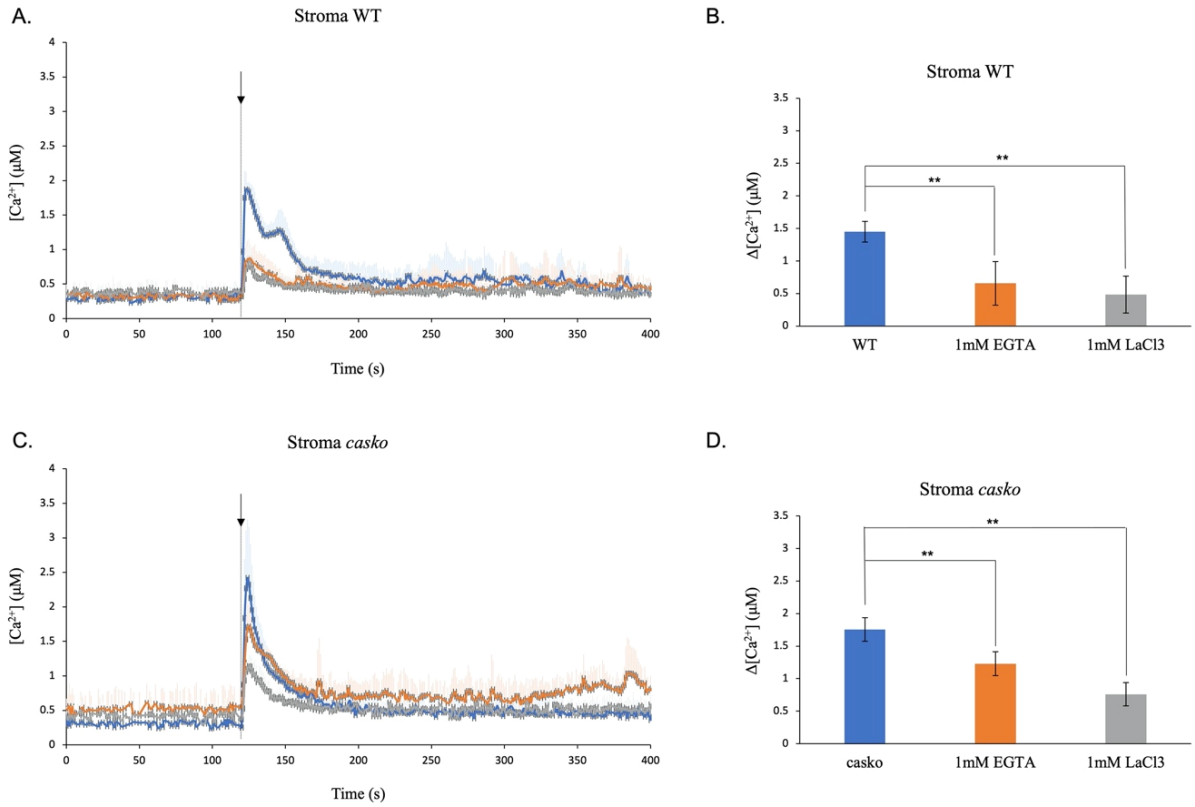

Figure 17. Inhibitory effect of pre-treatment with $LaCl_3$ and EGTA on Ca^{2+} response to NaCl in stroma of WT and *casko* plants. $[Ca^{2+}]_{str}$ changes in nine-days-old *A. thaliana* WT and *casko* seedlings in response to salt stress (200 mM NaCl) under 1 mM $LaCl_3$ or 1 mM EGTA. The $[Ca^{2+}]_{str}$ was measured using a luminometer in the stroma WT (A and B) and *casko* (C and D). Non treated samples of both WT and *casko* are presented with blue line and bar, samples pre-incubated in 1 mM EGTA are presented in orange, and samples pre-incubated in 1 mM $LaCl_3$ are presented in gray. The time point at which the stimuli was injected is marked with a black arrow (at 120 seconds). Values represent means ± SE of seven independent replicates (*P< 0.05 **P<0.01).

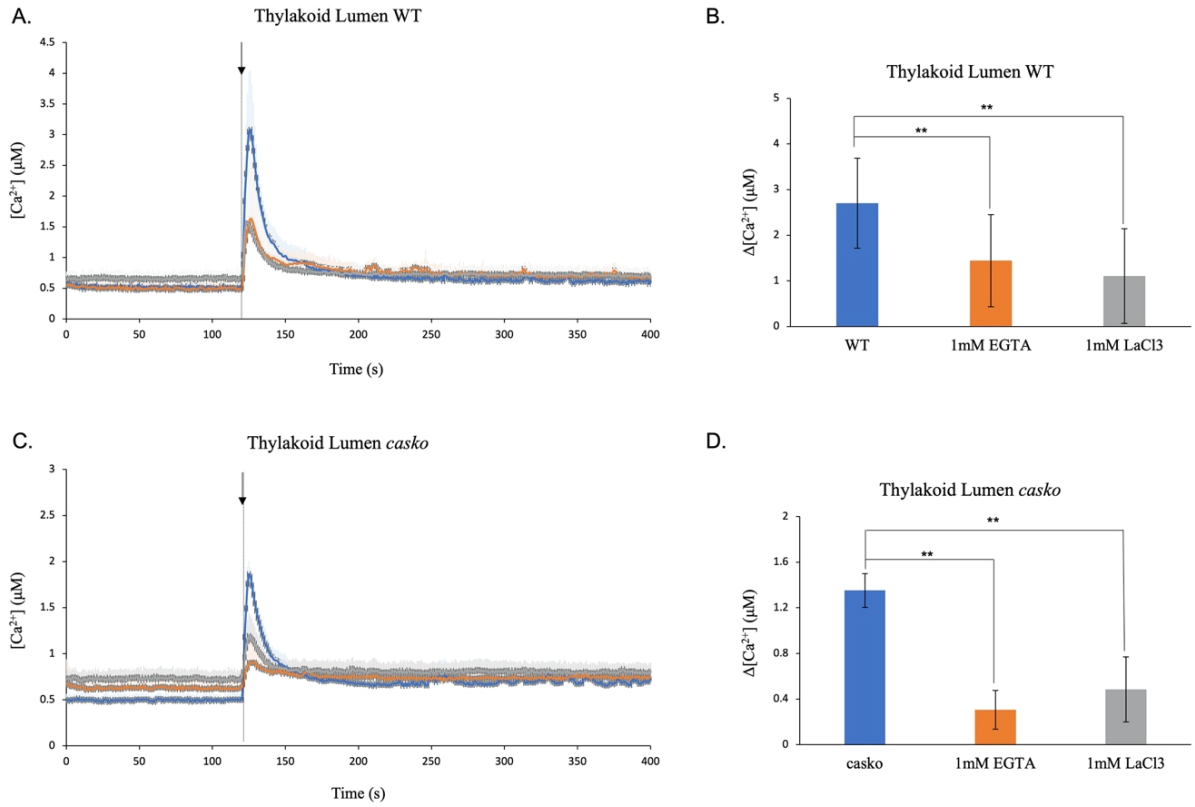

Figure 18. Inhibitory effect of pre-treatment with $LaCl_3$ and EGTA on Ca^{2+} response to NaCl in thylakoid lumen of WT and *casko* plants. $[Ca^{2+}]_{thyl}$ changes in nine-days-old *A. thaliana* WT and *casko* seedlings in response to salt stress (200 mM NaCl) under 1 mM $LaCl_3$ or 1 mM EGTA. The $[Ca^{2+}]_{thyl}$ was measured using a luminometer in the thylakoid lumen WT (A and B) and *casko* (C and D). Non treated samples of both WT and *casko* are presented with blue line and bar, samples pre-incubated in 1 mM EGTA are presented in orange, and samples pre-incubated in 1 mM $LaCl_3$ are presented in gray. The time point at which the stimuli was injected is marked with a black arrow (at 120 seconds). Values represent means ± SE of seven independent replicates (*P< 0.05 **P<0.01).

4.1.4.7 Ca^{2+} responses induced by mannitol

Mannitol is often used to mimic drought stress in Ca^{2+} signaling studies since it is a non-ionic osmotically active substance (Knight, et al., 1997). In this work, *A. thaliana* WT and *casko* mutant seedlings were injected with 300 mM mannitol. Upon injection, an immediate increase in [Ca^{2+}] was observed in all samples and reached a maximum within 5-7 seconds (**Figure 19**). The cytosol showed the strongest signal in both WT and *casko* lines compared to the stroma and the thylakoid lumen. Similar to the salt stress, WT and *casko* mutant plants displayed significant differences in the shape and amplitude of the Ca^{2+} response in the cytosol (**Figure 19A**). The WT sample showed a more extended and strong response compared to the *casko* sample. The response peak reached a maximum of 5.36 µM and 3.58 µM in WT and *casko*, respectively (**Figures 19A and B**). In the stroma lines, the differences between WT and *casko* were only evident in the shape of the curves and not significant in the peak amplitude (**Figure 19C**). Compared to the WT sample, the *casko* sample had a mildly longer response time. The amplitude of the peaks was at 1.7 µM and 1.8 µM in WT and *casko*, respectively (**Figure 19D**). The differences observed for the thylakoid lumen are detected not only in the pattern of the curves but also in the amplitude of the peak (**Figure 19E**). The peaks reached a maximum of 4.35 µM and 2.48 µM in WT and *casko*, respectively (**Figure 19F**).

The difference in Ca^{2+} dynamics indicated differences between the two plant lines WT and *casko* regarding the Ca^{2+} signaling components involved in response to mannitol/drought. In all cases, similar to the salt stress, the Ca^{2+} levels returned to near-resting levels after 50-60 seconds, indicating no prolonged organellar Ca^{2+} response to mannitol stress.

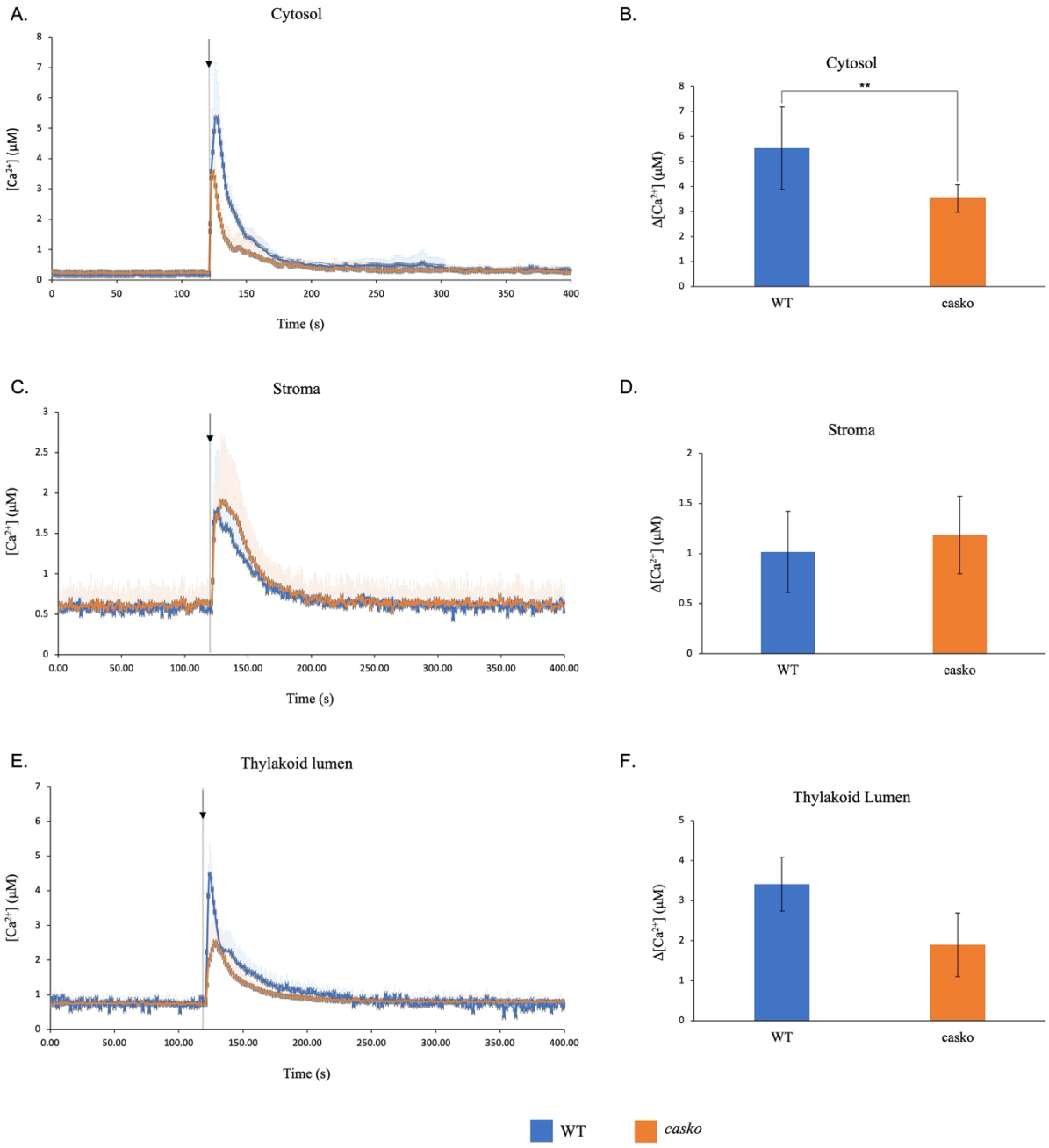

Figure 19. Induction of Ca^{2+} response to Mannitol in WT and *casko* plants. [Ca^{2+}] changes in nine-days-old *A. thaliana* WT and *casko* whole seedlings in response to mannitol stress (300 mM Mannitol). The [Ca^{2+}] was measured using a luminometer in the cytosol (A, B), stroma (C, D), and thylakoid lumen (E, F). WT is presented with blue lines and bars, and the *casko* is shown in orange lines and bars. The time point at which the stimulus was injected is marked with a black arrow (at 120 seconds). Values represent means ± SE of seven independent replicates (**P<0.01).

4.2 Analysis of CML36 sub-cellular localization

Calcium sensors such as calmodulin (CaM) and calmodulin-like proteins (CMLs) play an essential role in plant development and stress physiology through sensing and generating Ca^{2+} signals. *A. thaliana* genome encodes 7 CaMs and at least 50 CMLs. However, the function and the cellular localization of most of them are still unknown (Bussemer, et al., 2009; McCormack & Braam , 2003). Herein, this study has focused on identifying the subcellular localization of CML36.

Homology analysis of the amino acid sequence of CML36 with canonical CaM (CaM2) from *A. thaliana* showed that CML36 contains the CaM-typical four EF-hand motifs but differs from CaM2 by an extension in the N-terminus (**Figure 20.**) Based on bioinformatic analysis obtained from (http://aramemnon.uni-koeln.de) it appears that this extension could serve as a mitochondrial targeting signal through its Arginine (R), Alanine (A), and Serine-rich (S) sequence (von Heijne, et al., 1989).

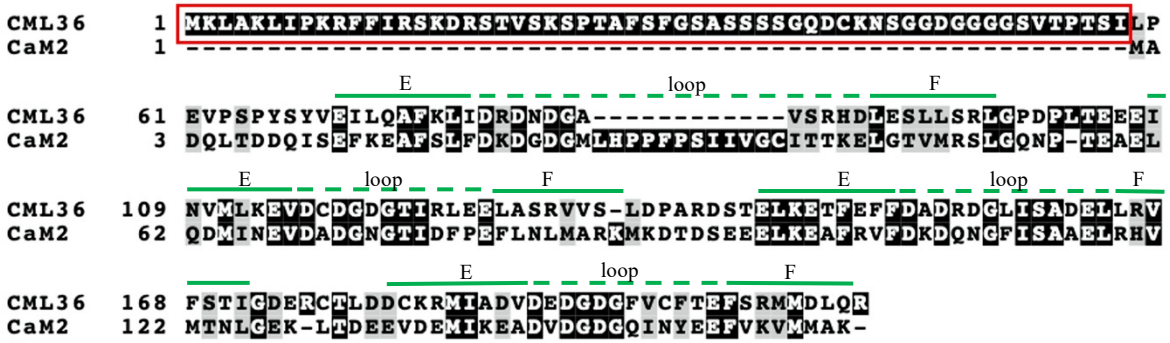

Figure 20. Alignment of CML36 with the canonical CaM2 from *A. thaliana*. The amino acid sequence alignment showed that the CML36 protein has an N-terminal extension which is lacking in CaM2. The black boxes present identical amino acid residues, and the gray boxes indicate a conserved amino acid substitution. The N-terminus extension is marked with a red box. The green bars above the sequence represent the four EF-hands, with the loops shown in dashed green lines.

As in-silico analysis can only make predictions based on comparisons with other known proteins, an in vivo analysis employing YFP tagged CML36 was employed to determine its intracellular localization.

4.2.1 Analysis of CML36 subcellular localization using YFP

CML36 fused to a full-length YFP-tag in a pBIN19 vector was transiently expressed in the tobacco leaves by infiltration with *A. tumefaciens* LBA1334 as described (**3.2.2.4 in material and methods**). The infiltrated leaves were then analyzed for YFP fluorescence using confocal laser scanning microscopy. The fluorescence patterns suggest an overall cytosolic localization of the YFP signal (**Figure 21, upper panel**). However, an overlay between YFP signals and the chlorophyll autofluorescence could be observed in some areas of the cells, indicating that CLM36 might also be located in the chloroplast. Agrobacterium-mediated plant transformation is a widely acknowledged approach, however, whole-leaf analysis has several limitations (Grønlund, et al., 2012). Therefore, isolation of protoplasts from tobacco leaves showing YFP signals was performed. The same results for the whole leaf tissue were obtained, showing an overall cytosolic localization in the protoplast and a partial overlay with chloroplasts (**Figure 21, lower panel**). However, whether the signal comes from the chloroplast surface remains unclear. Taken together, these results suggest that dual targeting of CML36 to the cytosol and chloroplasts might be possible, but further studies are required to confirm that.

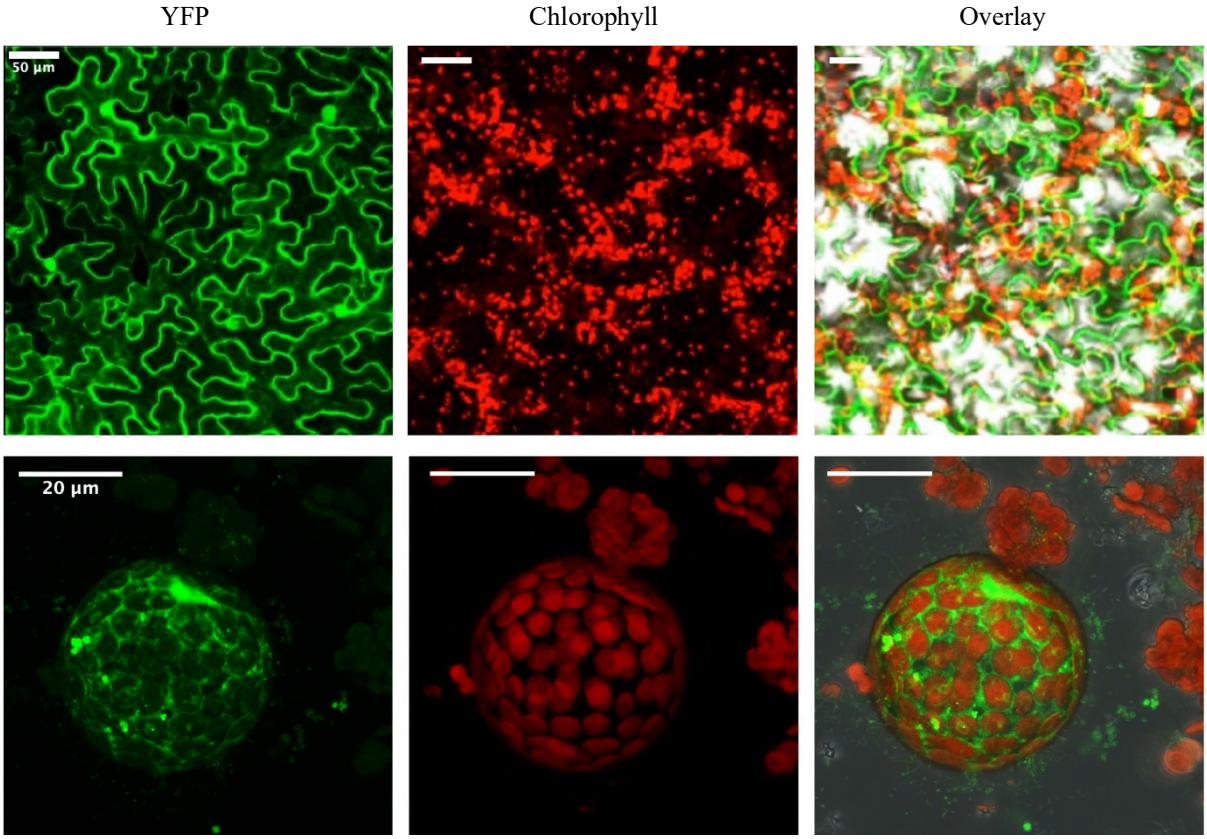

Figure 21. CML36 localization analysis using full-length YFP. Transient expression of the pBIN19 construct encoding for CML36 fused to YFP in tobacco leaves as visualized by confocal laser scanning microscopy in whole tissue (upper panel) and isolated protoplast (lower panel). Chloroplasts were detected by chlorophyll autofluorescence. Overlay: the overlay of YFP, chlorophyll as well as transmitting light images.

As discussed above, since the bioinformatic analysis of the CML36 amino acid sequence suggested mitochondrial localization of the CML36 protein, the cytosolic and possible chloroplast localization obtained here may indicate an inaccuracy in the prediction. To investigate this further, the saGFP system was used.

4.2.2 Analysis of CML36 subcellular localization using saGFP system

In the saGFP system, the 11 β-sheets of GFP are split into two fragments. One comprises the first 10 β-sheets ($saGFP_{1-10}$), and the other comprises the 11^{th} β-sheet ($saGFP_{11}$). These two parts of the GFP cannot produce a fluorescence signal independently. However, when localized to the same cellular sub-compartment, the two GFP fragments will reassemble, resulting in fluorescence signal emission. With regard to the analysis of subcellular localization, the saGFP

system has advantages due to the small size of the GFP_{11} fragment, which decreases interference with translocation, membrane insertion, or folding of proteins. It, therefore, often results in more reliable localization of tagged proteins than a full GFP-or YFP-tag. Also, in the case of dual localized proteins, it can separately visualize both localizations. Consequently, CML36 was fused C-terminally to $saGFP_{11}$, referred to as "CML36-$saGFP_{11}$" and co-infiltrated in *N. benthamiana* leaves with the complementary $saGFP_{1-10}$ fused to a marker protein with known cellular localization. After three days, the leaves were analyzed by confocal laser scanning microscopy.

Initially, the correct targeting of the marker proteins was confirmed in control experiments (**Figure 22**). For cytosolic localization, the marker protein $CPK17_{G2A}$, the mutated form of a membrane-associated calcium-dependent protein kinase, was used (**Figure 22**) (Harmon, et al., 2001; Li, et al., 2008; Asano, et al., 2010; Kiselev, et al., 2012). The G2A mutation abolishes myristylation of the protein, thus resulting in a cytosolic localization. The small subunit of the Ribulose-1,5-bisphosphate carboxylase-oxygenase (ssuRuBisCo) was utilized as a marker for the stroma of the chloroplast (**Figure 22**) (Jang, et al., 1999). The 2-Oxoglutaratdehydrogenase E1 (OGD) and MIA40 were used as a marker for mitochondria matrix and intermembrane space, respectively (Mesecke, et al., 2005; Riemer, et al., 2009; Nemeria, et al., 2014; Denton, et al., 2016). Co-expression of each marker fused to both $saGFP_{1-10}$ and $saGFP_{11}$ in tobacco leaves resulted in a visible GFP signal that resembles that of a mitochondrial protein (**Figure 22**), indicating the functionality of these constructs and that they are suitable for determining the localization of CML36. At this resolution, MIA40 and OGD appear similar (there is no discernible difference between the intermembrane space and the matrix).

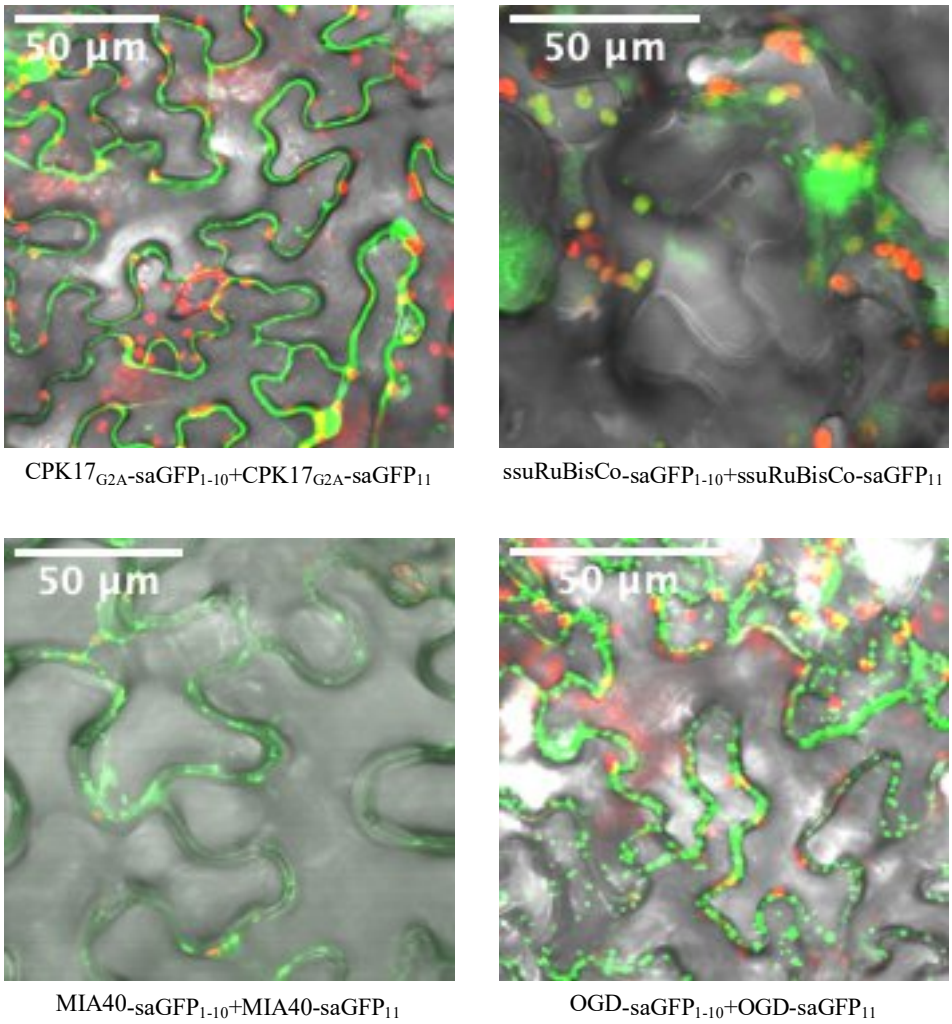

CPK17$_{G2A}$-saGFP$_{1-10}$+CPK17$_{G2A}$-saGFP$_{11}$ ssuRuBisCo-saGFP$_{1-10}$+ssuRuBisCo-saGFP$_{11}$

MIA40-saGFP$_{1-10}$+MIA40-saGFP$_{11}$ OGD-saGFP$_{1-10}$+OGD-saGFP$_{11}$

Figure 22. Functionality of the marker proteins. Co-expression of CPK17$_{G2A}$-saGFP$_{1-10}$+ CPK17$_{G2A}$-saGFP$_{11}$, ssuRuBisCo-saGFP$_{1-10}$+ ssuRuBisCo-saGFP$_{11}$, MIA40-saGFP$_{1-10}$+ MIA40-saGFP$_{11}$, OGD-saGFP$_{1-10}$+OGD-saGFP$_{11}$ in *N. benthamiana* leaves. CPK17$_{G2A}$: marker for the cytosol, ssuRuBisCo: marker for Chloroplast, MIA40: marker for the mitochondria intermembrane space and the OGD: marker of the matrix of the mitochondria. The images show the GFP signals in green and the chloroplasts autofluorescence in red. As expected for ssuRubisCo an overlap of both signals could be observed. The images show an overlay of YFP-chlorophyll autofluorescence as well as transmitting light.

For CML36, a co-expression of CML36-saGFP$_{11}$ and the mitochondrial markers OGD-saGFP$_{1-10}$ or MIA40-saGFP$_{1-10}$ showed no GFP signals in tobacco leaves (**Figure 23**), indicating that CML36 is not localized in the mitochondria and thus abolished the predicted mitochondrial localization suggested by bioinformatics analysis.

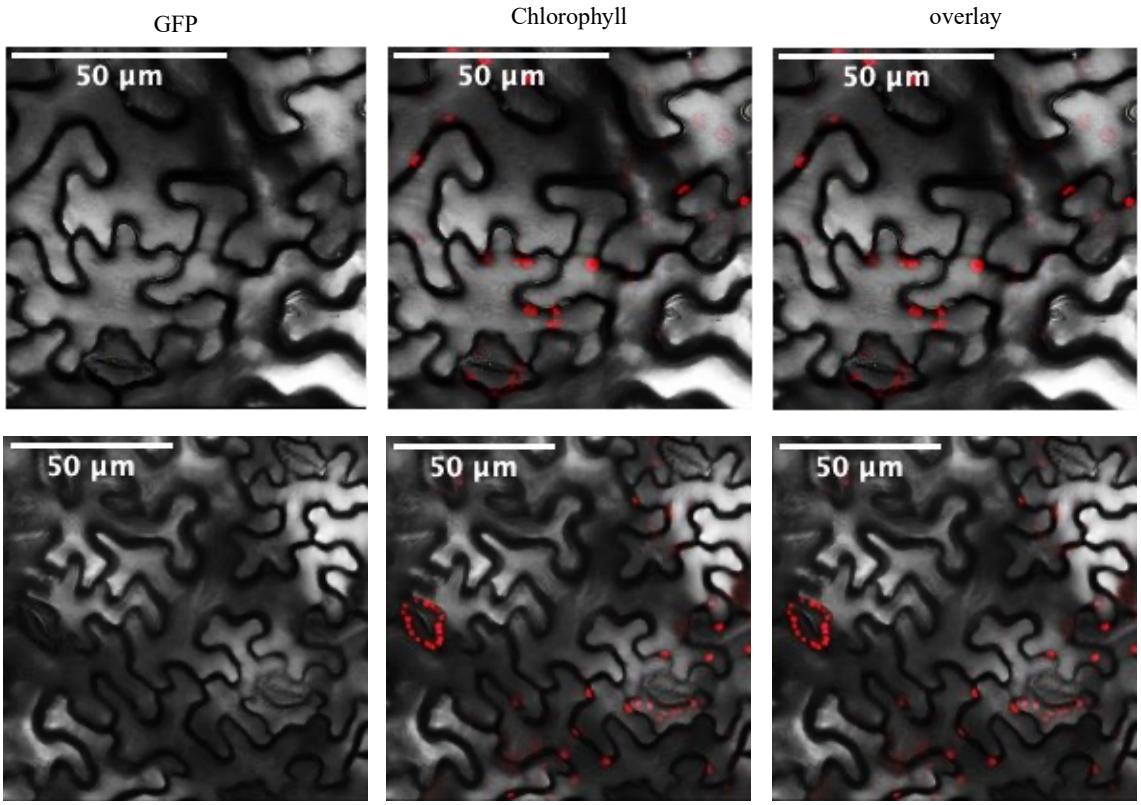

Figure 23. Subcellular analysis of CML36 localization using mitochondrial markers in *N.benthamiana* leaves. Co-expression of OGD-saGFP$_{1-10}$+CML36-saGFP$_{11}$ (upper panel) and the MIA40-saGFP$_{1-10}$ +CML36-saGFP$_{11}$ (Lower panel). No GFP signal was detected, indicating a lack of mitochondrial localization for the CML36.

When CML36-saGFP$_{11}$ was co-expressed with the cytosol marker CPK17$_{G2A}$ fused to saGFP$_{1-10}$, a strong and diffused GFP signal appeared throughout the cell, which did not overlap with the chlorophyll signals (**Figure 24**). This result indicates that at least major parts of the expressed CML36 are located in the cytosol and support the result obtained with the full-length YFP (**Figure 21**).

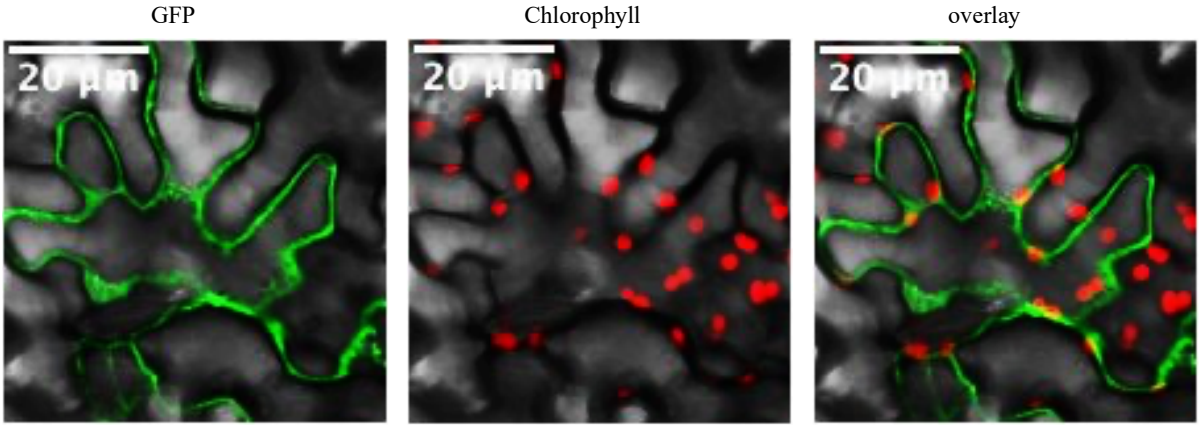

Figure 24. Subcellular localization of CML36 using cytosolic marker in *N. benthamiana* leaves. Co-expression of CPK17$_{G2A}$-saGFP$_{1-10}$ and CML36-saGFP$_{11}$. GFP signal appearing throughout the cell indicated a cytosolic localization for CML36.

The co-expression of CML36-saGFP$_{11}$ with the chloroplast marker ssuRuBisCo fused to saGFP$_{1-10}$ resulted in GFP signals that aligned perfectly with the red chlorophyll autofluorescence (**Figure 25, overlay**). This provides a strong indication for the localization of CML36 in the chloroplast.

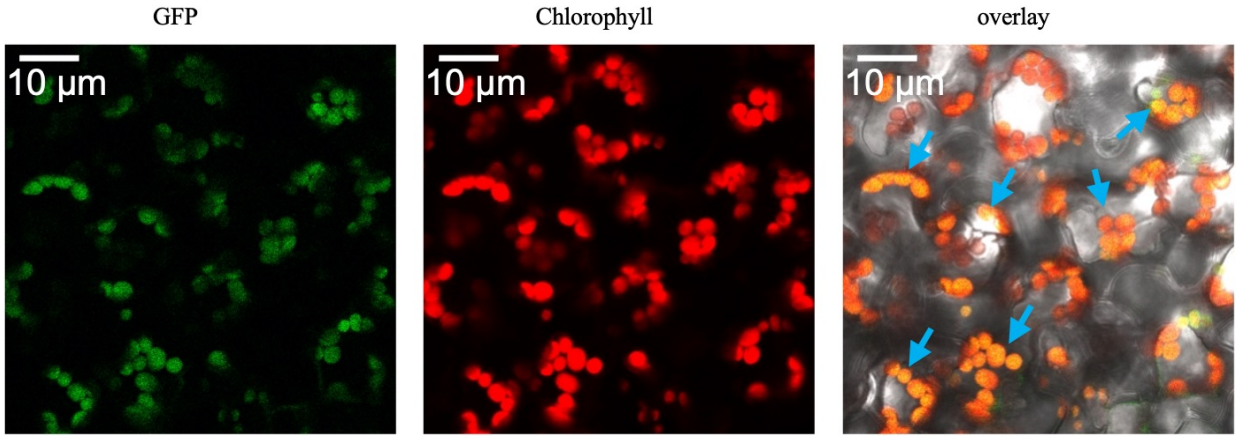

Figure 25. Subcellular localization of CML36 using chloroplastic marker in *N. benthamiana* leaves. Co-expression of ssu-RuBisCo-GFP$_{1-10}$ and CML36-GFP$_{11}$. GFP signal overlapping with the red chlorophyll autofluorescence throughout the cell (marked with blue arrows) indicated a chloroplastic localization for CML36. Overlay: the overlay of GFP, chlorophyll as well as transmitting light images.

Taken together, these results confirmed the dual localization of Cml36 in the cytosol and the chloroplast. To further support this dual localization, a competition experiment was carried out. In this study, infiltration of tobacco leaves was performed using a combination of three constructs: CML36-saGFP$_{11}$, CPK17$_{G2A}$-saGFP$_{1-10}$, and ssuRuBisCo-saGFP$_{1-10}$. Analysis of

the leaves using a confocal microscope showed the GFP as diffuse signals in the cytosol as well as spots overlapping with the red chlorophyll signals (**Figure 26**). This further supports the dual localization of CML36 in the cytosol and chloroplast.

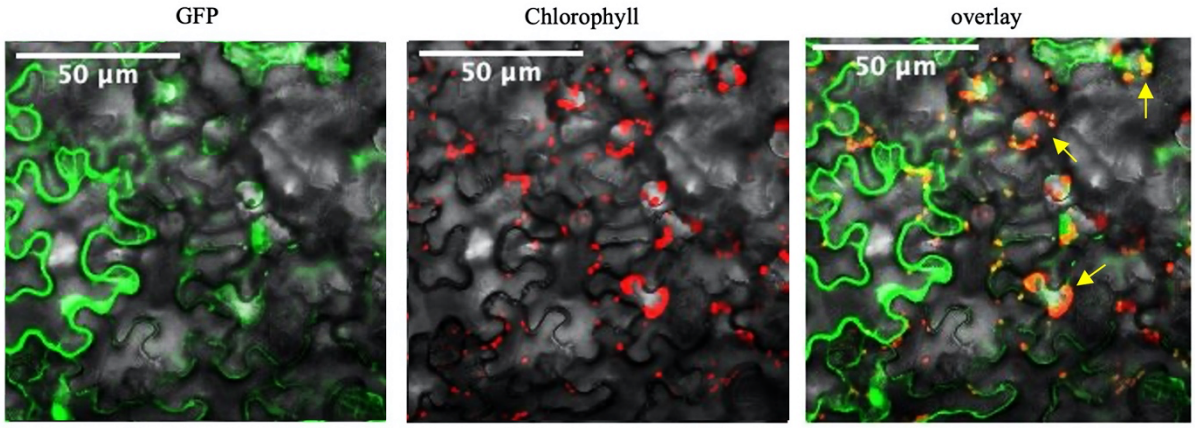

Figure 26. Subcellular localization of CML36 using the cytosolic and the chloroplastic markers simultaneously in *N. benthamiana* leaves. Using the CML36-saGFP$_{11}$, CPK17$_{G2A}$-saGFP$_{1-10}$ and ssuRuBisCo-saGFP$_{1-10}$ constructs. Positive GFP signal emitted from both cytosol in a diffused manner and the spot-like chloroplastic signals (marked with yellow arrows) indicate a dual localization for CML36.

5 Discussion

5.1 Identifying the protein complex of CAS and characterizing the CAS protein

In *Chlamydomonas reinhardtii*, an ortholog of CAS was detected to physically interact with a supercomplex composed of (PSI-LHCI)-(PSII-LHCII)-CYT*b6/f* in addition to FNR and the thylakoid protein PGR5-like1 (PGRL1) (Iwai, et al., 2010; Petroutsos, et al., 2009). This supercomplex is a component of the cyclic electron flow (CEF) which represents an alternative electron transfer pathway around PSI that contributes to the generation of the proton gradient across the thylakoid membrane and ATP synthesis without the accumulation of NADPH. CEF is crucial for a proper balance of NADPH and ATP in the thylakoid to protect the photosynthetic apparatus from photodamages (Munekage, et al., 2002; Takahashi & Milward, 2009; Suorsa, et al., 2012; Huang, et al., 2018). CAS is suggested to have a central role in the fine-tuning of photosynthesis in Chlamydomonas by affecting the CEF in a Ca^{2+}-depending manner (Yamori & Shikanai, 2016; Terashima, et al., 2012). A supercomplex containing all these complexes has not previously been described in *A. thaliana*. In the present study, the MS/MS analysis of BN-gels performed with isolated chloroplasts showed that CAS in *A. thaliana* plants co-migrate on the gel with the thylakoid membrane complexes such as PSI, PSII, and CYT*b6/f* complex. It seems as if these complexes are building at least three different supercomplexes at the level of bands A, B, and D, for which CAS is essential, since in its absence in the chloroplast of the *casko* mutant, the corresponding bands could not be detected (**Figure 5, bands A, B, and D**). With these results, it could be shown that CAS in *A. thaliana*, like its ortholog in Chlamydomonas, might be part of a supercomplex. However, while in Chlamydomonas, only one supercomplex could be identified, in *A. thaliana*, CAS seems to be involved in at least three supercomplexes with some differences in the protein composition (**Figure 5**). The main differences between bands A, B, and D, were in the case of FNR1 and 2, which were detected only in supercomplexes B and D but not in A. Also, LHC proteins showed a differential distribution within the *A. thaliana* supercomplexes: Supercomplex A contains (PSI-LHCA), (PSII-LHCB), CYT*b6/f*, and ATP-synthase, as well as the protein PGRL1. In supercomplex B, PSI-LHCA proteins, as well as PSII, CYT*b6/f*, ATP-synthase, and the proteins PGRL1 and FNR1/FNR2 were present, while in supercomplex D, PSI, (PSII-LHCB), CYT*b6/f*, ATP-synthase, and the proteins PGRL1 and FNR1/FNR2 were present. In *A. thaliana*, the supercomplexes also contain subunits of ATP-synthase, which were not described for Chlamydomonas. In *A. thaliana*, all three supercomplexes contain PGR5-like A (PGRL1),

which has already been described as a component of the CEF machinery in both *A. thaliana* as well as and *C. reinhardtii* (DalCorso, et al., 2008; Petroutsos, et al., 2009). Thus, it might be that the supercomplexes identified in this study are involved in *A. thaliana*'s CEF process, which is still largely unknown. The difference in the molecular weight of the three supercomplexes might be due to the differential distribution of the LHCs or due to additional components not detected in this analysis. These results indicate a potential role of CAS in the CEF reaction.

Additionally, these results agree with the conserved entropy network model and a co-expression network constructed based on the STRING database (https://string-db.org/). After constructing a network based on the sequenced proteins from MS/MS (**Figure 6**), CAS could be placed close to the proteins FNR1/FNR2, which are known to facilitate the last step of electron transfer from ferredoxin to NADPH, catalyzing the final step of electron flow thereby facilitating carbon fixation, along with PETC (PGR1), a subunit of the CYT*b6/f* complex, proposed to be involved in the CEF (Nikkanen, et al., 2018; Yamamoto & Shikanai, 2019). The results indicated that CAS is also associated with several other significant proteins, including LHCA3 and PSAf, both of which are components of light-harvesting complexes and PSI, respectively (**Figure 6**). Taken together, the results obtained with MS/MS sequencing and in-silico predictions in *A.thaliana* also tallies with the observations made in Chlamydomonas where CAS was shown to be a component involved in CEF along with other approved proteins involved in this process like FNR, PETC (PGR1) and PGRL1 (Terashima, et al., 2012; Leister & Shikanai, 2013).

Regulation of CEF may involve distinct mechanisms since green algae and plants, for example, use different plastoquinone reductases (Iwai, et al., 2010; Desplats, et al., 2009). It has been demonstrated that CEF in Chlamydomonas is regulated by stromal redox status, caused by an imbalance in the supply and demand of NADPH concerning ATP (Takahashi, et al., 2013; Lucker & Kramer, 2013). Higher plants, on the other hand, resist simplistic models that assume that a single redox carrier acts as a regulator (Livingston, et al., 2010). Despite this, a hypothetical model has been proposed where H_2O_2 production can regulate the activation of the CEF in the chloroplast of higher plants (Casano, et al., 2001; Strand, et al., 2015).

Besides the potential role of CAS and its supercomplexes in the CEF reaction, it seems that they are not essential for the growth and photosynthesis reactions in *A. thaliana* since the *casko* mutant showed no alterations in the phenotype and PSII yield activity when compared to the WT under normal growth conditions (**Figures 7B and C**). In a previous study, CAS RNAi antisense lines showed to exhibit earlier bolting compared to WT (Han, et al., 2003). Those,

however, do not conclude a phenotype for the *casko* lines, at least not under normal light conditions, which could be the result of CAS knockdown and not necessarily CAS dependent. However, the phenotype differences regarding the stomata aperture with the *casko* showing a larger stomata aperture than the WT (**Figure 7D**) match the results of previous studies (Nomura, et al., 2008; Weinl, et al., 2008). This indicates that CAS indeed plays a role in the regulation of stomatal closure. However, even under drought stress, no alteration in the phenotype could be observed, which was unexpected since the WT leaves showed 30% less stomata aperture than the *casko* mutant (**Figures 7D and E**).

The *casko* mutant has been previously shown to exhibit impaired de-excitation kinetics in the presence of excess light (Cutolo, et al., 2019). However, the effect of the lack of CAS protein on PSII activity had not been mentioned. Thus, to determine whether there is an association between the CAS and PSII, a comparison was made between the PSII yield in WT and *casko* plants (**Figures 7D and E**). Under control and salt conditions, the PSII performance was affected similarly between both plant lines. By contrast, when the plants were exposed to H_2O_2, the PSII performance decreased in the WT, while in the *casko*, it stayed unaffected (**Figures 7D and E**), indicating that plants might cope better with the H_2O_2 stress in the absence of CAS. This in turn, suggests that CAS might be a component of the machinery involved in response to H_2O_2. Previously a crosstalk has been shown between CAS-mediated Ca^{2+} transients and hydrogen peroxide (H_2O_2) production at the level of thylakoid membranes in mediating stomatal closure, suggesting that CAS is involved in both processes (Wang, et al., 2016).

One of the first events recorded in plants upon exposure to H_2O_2 is the increase of $[Ca^{2+}]$, indicating the involvement of the Ca^{2+} signaling pathway in the cellular response to H_2O_2. Whether CAS as a Ca^{2+} binding protein is involved in this process has been investigated by measurements of changes in $[Ca^{2+}]$ in a *casko* mutant compared to WT upon exposure to H_2O_2. For the Ca^{2+} measurements, *A. thaliana* lines expressing apoaequorin in the cytosol, stroma, and thylakoid lumen, were used. In plants, the AEQ bioluminescence marker system is a powerful tool that can be used to detect Ca^{2+} transients in response to biotic and abiotic stresses (Knight, et al., 1991; Jiang, et al., 2013). Changes in the $[Ca^{2+}]$ showed stimulus-specific spatial-temporal parameters, such as shape, frequency, amplitude, and duration, called "Ca^{2+} signatures" which define the specificity of the Ca^{2+} signaling in response to stimuli.

Under the application of exogenous H_2O_2, the cytosol produced a completely different Ca^{2+} signature compared to the stroma and the thylakoid lumen (**Figure 11**). The $[Ca^{2+}]_{Cyt}$ response to H_2O_2 appeared in the form of double peaks with quite similar dynamic patterns in both WT and *casko* mutants (**Figure 11A**). This result corresponds to previous studies in *A. thaliana*

(Rentel & Knight, 2004), which showed that the two $[Ca^{2+}]_{cyt}$ peaks are independent of each other, with the first peak being generated by the shoot and the second peak generated by the root, indicating that shoot and root tissues use separate H_2O_2 signal transduction/perception mechanisms (Rentel & Knight, 2004). In this study, the second peak is significantly higher in the WT compared to the *casko* (**Figure 11A**). This suggested that CAS might be implicated in the Ca^{2+} response to H_2O_2 in the roots of *A. thaliana*. The two $[Ca^{2+}]$ spikes obtained from the cytosol were significantly inhibited by La^{3+} and EGTA in WT as well as in *casko* (**Figure 12**). $LaCl_3$ has been widely used as a blocker of plasma membrane Ca^{2+} channels to inhibit Ca^{2+} influx from the apoplast into the cytosol (Tracy, et al., 2008). Additionally, (EGTA) is well-known to chelate Ca^{2+} in the cell wall, thus preventing it from entering the cytosol via the plasma membrane (Knight, et al., 1996). The significant inhibition of the two $[Ca^{2+}]_{cyt}$ spikes suggested that the $[Ca^{2+}]$ increases in the cytosol caused by H_2O_2 treatment came from external Ca^{2+} stores in both WT and *casko* plants.

In the case of the chloroplastic lines (the stroma and the thylakoid lumen), the Ca^{2+} signals are generally weaker as in thy cytosol, especially in the stroma, and showed completely different Ca^{2+} signatures. The results obtained in this study were consistent with those previously reported in WT plants (Sello, et al., 2018), in which the prolonged organellar Ca^{2+} response observed in the chloroplastic lines induced by 10 mM H_2O_2 did not dissipate within the 10 min. In the thylakoid lumen, the $[Ca^{2+}]$ increases showed quite similar dynamics in both lines with only one peak, which was much higher in WT than in *casko* (**Figure 11E**). Such patterns were observed in previous studies showing the necessity of the CAS protein for the chloroplast Ca^{2+} responses to elicitors, the light-dark transition (Nomura, et al., 2012), and heat stress (Lenzoni & Knight, 2019). It was indicated from the results that in the thylakoid lumen, the immediate sensing of the H_2O_2 was dependent on the presence of the CAS protein. However, the prolonged response was not CAS-dependent. The Ca^{2+} responses were significantly inhibited by La^{3+} and EGTA (**Figure 14**), indicating that the $[Ca^{2+}]$ increases in the thylakoid lumen caused by H_2O_2 application originated from external Ca^{2+}stores of both WT and *casko* plant lines.

In the stroma, the Ca^{2+} signatures were completely different between WT and *casko* lines, indicating the involvement of different Ca^{2+} signaling components in both lines. One of these components could be CAS protein itself which is absent in the *casko* mutant. On the other hand, the stroma presented the lowest response to H_2O_2 compared to the other two organelles. In plants, the removal of H_2O_2 is carried out by multiple enzymes in two distinct mechanisms: 1. Haem peroxidase and 2. The thiol-based peroxidase. In the chloroplast, the ascorbate peroxidase (APX), a peroxidase available in the haem reaction, and the yeast thiol peroxidase

(TPXs) remove H_2O_2 via ferredoxin using NADPH and photosynthetic electron transport (Smirnoff & Arnaud, 2019). The presence of the mentioned peroxidase in the stroma might explain the stroma's low sensitivity and unstable response to oxidative stress in this study.

Calcium influx in plant cells is also necessary for signaling mediated by the rapid and transient increase in cellular sub-compartment [Ca^{2+}], referred to as the Ca^{2+} signal. Physiological and gene expression responses are transduced by this signal from internal and external stimuli (Edel, et al., 2017). Since Ca^{2+} ions serve as key signals within cells, their concentration within the cell is tightly controlled. One mechanism by which Ca^{2+}-binding proteins limit free Ca^{2+} ions is buffering (Pangrsicˇ, et al., 2015). A cell contains a variety of proteins, including calcium channels, transporters, and pumps that, in conjunction with calcium buffers, provide structured intracellular Ca^{2+} signals (Schwaller, 2010). A Ca^{2+} buffer can be a Ca^{2+}-binding protein that modulates both the temporal and spatial aspects of intracellular Ca^{2+} signal transients. Many of these buffers can also be used as Ca^{2+} sensors in addition to their proven Ca^{2+} buffer functions (Schwaller, 2010).

So far, Ca^{2+}-binding proteins acting as buffers in chloroplasts have not been identified. However, chloroplasts may contain organellar Ca^{2+} buffering mechanisms that may play an essential role in creating heterogeneity in local Ca^{2+} concentrations (Navazio, et al., 2020). The chloroplast must maintain a low level of H_2O_2 as high levels of H_2O_2 can damage several macromolecular targets, including Calvin-Benson cycle enzymes regulated by the thioredoxin and are found within the stroma (Michelet, et al., 2013). Hence, another reason for the insensitivity of the stroma to oxidative stress observed in this study may be due to the CAS protein's role as a Ca^{2+} buffering protein within the chloroplast.

In the WT, the [Ca^{2+}] increases in the stroma showed two peaks. The first peak appeared almost immediately upon injection of H_2O_2, followed by a second and higher peak after 30 seconds of the injection (**Figure 11C**). These dynamics were quite similar to those observed in the cytosol, with a little delay compared to the cytosol, suggesting that the Ca^{2+} signals in the stroma induced by H_2O_2 might originate from the cytosol. However, the treatment with $LaCl_3$ and EGTA inhibited only the second peak in the stroma (**Figure 13**), while in the cytosol, both peaks were inhibited. These results indicated that the Ca^{2+} signals induced by H_2O_2 in the stroma might be both cytosol-independent (the first peak) and cytosol-dependent (the second peak). Since the inhibition did not affect the first peak, it can be suggested that the source of the [Ca^{2+}] increase here is not the apoplast but other internal Ca^{2+} stores, most likely the thylakoid lumen. In the stroma of the *casko* mutant, the first cytosol-independent peak is present, but not the second peak (**Figure 11C**). These results suggest that CAS is essential for

generating cytosol dependent Ca^{2+} signals induced by H_2O_2 treatment but not for those induced independently of the cytosol. In order to determine the effects of the absence of cytosol dependent Ca^{2+} signals on chloroplast functions and plant development, further studies are needed.

Next, the generation of $[Ca^{2+}]$ transients within the cytosol, stroma, and thylakoids under osmotic conditions induced by salinity (ionic) (**Figure 15**) or mannitol (non-ionic) (**Figure 19**), was studied. In the cytosol, the $[Ca^{2+}]_{Cyt}$ response to NaCl appeared in the form of a single peak with similar dynamic patterns in both WT and *casko* mutants (**Figure 15**). The Ca^{2+} responses were significantly inhibited by La^{3+} and EGTA (**Figure 16**), indicating that the $[Ca^{2+}]$ increases in the cytosol caused by NaCl application originated from external Ca^{2+}stores of in both plant lines. Chloroplastic lines (stroma and thylakoid lumen) exhibit weaker Ca^{2+} signals when subjected to NaCl stress. The difference in the amount of transient $[Ca^{2+}]$ between the cytosol and the stroma under salt stress matched the results of a previous study (Nomura, et al., 2012). The same study showed that both the cytosol and the stroma generate many secondary spikes, which were also observed in our study (**Figures 15A and C**). Although there is no true explanation for such secondary spikes, a previous study performed in barley (*Hordeum vulgare*) suggested that these inferior spikes might be induced by other factors such as H_2O_2 (Li, et al., 2008). In *A. thaliana*, it has been speculated that these secondary Ca^{2+} spikes might result from the response of different cell populations among root tissues as well as from the oscillatory nature of NaCl-induced changes in single cells (Kiegle, et al., 2000; Tracy, et al., 2008).

In the case of the stroma, the Ca^{2+} signatures were completely different between WT and *casko* lines, indicating the involvement of different Ca^{2+} signaling components in both lines. There were two peaks of $[Ca^{2+}]$ increases in the stroma in the WT; the first peak appeared immediately after injection of NaCl, then a second, lower peak appeared after 20 seconds of injection (**Figure 15**). By contrast, in the *casko* plants, only the first peak could be detected, indicating that CAS might mediate the generation of the second peak in the stroma. Under NaCl stress, EGTA and La^{3+} significantly inhibited Ca^{2+} responses in both lines (**Figure 17**).

In the thylakoid lumen, the $[Ca^{2+}]$ increases showed quite similar dynamics in both lines with only one peak, which is much higher in WT than in *casko* under NaCl stress (**Figure 15**). In all cellular sub-compartments, EGTA and La^{3+} significantly inhibited Ca^{2+} responses to NaCl, indicating the extracellular origin of Ca^{2+} in both WT and *casko* plants. However, the inhibition in none of the cases was 100%, demonstrating that $[Ca^{2+}]$ increases in response to NaCl are generated from internal Ca^{2+} stores.

Similar to NaCl, both plants showed a rapid initial [Ca^{2+}] increase in response to mannitol; however, a greater response was observed in WT cytosol in comparison to *casko* cytosol, and the cytosol as a whole responded more strongly than other sub-compartments (**Figure 19**). In contrast to NaCl, the stroma in both WT and *casko* plants showed only one [Ca^{2+}] peak.

Under NaCl and mannitol stress in both the WT and the *casko* samples, the order of the appearance of the transient [Ca^{2+}] in the three cellular sub-compartments was similar. Regardless of the type of osmotic stress, calcium levels dropped to approximately the resting level after 50 to 60 seconds, indicating no prolonged organellar Ca^{2+} response (**Figures 15 and 19**). It has previously been described that the activation of thylakoid lumen Ca^{2+} signal may be crucial for rapidly restoring low basal stromal concentrations of calcium after a Ca^{2+} signal transient that traverses into the organelle from the cytosol without prolonging the transient in the organelle using a back flux (Sello, et al., 2018).

By using MS/MS analysis, this study has been able to gain a better understanding of the supercomplexes in which CAS might be involved and its role in the CEF in *A. thaliana*. Meanwhile, PSII yield results, along with Ca^{2+} measurements, suggested that CAS may be a component of the H_2O_2 mediated response mechanism in the chloroplast. However, these claims should be confirmed by further detailed studies that will need to be conducted.

5.2 Sub-cellular localization of CML36

In order to decode Ca^{2+} signals, Ca^{2+}-binding proteins (CBPs) are required. Upon binding of Ca^{2+}, CBPs activate (or deactivate) downstream target proteins, which then induce the stimulus-appropriate cellular response. This work analyzed the localization of CML36, one of the 50 CMLs in *A. thaliana*. CML36 has four EF-hand motifs and contains an N-terminal extension absent in canonical CaMs (**Figure 20**). Bioinformatical analyses predict this N-terminal extension to be a targeting signal for the mitochondria. Nevertheless, saGFP analysis results obtained in this work showed that CML36 is dual localized in the cytosol and the chloroplast and not targeted to the mitochondria (**Figure 23**).

The cytosolic localization was clearly observable when CML36 was fused to the full-length YFP tag (**Figure 21**). Similar results had been obtained previously when GFP-fusions of CML36 was expressed in *A. thaliana* leaf protoplasts (Dell'Aglio, et al., 2016). This localization is also in good accordance with the findings of Astegno and co-workers, which revealed the interaction of CML36 with ACA8, a Ca^{2+}-ATPase localized on the plasma

membrane (Astegno, et al., 2017). However, the YFP signal of CML36-YFP in our study also showed an overlap in some areas with the chlorophyll fluorescence (**Figure 21**), suggesting a possible second localization of CML36 in the chloroplast. This localization could be confirmed using the saGFP system to co-express CML36-saGFP$_{11}$ with a chloroplast marker ssuRuBisCo-saGFP$_{1-10}$ (**Figure 25**). The dual targeting of the CML36 was supported when CML36 was simultaneously co-expressed with CPK17$_{G2A}$ and ssuRuBisCo, and the GFP signal could be detected in both the cytosol and the chloroplasts (**Figure 26**). A similar dual-targeting feature was previously shown for another CML in *A. thaliana*, CML30, which targeted both the cytosol and mitochondria (Chigri, et al., 2012).

In the chloroplast, CaM regulation has been connected to the translocation of nuclear-encoded proteins into the organelle (Chigri, et al., 2005; Chigri, et al., 2006), a vesicle transport system inside chloroplasts (Westphal, et al., 2001; Westphal, et al., 2003), and phosphorylation of thylakoid membrane proteins (Jarrett, et al., 1982; Li, et al., 1998).

Moreover, several CaM-binding proteins in the chloroplasts were identified. One of the well-studied CaM-binding proteins localized in the chloroplast is the Tic32 (Chigri, et al., 2006). Additionally, four potential CaM-binding proteins were identified as a result of screening for potential CaM-binding proteins in *A. thaliana* (Reddy, et al., 2002). These proteins include PsaN, a component of photosystem I, AAA-ATPase encoded by At3g56990, ACA1, and Cpn10. Cpn10, together with the chaperonin Cpn60, seems to be involved in the assembly of the RuBisCo, the critical enzyme in photosynthetic CO_2-fixation (Yang & Poovaiah, 2000). Several plant members of the ATPases associated with different cellular activities (AAA) protein families have been described previously. Although some of these proteins, such as the AAA-ATPase encoded by At3g56990 (CIP111) and the AAA+-ATPase AFGL1 (Buaboocha, et al., 2001; Bussemer, et al., 2009), have been established as CaM binding proteins located in the chloroplast, many questions still remain about their specific function. ACA1 is a Ca^{2+}-ATPase localized in the envelope of the chloroplast and is suggested to have a function as a Ca^{2+}-transporter (Huang, et al., 1993). Despite the increasing evidence that CaM-type proteins are associated with some chloroplast functions, in neither case was the CaM involved clearly identified. Therefore, our results present for the first-time confirmation of the existence of a CML within the chloroplasts. So far, the target of CML36 in chloroplasts has not been identified. Thus, further studies are required to determine whether CML36 interacts with one of the above-mentioned potential CaM-targets or is involved in one of the processes regulated by CaM in the chloroplasts. In addition, the dual localization of CML36 might provide a means

to regulate specific functions in both cellular compartments, cytosol, and chloroplast, in a concerted manner via incorporation into the Ca^{2+} signaling network of the cell.

Summary

Plants, as immobile organisms, cannot escape the environmental biotic and abiotic cues they are faced with. To deal with the stress, plants have evolved different pathways that enable them to recognize the stimuli and initiate various downstream processes, which result in cellular responses, leading to plant survival. The Ca^{2+}- signaling has been recognized for several decades as one of the key mechanisms used by plants to respond to stimuli. Recently, chloroplasts have been considered as more than just a source of energy in plants, but as an essential signaling hub as well. Several Ca^{2+} binding proteins have been identified in the chloroplasts and have been considered as potential key players in the chloroplast Ca^{2+} signaling pathway. One of these proteins is the calcium sensing protein (CAS), that is still poorly characterized in plants.

In the present work, it has been shown that CAS is an essential component of at least three different supercomplexes containing PSI, PSII, LHCs, CYT*b6/f*, ATPsynthase in addition to FNR and PGRL1 in the chloroplast of *A. thaliana*. Such CAS-supercomplex was identified in the chloroplast of *Chlamydomonas reinhardtii,* and the interaction of CAS with PGRL1, a component of alternative cyclic electron flow (CEF), leads to the assumption that CAS might play a function in CEF. Despite this potential function, the lack of CAS appears to have no effect either on the phenotype of the plants or on the photosynthesis activity under normal growth conditions. However, the application of exogenous H_2O_2 did not affect the PSII activity in the t-DNA inserted CAS line (*casko*) compared to WT plants. This difference could be due to differences observed between WT and *casko* plants in the dynamics of the $[Ca^{2+}]$ changes induced by H_2O_2 in the stroma and thylakoids. Changes in the $[Ca^{2+}]$ were measured using the Ca^{2+} indicator aequorin targeted to the cytosol, stroma, and thylakoid lumen of WT and *casko A. thaliana* lines. By contrast, for other stresses such as salt and mannitol, the differences in $[Ca^{2+}]$ dynamics between both lines were mostly observed in the cytosol. All these results indicated that CAS is involved in the Ca^{2+} signaling in both the cytosol and in the chloroplast in a stimulus-dependent manner.

Additionally, using transiently transfected tobacco leaves and isolated protoplasts, this thesis focused on finding the localization of CML36, one of fifty CML proteins present in *A. thaliana*. Using the self-assembly GFP (saGFP) method, a dual localization of the cytosol and the chloroplast was proposed for the CML36.

Zusammenfassung

Als sessile Organismen können Pflanzen den biotischen und abiotischen Umweltreizen, denen sie ausgesetzt sind, nicht entkommen. Um mit dem Stress fertig zu werden, haben Pflanzen verschiedene Wege entwickelt, die es ihnen ermöglichen, die Reize zu erkennen und verschiedene nachgeschaltete Prozesse in Gang zu setzen, die zu zellulären Reaktionen führen um das Überleben der Pflanze zu sichern. Die Ca^{2+}-Signalübertragung ist seit mehreren Jahrzehnten als einer der wichtigsten Mechanismen bekannt, mit denen Pflanzen auf Stimuli reagieren. In jüngster Zeit werden die Chloroplasten nicht nur als Energiequelle in Pflanzen betrachtet, sondern auch als ein wichtiger Knotenpunkt für die Signalübertragung. In den Chloroplasten wurden mehrere Ca^{2+}-bindende Proteine als potenzielle Hauptakteure im Ca^{2+} -Signalweg der Chloroplasten indentifiziert. Eines dieser Proteine ist das Calcium Sensing Protein (CAS), das in Pflanzen bisher wenig charakterisiert ist.

In der vorliegenden Arbeit wurde gezeigt, dass CAS ein wesentlicher Bestandteil von mindestens drei verschiedenen Superkomplexen ist, die PSI, PSII, LHCs, CYT*b6/f*, ATPsynthase sowie FNR und PGRL1 im Chloroplasten von *A. thaliana*. Ein solcher CAS-Superkomplex wurde bereits im Chloroplasten von *Chlamydomonas reinhardtii* beschrieben, und es wurde gezeigt, dass er am zyklischen Elektronenfluss (CEF) beteiligt ist, was zu der Vermutung führte, dass CAS auch eine Rolle im CEF der Chloroplasten von *A. thaliana* spielen könnte. Trotz dieser potenziellen Funktion scheint das Fehlen von CAS weder auf den Phänotyp der Pflanzen noch auf die Photosyntheseaktivität unter normalen Wachstumsbedingungen Auswirkungen zu haben. Die PSII-Aktivität in den *casko*-Pflanzen wurde im Vergleich zu WT-Pflanzen allerdings nicht nicht durch eine exogene H_2O_2 Anwendung beeinflusst. Dieser Unterschied könnte auf die zwischen WT- und *casko*-Pflanzen beobachteten Unterschiede in der Dynamik der durch H_2O_2 induzierten [Ca^{2+}]-Veränderungen im Stroma und in den Thylakoiden zurückzuführen sein. Die [Ca^{2+}]-Veränderungen wurden mit dem Ca^{2+}-Indikator Aequorin im Cytosol, Stroma und Thylakoidlumen der WT- und *casko- A. thaliana* -Linien gemessen. Im Gegensatz dazu wurden bei anderen Stressfaktoren wie Salz und Mannitol die Unterschiede in der [Ca^{2+}]-Dynamik zwischen beiden Linien hauptsächlich im Zytosol beobachtet. All diese Ergebnisse deuten darauf hin, dass CAS sowohl im Zytosol als auch im Chloroplasten in einer stimulusabhängigen Weise an der Ca^{2+}-Signalübertragung beteiligt ist.

Darüber hinaus wurde in dieser Arbeit mit transient transfizierten Tabakblättern und isolierten Protoplasten die Lokalisierung von CML36, einem der fünfzig CML-Proteine in *A. thaliana*, untersucht. Eine Self-Assembly-GFP-Analyse (saGFP) deutet dabei auf eine duale Lokalisierung von CML36 im Zytosol im Chloroplasten.

References

Agarwal, S. et al., 2005. Role of ABA, salicylic acid, calcium and hydrogen peroxide on antioxidant enzymes induction in wheat seedlings. *Plant Science,* 169(3), pp. 559-570.

Albertsson, P. Å., 2001. A quantitative model of the domain structure of the photosynthetic membrane. *Trends in plant science,* 6(8), pp. 349-354.

Allen, D. G. & Prendergast, F. G., 1977. Aequorin luminescence: relation of light emission to calcium concentration—a calcium-independent component.. *Science,* 195(4282), pp. 996-998.

Allen, G. et al., 2000. Alteration of stimulus-specific guard cell calcium oscillations and stomatal closing in Arabidopsis det3 mutant. *Science,* 189(5488), pp. 2338-2342.

Andersson , I. & Backlund, A., 2008. Structure and function of Rubisco. *Plant Physiology and Biochemistry,* 46(3), pp. 275-291.

Andersson, B. & Anderson, J. M., 1980. Lateral heterogeneity in the distribution of chlorophyll-protein complexes of the thylakoid membranes of spinach chloroplasts. *Biochimica et Biophysica Acta (BBA)-Bioenergetics,* 593(2), pp. 427-440.

Anuradha, S. & Rao , S. S. R., 2001. Effect of brassinosteroids on salinity stress induced inhibition of seed germination and seedling growth of rice (Oryza sativa L.). *Plant Growth Regulation,* 33(2), pp. 151-153.

Apel, K. & Hirt, H., 2004. Reactive oxygen species: metabolism, oxidative stress, and signal transduction.. *Annu. Rev. Plant Biol.,* Volume 55, pp. 373-399.

Asada, K., 1994. Production and action of active oxygen species in photosynthetic tissues," in Photo-oxidative stresses in plants: causes and amelioration.. *Ed. C. Foyer and P. Mullineaux (BocaRaton: CRC Press Inc.),* pp. 77-104.

Asada, K., 2006. Production and Scavenging of Reactive Oxygen Species in Chloroplasts and Their Functions. *Plant Physiol,* Volume 141, pp. 391-396.

Asano, T. et al., 2010. Overexpression of a calcium-dependent protein kinase gene enhances growth of rice under low-nitrogen conditions. *Plant biotechnology,* 27(4), pp. 369-373.

Astegno, A. et al., 2017. Arabidopsis calmodulin-like protein CML36 is a calcium (Ca2+) sensor that interacts with the plasma membrane Ca2+-ATPase isoform ACA8 and stimulates its activity.. *Journal of Biological Chemistry,* pp. 15049-15061.

Babbs, C. F., Pham, J. A. & Coolbaugh, R. C., 1989. Lethal Hydroxyl Radical Production in Paraquat-Treated Plants. *Plant Physiology,* 90(4), pp. 1267-1270.

Babu, M. A., Singh, D. & Gothandam, K. M., 2012. The effect of salinity on growth, hormones and mineral elements in leaf and fruit of tomato cultivar PKM1.. *J Anim Plant Sci,* 22(1), pp. 159-164.

Bannai, H. et al., 2002. Extensive feature detection of N-terminal protein sorting signals. *Bioinformatics,* 18(2), pp. 298-305.

Barr, R., Troxel, K. S. & Crane, F. L., 1980. EGTA, a calcium chelator, inhibits electron transport in photosystem II of spinach chloroplasts at two different sites.. *Biochemical and biophysical research communications,* 92(1), pp. 206-212.

Bartels, D. & Nelson, D., 1994. Approaches to improve stress tolerance using molecular genetics. *Plant, Cell & Environment,* 17(5), pp. 659-667.

Basu, S. et al., 2013. Divergence of Erv1-associated mitochondrial import and export pathways in trypanosomes and anaerobic protists.. *Eukaryotic cell,* 12(2), pp. 343-355.

Batistič, O. & Kudla, J., 2012. Analysis of calcium signaling pathways in plants. *Biochim Biophys Acta,* pp. 1283-93.

Behrens, C. et al., 2013. The 'protein complex proteome' of chloroplasts in Arabidopsis thaliana. *Journal of proteomics,* Volume 91, pp. 73-83.

Benetka, W. et al., 2008. Experimental testing of predicted myristoylation targets involved in asymmetric cell division and calcium-dependent signalling. *Cell Cycle,* 7(23), pp. 3709-3719.

Berridge, M. J., Lipp, P. & Bootman, M. D., 2000. The versatility and universality of calcium signalling. *Nature reviews Molecular cell biology,* pp. 11-21.

Bertens, P., Van der Wel, N., Wellink, J. & Van Kammen, A., 2003. Studies on the C-terminus of the Cowpea mosaic virus movement protein. *Archives of virology,* 148(2), pp. 265-279.

Bevan, M., 1984. Binary Agrobacterium vectors for plant transformation.. *Nucleic acids research,* 12(22), pp. 8711-8721..

Bhattacharya, S., Bunick, C. G. & Chazin, W. J., 2004. Target selectivity in EF-hand calcium binding proteins.. *Biochimica et Biophysica Acta (BBA)-Molecular Cell Research,* 1742(1), pp. 69-79.

Billker, O., Lourido, S. & Sibley, D. L., 2009. Calcium-dependent signaling and kinases in apicomplexan parasites. *Cell host & microbe,* 5(6), pp. 612-622.

Bonza, M. & Michelis, M. D., 2011. The plant Ca2+-ATPase repertoire: biochemical features and physiological functions.. *Plant Biology,* 13(3), pp. 421-430.

Bowler, C., Montagu, M. V. & Inzé, D., 1992. Superoxide dismutase and stress tolerance.. *Annual review of plant biology,* 43(1), pp. 83-116.

Boyer, J. S., 1982. Plant productivity and environment.. *Science,* pp. 443-448.

Brand, J. J. & Becker, D. W., 1984. Evidence for direct roles of calcium in photosynthesis. *Journal of bioenergetics and biomembranes,* pp. 239-249.

Brini, M. et al., 1993. Nuclear Ca2+ concentration measured with specifically targeted recombinant aequorin. *The EMBO journal,* 12(12), pp. 4813-4819.

Buaboocha, T., Liao, B. & Zielinski, R. E., 2001. Isolation of cDNA and genomic DNA clones encoding a calmodulin-binding protein related to a family of ATPases involved in cell division and vesicle fusion. *Planta,* Volume 212, pp. 774-781.

Bush, D. S., 1995. Calcium regulation in plant cells and its role in signaling.. *Annual review of plant biology,* 46(1), pp. 95-122.

Bussemer, J., Vothknecht, U. C. & Chigri, F., 2009. Calcium regulation in endosymbiotic organelles of plants. *Plant signaling & behavior,* 4(9), pp. 805-808.

Cabantous, S., Terwilliger, T. C. & Waldo, G. S., 2005. Protein tagging and detection with engineered self-assembling fragments of green fluorescent protein. *Nature,* 23(1), pp. 102-107.

Callaham, D. A. & Hepler, P. K., 1991. Measurement of free calcium in plant cells.. *Cellular Calcium: A Practical Approach,* pp. 383-410.

Campbell, A. K., 1988. *Chemiluminescence. Principles and applications in biology and medicine.* s.l.:s.n.

Carrie, C. et al., 2010. Conserved and novel functions for Arabidopsis thaliana MIA40 in assembly of proteins in mitochondria and peroxisomes. *Journal of Biological Chemistry,* 285(46), pp. 36138-36148.

Casano, L. M., Martin, M. & Sabater, B., 2001. "Hydrogen peroxide mediates the induction of chloroplastic Ndh complex under photooxidative stress in barley.. *Plant Physiology,* 125(3), pp. 1450-1458.

Cen, H. et al., 2017. Chlorophyll fluorescence imaging uncovers photosynthetic fingerprint of citrus Huanglongbing.. *Frontiers in plant science,* Volume 8, p. 1509.

Chaal, B. K. & Green, B. R., 2005. Protein import pathways in 'complex' chloroplasts derived from secondary endosymbiosis involving a red algal ancestor. In: M. Seki, ed. *Plant molecular biology.* s.l.:springer, pp. 333-342.

Chalfie, M. T. Y. E. G. W. W. a. P. D., 1994. Green fluorescent protein as a marker for gene expression.. *Science,* 263(5148), pp. 802-805.

Chan, K. X. et al., 2016. Learning the languages of the chloroplast: retrograde signaling and beyond.. *Annual review of plant biology,* Volume 67, pp. 25-53.

Chapman, J. M. J. G. S. a. M. G., 2019. RBOH-dependent ROS synthesis and ROS scavenging by plant specialized metabolites to modulate plant development and stress responses.. *Chemical research in toxicology,* 32(3), pp. 370-396.

Cheng, S.-H., Willmann, M. R., Chen, H. & Sheen, J., 2002. Calcium Signaling through Protein Kinases. The Arabidopsis Calcium-Dependent Protein Kinase Gene Family. *Plant physiology,* 129(2), pp. 469-485.

Chen, H., Zhang, B., Hicks, L. M. & Xiong, L., 2011. A nucleotide metabolite controls stress-responsive gene expression and plant development. *PLoS One,* 6(10), p. e26661.

Chigri, F. et al., 2012. The Arabidopsis calmodulin-like proteins AtCML30 and AtCML3 are targeted to mitochondria and peroxisomes, respectively.. *Plant molecular biology,* 78(3), pp. 211-222.

Chigri, F. et al., 2006. Calcium regulation of chloroplast protein translocation is mediated by calmodulin binding to Tic32. *Proceedings of the National Academy of Sciences,* 103(43), pp. 16051-16056.

Chigri, F., Soll, J. & Vothknecht, U. C., 2005. Calcium regulation of chloroplast protein import.. *The Plant Journal,* 42(6), pp. 821-831.

Choi, W. T. M. K. S. H. R. a. G. S., 2014. Salt stress-induced Ca2+ waves are associated with rapid, long-distance root-to-shoot signaling in plants.. *Proceedings of the National Academy of Sciences ,* 111(17), pp. 6497-6502.

Costa, A., Navazio, L. & Szabo, I., 2018. The contribution of organelles to plant intracellular Calcium signalling. *J Exp Bot. 69 ,* pp. 4175-4193.

Cramer, G. R. et al., 2011. Effects of abiotic stress on plants: a systems biology perspective.. *BMC plant biolog,* pp. 1-14.

Creissen, G., Reynolds, H., Xue , Y. & Mullineaux, P., 1995. Simultaneous targeting of pea glutathione reductase and of a bacterial fusion protein to chloroplasts and mitochondria in transgenic tobacco.. *The Plant Journal,* 8(2), pp. 167-175.

Cutolo, E. et al., 2019. The High Light Response in Arabidopsis Requires the Calcium Sensor Protein CAS, a Target of STN7- and STN8-Mediated Phosphorylation. *Front. Plant Sci,* p. 974.

Cutolo, E., Ph.D. 2018.

Cyert, M. S., 2001. Genetic analysis of calmodulin and its targets in Saccharomyces cerevisiae.. *Annual review of genetics,* 35(1), pp. 647-672.

Dai, Y. et al., 2002. Effects of rare earth compounds on growth and apoptosis of leukemic cell lines. *n Vitro Cellular & Developmental Biology-Animal ,* 38(7), pp. 373-375.

DalCorso, G. et al., 2008. A complex containing PGRL1 and PGR5 is involved in the switch between linear and cyclic electron flow in Arabidopsis.. *Cell,* 132(2), pp. 273-285.

Dark, A. et al., 2011. Release of extracellular purines from plant roots and effect on ion fluxes.. *Plant signaling & behavior,* 6(11), pp. 1855-1857.

Dash, M. & Panda, S., 2001. Salt stress induced changes in growth and enzyme activities in germinating Phaseolus mungo seeds. *Biologia plantarum,* 44(4), pp. 587-589.

Davies, W., Wilson, J., Sharp, R. & Osonubi, O., 1981. Control of stomatal behaviour in water stressed plants.. *Cambridge university press,* pp. 163-185.

Day, I. S., Reddy, V. S., Ali, G. s. & Reddy, A., 2002. Analysis of EF-hand-containing proteins in Arabidopsis. *Genome biology,* pp. 1-24.

De Michele, R., Formentin, E. & Lo Schiavo, F., 2009. Legume leaf senescence: a transcriptional analysis. *Plant Signal Behav.,* 4(4), pp. 319-320.

Dekker, J. P. & Boekema, E. J., 2005. Supramolecular organization of thylakoid membrane proteins in green plants. *Biochimica et Biophysica Acta (BBA)-Bioenergetics ,* 1706(1-2), pp. 12-39.

Dell'Aglio, E. et al., 2016. No plastidial calmodulin-like proteins detected by two targeted mass-spectrometry approaches and GFP fusion proteins. *New Negatives in Plant Science,* Volume 3, pp. 19-26.

Delwiche, C. F., Kuhsel, M. G. & Palmer, J. D., 1995. Phylogenetic analysis of tufA sequences indicates a cyanobacterial origin of all plastids. *Molecular phylogenetics and evolution,* 4(2), pp. 110-128.

Demidchik, V. et al., 2010. Arabidopsis root K+-efflux conductance activated by hydroxyl radicals: single-channel properties, genetic basis and involvement in stress-induced cell death. *Journal of cell science,* 123(9), pp. 1468-1479.

Demidchik, V. & Maathuis, F. J. M., 2007. Physiological roles of nonselective cation channels in plants: from salt stress to signalling and development. *New Phytologist,* 175(3), pp. 387-404.

Demidchik, V. et al., 2003. Is ATP a signaling agent in plants?. *Plant Physiology ,* 133(2), pp. 456-461.

Demidchik, V. et al., 2014. Stress-induced electrolyte leakage: the role of K+-permeable channels and involvement in programmed cell death and metabolic adjustment.. *Journal of experimental botany,* 65(5), pp. 1259-1270.

Deng, L. et al., 2005. All three Ca2+-binding loops of photoproteins bind calcium ions: The crystal structures of calcium-loaded apo-aequorin and apo-obelin.. *Protein science,* 14(3), pp. 663-675.

Denton, R. M. et al., 2016. Calcium-insensitive splice variants of mammalian E1 subunit of 2-oxoglutarate dehydrogenase complex with tissue-specific patterns of expression.. *Biochemical Journal,* 473(9), pp. 1165-1178.

Desplats, C. et al., 2009. Characterization of Nda2, a plastoquinone-reducing type II NAD (P) H dehydrogenase in Chlamydomonas chloroplasts. *Journal of Biological Chemistry,* 284(7), pp. 4148-4157.

DeWald, D. B. et al., 2001. Rapid Accumulation of Phosphatidylinositol 4,5-Bisphosphate and Inositol 1,4,5-Trisphosphate Correlates with Calcium Mobilization in Salt-Stressed Arabidopsis. *Plant Physiology,* 126(2), pp. 759-769.

Dodd, A. N. et al., 2006. Time of day modulates low-temperature Ca2+ signals in Arabidopsis.. *The Plant Journal,* 48(6), pp. 962-973.

Dodd, A. N., Kudla, J. & Sanders, D., 2010. The language of calcium signaling.. *Annual review of plant biology,* Volume 61, pp. 593-620.

Dodge, A. D., 1989. *Herbicides interacting with photosystem I.* UK: Cambridge University Press.

Drög, W., 2002. Free radicals in the physiological control of cell function.. *Physiological reviews,* 82(1), pp. 47-95.

Drerup, M. S. K. H. K. M. P. S. L. K. K. a. K. J., 2013. The calcineurin B-like calcium sensors CBL1 and CBL9 together with their interacting protein kinase CIPK26 regulate the Arabidopsis NADPH oxidase RBOHF. *Molecular Plant,* 6(2), pp. 559-569.

Edel, K. H. et al., 2017. The evolution of calcium-based signalling in plants." Current Biology 27.13 (2017): R667-R679.. *Current Biology 27.13 (2017): R667-R679.,* 27(13), pp. R667-R679.

Ellis, R. J., 1981. Chloroplast proteins: synthesis, transport, and assembly. *Annual Review of Plant Physiology,* 32(1), pp. 111-137.

Estavillo, G. M. et al., 2011. Evidence for a SAL1-PAP chloroplast retrograde pathway that functions in drought and high light signaling in Arabidopsis.. *The Plant Cell ,* 23(11), pp. 3992-4012.

Evans, D. E., 1994. Calmodulin-stimulated calcium pumping ATPases located at higher plant intracellular membranes: a significant divergence from other eukaryotes?. *Physiologia Plantarum,* 90(2), pp. 420-426.

Evans, J. L., Maddux, B. A. & Goldfine, I. D., 2005. The molecular basis for oxidative stress-induced insulin resistance.. *Antioxidants & redox signaling,* 7(7.7-8), pp. 1040-1052.

Fernández, A. P. & Strand, Å., 2008. Retrograde signaling and plant stress: plastid signals initiate cellular stress responses.. *Current opinion in plant biology ,* 11(5), pp. 509-513.

Ferreira, K. N. et al., 2004. Architecture of the photosynthetic oxygen-evolving center.. *Science ,* 303(5665), pp. 1831-1838.

Finazzi, G. et al., 2015. Ions channels/transporters and chloroplast regulation.. *Cell calcium,* 58(1), pp. 86-97.

Fischer, R. L. Y., Hoffmann, K., Schillberg, S. & Emans, N., 1999. Molecular farming of recombinant antibodies in plants..

Foyer, C. H., Descourvières, P. & Kunert, K. J., 1994. Protection against oxygen radicals: an important defence mechanism studied in transgenic plants. *Plant, Cell & Environment ,* 17(5), pp. 507-523.

Foyer, C. H., Lelandais, M. & Kunert, K. J., 1994. Photooxidative stress in plants. pp. 697-717.

Foyer, C. H. & Noctor, G., 2009. Redox regulation in photosynthetic organisms: signaling, acclimation, and practical implications.. *Antioxidants & redox signaling,* 11(4), pp. 861-905.

Frank, J. et al., 2019. Chloroplast-localized BICAT proteins shape stromal calcium signals and are required for efficient photosynthesis. *New Phytologist,* 221(2), pp. 866-880.

Fuchs, M., Vothknecht, U. C. & Chigri, F., 2011. Calmodulin and calmodulin-like proteins in Arabidopsis thaliana. *Journal of Endocytobiosis and cell research,* pp. 114-121.

Fuchs, P. et al., 2020. Single organelle function and organization as estimated from Arabidopsis mitochondrial proteomics.. *The Plant Journal,* 101(2), pp. 420-441.

Fuerst, E. P. & Norman, M. A., 1991. Interactions of herbicides with photosynthetic electron transport.. *Weed Science,* 39(3), pp. 458-464.

Garg, N. & Manchanda, G., 2009. Role of arbuscular mycorrhizae in the alleviation of ionic, osmotic and oxidative stresses induced by salinity in Cajanus cajan (L.) Millsp.(pigeonpea). *Journal of Agronomy and Crop Science,* 195(2), pp. 110-123.

Gifford, J. L., Walsh, M. P. & Vogel, H. J., 2007. Structures and metal-ion-binding properties of the Ca2+-bindinghelix–loop–helix EF-hand motifs. *Biochemical Journal ,* 405(2), pp. 199-221.

Goldental-Cohen, S. et al., 2017. Ethephon induced oxidative stress in the olive leaf abscission zone enables development of a selective abscission compound.. *BMC plant biology ,* 17(1), pp. 1-17.

Gong, M., Van der Luit, A. H., Knight, M. R. & Trewavas, A. J., 1998. Heat-Shock-Induced Changes in Intracellular Ca2+Level in Tobacco Seedlings in Relation to Thermotolerance. *Plant Physiol.,* Volume 116, pp. 429-437.

Grønlund, J. T. et al., 2012. Cell Specific Analysis of Arabidopsis Leaves Using Fluorescence Activated Cell Sorting. *JoVE (Journal of Visualized Experiments) ,* Volume 68, p. e4214.

Gunz, D. W. & Hoffmann, M. R., 1990. Atmospheric chemistry of peroxides: a review.. *Atmospheric Environment. Part A. General Topics,* 24(7), pp. 1601-1633.

Guo, H. et al., 2016. Plastid-nucleus communication involves calcium-modulated MAPK signalling. *Nature Communications,* 7(1), pp. 1-15.

Han, S. et al., 2003. A cell surface receptor mediates extracellular Ca2+ sensing in guard cells. *Nature,* 425(6954), pp. 196-200.

Harmon, A. C., Gribskov, M., Gubrium , E. & Harper, J. F., 2001. The CDPK superfamily of protein kinases.. *New Phytologist,* 151(1), pp. 175-183.

Harmon, A. C., Gribskov, M. & Harper, J. F., 2000. CDPKs–a kinase for every Ca2+ signal?. *rends in plant science 5.4,* pp. 154-159.

Haswell, E. S. & Meyerowitz, E. M., 2006. MscS-like Proteins Control Plastid Size and Shape in Arabidopsis thaliana. *Current biology ,* 16(1), pp. 1-11.

Heffeter, P. et al., 2006. Anticancer activity of the lanthanum compound [tris (1, 10-phenanthroline) lanthanum (III)] trithiocyanate (KP772; FFC24).. *Biochemical pharmacology,* 71(4), pp. 426-440.

Hirsch, J. et al., 2011. A novel fry1 allele reveals the existence of a mutant phenotype unrelated to 5′-> 3′ exoribonuclease (XRN) activities in Arabidopsis thaliana roots. *PLoS One,* 6(2), p. e16724.

Hochmal, A. K., Schulze, S., Trompelt, K. & Hippler, M., 2015. Calcium-dependent regulation of photosynthesis. *Biochimica et Biophysica Acta (BBA)-Bioenergetics 1847.9,* pp. 993-1003.

Huang, L., Berkelman, T., Franklin, A. E. & Hoffman, N. E., 1993. Characterization of a gene encoding a Ca (2+)-ATPase-like protein in the plastid envelope.. *Proceedings of the National Academy of Sciences,* 90(21), pp. 10066-10070.

Huang, W., Yang, Y.-J., Zhang, S.-B. & Liu, T., 2018. Cyclic Electron Flow around Photosystem I Promotes ATP Synthesis Possibly Helping the Rapid Repair of Photodamaged Photosystem II at Low Light. *Frontiers in plant science,* Volume 9, p. 239.

Humplík, J. F. et al., 2015. Automated integrative high-throughput phenotyping of plant shoots: a case study of the cold-tolerance of pea (Pisum sativum L.). *Plant methods,* 11(1), pp. 1-11.

Inzé, D. & Montague, M. V., 1995. Oxidative stress in plants.. *Current opinion in Biotechnology ,* 6(2), pp. 153-158.

Iwai, M. et al., 2010. Isolation of the elusive supercomplex that drives cyclic electron flow in photosynthesis.. *Nature,* 464(7292), pp. 1210-1213.

Jaleel, C. A. et al., 2009. Drought stress in plants: a review on morphological characteristics and pigments composition. *Int. J. Agric. Biol ,* 11(1), pp. 100-105.

Jang, I.-C., Nahm, B. H. & Kim, J.-K., 1999. Subcellular targeting of green fluorescent protein to plastids in transgenic rice plants provides a high-level expression system. *Molecular Breeding,* 5(5), pp. 453-461.

Jarrett, H. W., Brown, C. J., Black, C. C. & Cormier, M. J., 1982. Evidence that calmodulin is in the chloroplast of peas and serves a regulatory role in photosynthesis. *Journal of Biological Chemistry,* 257(22), pp. 13795-13804.

Jiang, Z. et al., 2013. Relationship between NaCl-and H2O2-induced cytosolic Ca2+ increases in response to stress in Arabidopsis.. *PloS one,* 8(10), p. e76130.

Ji, R. et al., 2017. Calcium-dependent protein kinase CPK31 interacts with arsenic transporter AtNIP1;1 and regulates arsenite uptake in Arabidopsis thaliana. *PLoS One,* 12(3), p. e0173681.

Johnson, C. H. et al., 1995. Circadian oscillations of cytosolic and chloroplastic free calcium in plants. *Science 269.5232 ,* pp. 1863-1865.

Joliot, P. & Joliot, A., 2002. Cyclic electron transfer in plant leaf.. *Proceedings of the National Academy of Sciences,* 99(15), pp. 10209-10214.

Jung, H.-S.et al., 2013. Subset of heat-shock transcription factors required for the early response of Arabidopsis to excess light.. *Proceedings of the National Academy of Sciences,* 110(35), pp. 14474-14479.

Karniely, S. & Pines, O., 2005. Single translation—dual destination: mechanisms of dual protein targeting in eukaryotes. *EMBO reports,* 6(5), pp. 420-425.

Katembe, W. J., Ungar, I. A. & Mitchell, J. P., 1998. Effect of salinity on germination and seedling growth of twoAtriplexspecies (Chenopodiaceae).. *Annals of Botany,* 82(2), pp. 167-175.

Kawasaki, H., Nakayama, S. & Kretsinger, R. H., 1998. Classification and evolution of EF-hand proteins.. *Biometals,* 11(4), pp. 277-295.

Kiegle, E. et al., 2000. Cell-type-specific calcium responses to drought, salt and cold in the Arabidopsis root.. *The Plant Journal ,* 23(2), pp. 267-278.

Kirschhoff, H., 2013. Architectural switches in plant thylakoid membranes. *Photosynthesis research,* 116(2), pp. 481-487.

Kirschhoff, H., 2019. Chloroplast ultrastructure in plants. *New Phytologist,* 223(2), pp. 565-574.

Kiselev, K. V., Turlenko, A. V. & Zhuravlev, Y. N., 2012. Structure and expression profiling of a novel calcium-dependent protein kinase gene PgCDPK1a in roots, leaves, and cell cultures of Panax ginseng. *Plant Cell, Tissue and Organ Culture (PCTOC) ,* 103(2), pp. 197-204.

Knight, H., 1999. Calcium signaling during abiotic stress in plants.. *International review of cytology.,* 195(Academic Press), pp. 269-324.

Knight, H., Brandt, S. & Knight, M. R., 1998. A history of stress alters drought calcium signalling pathways in Arabidopsis.. *The Plant Journal,* 16(6), pp. 681-687.

Knight, H. & Knight, M. R., 1995. Recombinant aequorin methods for intracellular calcium measurement in plants.. *Methods in cell biology,* Volume 49, pp. 201-216.

Knight, H., Trewavas, A. J. & Knight, M. R., 1996. Cold calcium signaling in Arabidopsis involves two cellular pools and a change in calcium signature after acclimation.. *The Plant Cell,* 8(3), pp. 489-503.

Knight, H., Trewavas, A. J. & Knight, M. R., 1997. Calcium signalling in Arabidopsis thaliana responding to drought and salinity.. *The Plant Journal,* Volume 12.5, pp. 1067-1078.

Knight, H., Trewavas, A. J. & Read, N. D., 1993. Confocal microscopy of living fungal hyphae microinjected with Ca2+-sensitive fluorescent dyes. *Mycological Research,* 97(12), pp. 1505-1515.

Knight, M. R., Campbell, A. K., Smith, S. M. & Trewavas, A. J., 1991. Transgenic plant aequorin reports the effects of touch and cold-shock and elicitors on cytoplasmic calcium.. *Nature,* 352(6335), pp. 524-526.

Krause, G. H. & Weis, E., 1991. Chlorophyll fluorescence and photosynthesis: the basics. *Annual review of plant biology,* 42(1), pp. 313-349.

Krebs, M. et al., 2012. FRET-based genetically encoded sensors allow high-resolution live cell imaging of Ca2+ dynamics. *The Plant Journal,* 69(1), pp. 181-192.

Kudla, J., Batistič, O. & Hashimoto, K., 2010. Calcium signals: the lead currency of plant information processing. *The Plant Cell,* Issue 22.3, pp. 541-563.

Kurusu, T. et al., 2013. Plant mechanosensing and Ca2+ transport.. *Trends in plant science,* 18(4), pp. 227-233.

La Verde, V., Dominici, P. & Astegno, A., 2018. Towards Understanding Plant Calcium Signaling through Calmodulin-Like Proteins: A Biochemical and Structural Perspective. *nternational journal of molecular sciences,* 19(5), p. 1331.

Larkum, A. W., 1968. Ionic relations of chloroplasts in vivo. *Nature,* pp. 447-449.

Lascano, H. R., Casano, L. M., Martin, M. & Sabater, B., 2003. "The activity of the chloroplastic Ndh complex is regulated by phosphorylation of the NDH-F subunit.. *Plant Physiology ,* 132(1), pp. 256-262.

Lecourieux, D. et al., 2002. Analysis and effects of cytosolic free calcium increases in response to elicitors in Nicotiana plumbaginifolia cells. *The plant Cell,* 14(10), pp. 2627-2641.

Lecourieux, D., Ranjeva, R. & Pugin, A., 2006. Early signaling events induced by elicitors of plant defenses. *Molecular plant-microbe interactions,* 19(7), pp. 711-724.

Leister, D., 2012. Retrograde signaling in plants: from simple to complex scenarios. *Frontriers in plant science,* 3(135).

Leister, D. & Shikanai, T., 2013. Complexities and protein complexes in the antimycin A-sensitive pathway of cyclic electron flow in plants.. *Frontiers in plant science,* Volume 4, p. 161.

Le, M. H., Cao, Y., Zhang, X.-C. & Stacey, G., 2014. LIK1, A CERK1-Interacting Kinase, Regulates Plant Immune Responses in Arabidopsis. *PloS one,* p. e102245.

Lenzoni, G. & Knight, M. R., 2019. Increases in Absolute Temperature Stimulate Free Calcium Concentration Elevations in the Chloroplast. *Plant cell Physiol,* Volume 60, pp. 538-548.

Lettvin, J. P. W. M. W. a. P. W., 1964. A theory of passive ion flux through axon membranes.. *Nature,* 202(4939), pp. 1338-1339.

Liao, C., Zheng, Y. & Guo, Y., 2017. MYB30 transcription factor regulates oxidative and heat stress responses through ANNEXIN-mediated cytosolic calcium signaling in Arabidopsis. *New Phyto,* Volume 216, pp. 163-177.

Li, A.-L.et al., 2008. Evolutionary and functional study of the CDPK gene family in wheat (Triticum aestivum L.). *Plant molecular biology ,* 66(4), pp. 429-443.

Li, C., Xiang, Z., Ling, Q. & Shang, K., 1998. Effects of calmodulin and calmodulin binding protein BP-10 on phosphorylation of thylakoid membrane protein. *Science in China Series C: Life Sciences,* 41(1), pp. 64-70.

Li, Q.-Y.et al., 2008. Protective role of exogenous nitric oxide against oxidative-stress induced by salt stress in barley (Hordeum vulgare).. *Colloids and Surfaces B: Biointerfaces,* 65(2), pp. 220-225.

Livingston, A. K., Kanazawa, A., Cruz, J. A. & Kramer, D. M., 2010. Regulation of cyclic electron flow in C3 plants: differential effects of limiting photosynthesis at ribulose-1,5-bisphosphate carboxylase/oxygenase and glyceraldehyde-3-phosphate dehydrogenase. *Plant, Cell & Environment ,* 33(11), pp. 1779-1788.

Li, X. & Imlay, J. A., 2018. Improved measurements of scant hydrogen peroxide enable experiments that define its threshold of toxicity for Escherichia coli. *Free Radical Biology and Medicine,* Volume 120, pp. 217-227.

Logan, D. C. & Knight, M. R., 2003. Mitochondrial and cytosolic calcium dynamics are differentially regulated in plants. *Plant Physiology 133.1,* pp. 21-24.

Loro, G. et al., 2016. Chloroplast-Specific in Vivo Ca2+ Imaging Using Yellow Cameleon Fluorescent Protein Sensors Reveals Organelle-Autonomous Ca2+ Signatures in the Stroma. *Plant Physiology,* pp. 2317-2330.

Luan, S. et al., 2002. Calmodulins and calcineurin B–like proteins: Calcium sensors for specific signal response coupling in plants.. *The Plant Cell ,* 14((suppl 1)), pp. S389-S400.

Lucker, B. & Kramer, D. M., 2013. Regulation of cyclic electron flow in Chlamydomonas reinhardtii under fluctuating carbon availability.. *Photosynthesis research,* 117(1), pp. 449-459.

Lu, L. et al., 2021. CIPK11: a calcineurin B-like protein-interacting protein kinase from Nitraria tangutorum, confers tolerance to salt and drought in Arabidopsis. *BMC Plant Biology,* 21(1), pp. 1-16.

Manohar, M., Shigaki, T. & Hirschi, K. D., 2011. Plant cation/H+ exchangers (CAXs): biological functions and genetic manipulations. *Plant biology,* 13(4), pp. 561-569.

Manzoor, H. et al., 2012. Calcium signatures and signaling in cytosol and organelles of tobacco cells induced by plant defense elicitors.. *Cell calcium,* 51(6), pp. 434-444.

Manzoor, H. et al., 2015. Calcium signatures and signaling in cytosol and organelles of tobacco cells induced by plant defense elicitors. *Cell Calcium,* pp. 434-444.

Marcec, M. J. & Tanaka, K., 2022. Crosstalk between Calcium and ROS Signaling during Flg22-Triggered Immune Response in Arabidopsis Leaves.. *Plants,* 11(1), p. 14.

Martin, W. et al., 2002. Evolutionary analysis of Arabidopsis, cyanobacterial, and chloroplast genomes reveals plastid phylogeny and thousands of cyanobacterial genes in the nucleus.. *Proceedings of the National Academy of Sciences,* 99(19), pp. 12246-12251.

Maruta, T., Sawa, Y., Shigeoka, S. & Ishikawa, T., 2016. Diversity and Evolution of Ascorbate Peroxidase Functions in Chloroplasts: More Than Just a Classical Antioxidant Enzyme?. *Plant Cell Physiol. ,* 57(7), pp. 1377-1386.

McAinish, M. R., Clayton, H., Mansfield, T. A. & Hetherington, A. M., 1996. Changes in Stomatal Behavior and Guard Cell Cytosolic Free Calcium in Response to Oxidative Stress. *Plant Physiol,* Volume 111, pp. 1031-1042.

McAinsh, M. R. & Hetherington, A. M., 1998. Encoding specificity in Ca2+ signalling systems.. *Trends in Plant Science,* 3(1), pp. 32-36.

McAinsh, M. R. & Pittman, J. K., 2009. Shaping the calcium signature. *Phytol .,* pp. 275-294.

McCormack, E. & Braam , J., 2003. Calmodulins and related potential calcium sensors of Arabidopsis. *New Phytologist,* pp. 585-598.

McCurdy, D. W. & Harmon, A. C., 1991. Calcium-dependent protein kinase in the green alga Chara.. *Planta,* 188(1), pp. 54-61.

Mehlmer, N. et al., 2012. A toolset of aequorin expression vectors for in planta studies of subcellular calcium concentrations in Arabidopsis thaliana. *Journal of experimental botany,* 63(4), pp. 1751-1761.

Mereschkowski, K. S., 1905. Über Natur und Ursprung der Chromatophoren im Pflanzenreiche, Biol.

Mesecke, N. et al., 2005. A disulfide relay system in the intermembrane space of mitochondria that mediates protein import.. *Cell,* 121(7), pp. 1059-1069.

Michelet, L. et al., 2013. Redox regulation of the Calvin–Benson cycle: something old, something new.. *Frontiers in plant science,* Volume 4, p. 470.

Miller, G. & Mittler, R., 2006. Could heat shock transcription factors function as hydrogen peroxide sensors in plants?. *Annals of botany,* 98(2), pp. 279-288.

Miller, G. et al., 2009. The plant NADPH oxidase RBOHD mediates rapid systemic signaling in response to diverse stimuli.. *Science signaling,* 2(84), pp. ra45-ra45.

Mittler, R., 2017. ROS are good.. *Trends in plant science,* 22(1), pp. 11-19.

Morgan, A. J. & Galione, A., 2014. Two-pore channels (TPCs): Current controversies. *Bioessays,* 36(2), pp. 173-183.

Mugnai, S. et al., 2014. Oxidative stress and NO signalling in the root apex as an early response to changes in gravity conditions.. *BioMed research international.*

Mullineaux, P. M., Exposito-Rodriguez, M., Laissue, P. P. & Smirnoff, N., 2018. ROS-dependent signalling pathways in plants and algae exposed to high light: comparisons with other eukaryotes.. *Free Radical Biology and Medicine ,* Volume 122, pp. 52-64.

Munekage, Y. et al., 2002. PGR5 Is Involved in Cyclic Electron Flow around Photosystem I and Is Essential for Photoprotection in Arabidopsis.. *Cell,* 110(3), pp. 361-371.

Munns, R., 2002. Comparative physiology of salt and water stress. *Plant, cell & environment,* 25(2), pp. 239-250.

Munns, R. & Tester, M., 2008. Mechanismsofsalinitytolerance.. *AnnuRev PlantBiol,* Volume 59, pp. 651-681.

Muñoz, P. & Munné-Bosch, S., 2018. Photo-oxidative stress during leaf, flower and fruit development. *Plant Physiology ,* 176(2), pp. 1004-1014.

Navazio, L., Formentin, E., Cendron, L. & Szabò, I., 2020. Chloroplast Calcium Signaling in the Spotlight. *Frontiers in plant science,* Volume 11, p. 186.

Neish, A. C., 1939. Studies on chloroplasts Their chemical composition and the distribution of certain metabolites between the chloroplasts and the remainder of the leaf. *Biochem J,* pp. 300-308.

Nemeria, N. S. et al., 2014. Human 2-oxoglutarate dehydrogenase complex E1 component forms a thiamin-derived radical by aerobic oxidation of the enamine intermediate. *Journal of Biological Chemistry,* 289(43), pp. 29859-29873.

Nevo, R., Charuvi, D., Tsabari, O. & Reich, Z., 2012. Composition, architecture and dynamics of the photosynthetic apparatus in higher plants. *The Plant Journal,* 70(1), pp. 157-176.

Nikkanen, L. et al., 2018. Regulation of cyclic electron flow by chloroplast NADPH-dependent thioredoxin system.. *Plant Direct,* 2(11), p. e00093.

Nixon, A. E. & Benkovic, S. J., 2000. Improvement in the efficiency of formyl transfer of a GAR transformylase hybrid enzyme. *Protein engineering ,* 13(5), pp. 323-327.

Noctor, G. & Foyer, C. H., 1998. Ascorbate and glutathione: keeping active oxygen under control.. *Annual review of plant biology,* 49(1), pp. 249-279.

Noctor, G., Lelarge-Trouverie, C. & Mhamdi, A., 2015. The metabolomics of oxidative stress.. *Phytochemistry,* Volume 112, pp. 33-53.

Nomura, H. et al., 2008. Evidence for chloroplast control of external Ca2+-induced cytosolic Ca2+ transients and stomatal closure. *The plant journal,* 53(6), pp. 988-998.

Nomura, H. et al., 2012. Chloroplast-mediated activation of plant immune signalling in Arabidopsis.. *Nature communications,* 3(1), pp. 1-11.

Nomura, H. et al., 2012. Chloroplast-mediated activation of plant immune signalling in Arabidopsis.. *Nature communications 3.1,* pp. 1-11.

Nomura, H. & Takashi, S., 2014. Calcium signaling in plant endosymbiotic organelles: mechanism and role in physiology. *Molecular plant,* 7(7), pp. 1094-104.

O'keefe, D. P. & Dilley, R. A., 1977. The effect of chloroplast coupling factor removal on thylakoid membrane ion permeability.. *Biochimica et Biophysica Acta (BBA)-Bioenergetics 461.1,* pp. 48-60.

Pangrsicˇ, T. et al., 2015. EF-hand protein Ca2+ buffers regulate Ca2+ influx and exocytosis in sensory hair cells. *Proceedings of the National Academy of Sciences,* 112(9), pp. E1028-1037.

Peng, Y., Wersch, R. v. & Zhang, Y., 2018. Convergent and divergent signaling in PAMP-triggered immunity and effector-triggered immunity.. *Molecular Plant-Microbe Interactions ,* 31(4), pp. 403-409.

Pérez-Salamó, I. et al., 2014. The heat shock factor A4A confers salt tolerance and is regulated by oxidative stress and the mitogen-activated protein kinases MPK3 and MPK6.. *Plant physiology,* 165(1), pp. 319-334.

Perruc, E. et al., 2004. A novel calmodulin-binding protein functions as a negative regulator of osmotic stress tolerance in Arabidopsis thaliana seedlings. *The Plant Journal,* 38(3), pp. 410-420.

Petroutsos, D. et al., 2009. PGRL1 participates in iron-induced remodeling of the photosynthetic apparatus and in energy metabolism in Chlamydomonas reinhardtii.. *Journal of Biological Chemistry ,* 284(47), pp. 32770-32781.

Petrov, V. D. & Breusegem, F. V., 2012. Hydrogen peroxide—a central hub for information flow in plant cells. *AoB plants.*

Peuke, A. D. & Jeschke, W., 1999. The characterization of inhibition of net nitrate uptake by salt in salt-tolerant barley (Hordeum vulgare L. cv. California Mariout).. *Journal of experimental botany ,* 50(337), pp. 1365-1372.

Pirayesh, N. et al., 2021. Organellar Calcium Signaling in Plants: An Update. *Biochimica et Biophysica Acta (BBA)-Molecular Cell Research,* p. 118948.

Pirayesh, N., Master thesis 2017.

Porra, R., Thompson, W. & Kriedemann, P., 1989. Determination of accurate extinction coefficients and simultaneous equations for assaying chlorophylls a and b extracted with four different solvents: verification of the concentration of chlorophyll standards by atomic absorption spectroscopy.. *Biochimica et Biophysica Acta (BBA)-Bioenergetics,* 975(3), pp. 384-394.

Portis Jr, A. R. & Heldt, H. W., 1976. Light-dependent changes of the Mg2+ concentration in the stroma in relation to the Mg2+ dependency of CO2 fixation in intact chloroplasts.. *Biochimica et Biophysica Acta (BBA)-Bioenergetics,* 449(3), pp. 434-446.

Price, M. B., Jelesko, J. & Okumoto, S., 2012. Glutamate receptor homologs in plants: functions and evolutionary origin. *Frontiers in Plant Science,* Volume 3, p. 235.

Qiu, Q.-S.et al., 2002. Regulation of SOS1, a plasma membrane Na+/H+ exchanger in Arabidopsis thaliana, by SOS2 and SOS3.. *Proceedings of the National Academy of Sciences,* 99(12), pp. 8436-8441.

Ramachandran, S. R., Kumar, S. & Tanaka, K., 2019. Quantification of Extracellular ATP in Plant Suspension Cell Cultures.. *Methods in molecular biology ,* Volume 1991, pp. 43-54.

Ramel, F. et al., 2012. Carotenoid oxidation products are stress signals that mediate gene responses to singlet oxygen in plants. *Proceedings of the National Academy of Sciences,* 109(14), pp. 5535-5540.

Ranf, S. et al., 2008. Loss of the vacuolar cation channel, AtTPC1, does not impair Ca2+ signals induced by abiotic and biotic stresses.. *The Plant Journal ,* 53(2), pp. 287-299.

Reddy, V. S., Ali, G. S. & Reddy, A. S., 2002. Genes Encoding Calmodulin-binding Proteins in the Arabidopsis Genome* 210. *Journal of Biological Chemistry,* 277(12), pp. 9840-9852.

Remington, S. J., 2011. Green fluorescent protein: a perspective.. *Protein Science,* 20(9), pp. 1509-1519.

Rensink, W. A., Pilon, M. & Weisbeek, P., 1998. Domains of a transit sequence required for in vivo import in Arabidopsis chloroplasts. *Plant Physiol,* Volume 118, pp. 691-699.

Rentel, M. C. & Knight, M. R., 2004. Oxidative Stress-Induced Calcium Signaling in Arabidopsis. *Plant Physiology,* 135(3), pp. 1471-1479.

Riemer, J., Bulleid, N. & Herrmann, J., 2009. Disulfide Formation in the ER and Mitochondria: Two Solutions to a Common Process. *Science,* 324(5932), pp. 1284-1287.

Rizhsky, L., Liang, H. & Mittler, R., 2003. The water-water cycle is essential for chloroplast protection in the absence of stress.. *Journal of Biological Chemistry,* 278(40), pp. 38921-38925.

Rocha, A. G. et al., 2014. Phosphorylation of Arabidopsis transketolase at Ser428 provides a potential paradigm for the metabolic control of chloroplast carbon metabolism. *Biochemical Journal,* 458(2), pp. 313-322.

Rocha, A. G. & Vothknecht, U. C., 2012. The role of calcium in chloroplasts—an intriguing and unresolved puzzle. *Protoplasma ,* 249(4), pp. 957-966.

Rodermel, S. & Park, S., 2003. Pathways of intracellular communication: Tetrapyrroles and plastid-to-nucleus signaling.. *Bioessays,* 25(7), pp. 631-636.

Roychoudhury, A., Basu, S., Sarkar, S. N. & Sengupta, D. N., 2008. Comparative physiological and molecular responses of a common aromatic indica rice cultivar to high salinity with non-aromatic indica rice cultivars. *Plant cell reports,* 27(8), pp. 1395-1410.

Rudd, J. J. & Franklin-Tong, V. E., 1999. Calcium signaling in plants.. *Cellular and Molecular Life Sciences CMLS ,* 55(2), pp. 214-32.

Sai, J. & Hirschie Johnson, C., 2002. Dark-stimulated calcium ion fluxes in the chloroplast stroma and cytosol.. *The Plant Cell 14.6 ,* pp. 1279-1291. .

Sato, T., Hashizume, M., Hotta, Y. & Okahata, Y., 1998. Morphology and proliferation of B16 melanoma cells in the presence of lanthanoid and Al 3+ ions.. *Biometals,* 11(2), pp. 107-112.

Savoure, A. et al., 1995. Isolation, characterization, and chromosomal location of a gene encoding the Δ 1-pyrroline-5-carboxylate synthetase in Arabidopsis thaliana. *FEBS letters,* 372(1), pp. 13-19.

Scarse-Field, S. A. & Knight, M. R., 2003. Calcium: just a chemical switch?. *Current opinion in plant biology,* pp. 500-506.

Schmidt, R. et al., 2013. SALT-RESPONSIVE ERF1 regulates reactive oxygen species–dependent signaling during the initial response to salt stress in rice.. *The Plant Cell,* 25(6), pp. 2115-2131.

Schwaller, B., 2010. Cytosolic Ca2+ buffers.. *Cold Spring Harbor perspectives in biology,* 2(11), p. a004051.

Schwarzländer, M., Fricker, M. D. & Sweetlove , L. J., 2009. Monitoring the in vivo redox state of plant mitochondria: Effect of respiratory inhibitors, abiotic stress and assessment of

recovery from oxidative challenge. *Biochimica Et Biophysica Acta (BBA)-Bioenergetics,* 1787(5), pp. 468-475.

Seigneurin-Berny, D. et al., 2008. Percoll-purified and photosynthetically active chloroplasts from Arabidopsis thaliana leaves.. *Plant Physiology and Biochemistry,* 46(11), pp. 951-955.

Sello, S. et al., 2018. Chloroplast Ca2+ fluxes into and across thylakoids revealed by thylakoid-targeted aequorin probes. *Plant physiology,* 177(1), pp. 38-51.

Sello, S. et al., 2016. Dissecting stimulus-specific Ca2+ signals in amyloplasts and chloroplasts of Arabidopsis thaliana cell suspension cultures. *Journal of Experimental Botany,* pp. 3965-3974.

Sétif, P., 2015. Electron-transfer kinetics in cyanobacterial cells: Methyl viologen is a poor inhibitor of linear electron flow.. *Biochimica et Biophysica Acta (BBA)-Bioenergetics,* 1847(2), pp. 212-222.

Shi, L.-X. & Theg, S. M., 2013. The chloroplast protein import system: from algae to trees. *Biochimica et Biophysica Acta (BBA)-Molecular Cell Research,* 1833(2), pp. 314-331.

Shimomura, O. J. F. H. a. S. Y., 1962. Extraction, purification and properties of aequorin, a bioluminescent protein from the luminous hydromedusan, Aequorea.. *Journal of cellular and comparative physiology,* 59(3), pp. 223-239.

Shi, Y. et al., 2014. Silicon improves seed germination and alleviates oxidative stress of bud seedlings in tomato under water deficit stress.. *Plant Physiology and Biochemistry,* Volume 78, pp. 27-36.

Sierla, M. et al., 2013. Apoplastic and chloroplastic redox signaling networks in plant stress responses.. *Antioxidants & redox signaling,* 18(16), pp. 2220-2239.

Smirnoff, N. & Arnaud, D., 2019. Hydrogen peroxide metabolism and functions in plants. *New Phytologist ,* Volume 221, pp. 1197-1214.

Song, C. J., 2006. Extracellular ATP induces the accumulation of superoxide via NADPH oxidases in Arabidopsis. *Plant physiology,* 140(4), pp. 1222-1232.

Stael, S. et al., 2011. Arabidopsis calcium-binding mitochondrial carrier proteins as potential facilitators of mitochondrial ATP-import and plastid SAM-import. *FEBS letters,* 585(24), pp. 3935-40.

Stael, S. et al., 2012 a.. Cross-talk between calcium signalling and protein phosphorylation at the thylakoid. *Journal of experimental botany,* 63(4), pp. 1725-1733.

Stael, S. et al., 2012 b.. Plant organellar calcium signalling: an emerging field. *Journal of experimental botany,* 63(4), pp. 1525-1542.

Strand, D. D. et al., 2015. Activation of cyclic electron flow by hydrogen peroxide in vivo. *PNAS,* 112(17), pp. 5539-5544.

Sugiura, M., 1995. The chloroplast genome. *Essays in biochemistry ,* Volume 30, pp. 49-57.

Suorsa, M. et al., 2012. PROTON GRADIENT REGULATION5 is essential for proper acclimation of Arabidopsis photosystem I to naturally and artificially fluctuating light conditions.. *The Plant Cell,* 24(7), pp. 2934-2948.

Susek, R. E., Ausubel, F. & Chory, J., 1993. Signal transduction mutants of arabidopsis uncouple nuclear CAB and RBCS gene expression from chloroplast development. *Cell,* 74(5), pp. 787-799.

Takahashi, H. et al., 2013. Cyclic electron flow is redox-controlled but independent of state transition.. *Nature communications,* 4(1), pp. 1-8.

Takahashi, S. & Milward, S., 2009. How does cyclic electron flow alleviate photoinhibition in Arabidopsis?. *Plant physiology,* 149(3), pp. 1560-1567.

Takata, M. P. W. L. J. a. M. J., 1966. Ionic conductance changes in lobster axon membrane when lanthanum is substituted for calcium.. *The Journal of general physiology,* 50(2), pp. 461-471.

Tanaka, K. & Heil, M., 2021. Damage-Associated Molecular Patterns (DAMPs) in Plant Innate Immunity: Applying the Danger Model and Evolutionary Perspectives.. *Annual Review of Phytopathology,* Volume 59.

Tanaka, K., Swanson, S. J., Gilroy, S. & Stacey, G., 2010. Extracellular nucleotides elicit cytosolic free calcium oscillations in Arabidopsis. *Plant Physiology,* 154(2), pp. 705-719.

Tang, L. et al., 2020. An effector of a necrotrophic fungal pathogen targets the calcium-sensing receptor in chloroplasts to inhibit host resistance. *Molecular plant pathology,* 21(5), pp. 686-701.

Tang, R.-H.et al., 2007. Coupling diurnal cytosolic Ca2+ oscillations to the CAS-IP3 pathway in Arabidopsis.. *Science,* 315(5817), pp. 1423-1426.

Teardo, E. et al., 2015. Alternative splicing-mediated targeting of the Arabidopsis GLUTAMATE RECEPTOR3. 5 to mitochondria affects organelle morphology. *Plant Physiology,* 167(1), pp. 216-227.

Teardo, E. et al., 2011. Dual localization of plant glutamate receptor AtGLR3.4 to plastids and plasmamembrane. *Biochimica et Biophysica Acta (BBA)-Bioenergetics,* 1807(3), pp. 359-367.

Teardo, E. et al., 2010. Characterization of a plant glutamate receptor activity.. *Cellular Physiology and Biochemistry ,* 26(2), pp. 253-262.

Terashima, M. et al., 2012. Calcium-dependent regulation of cyclic photosynthetic electron transfer by a CAS, ANR1, and PGRL1 complex. *Proceedings of the National Academy of Sciences,* 109(43), pp. 17717-17722.

Thomson, S. M., Pulido, P. & Jarvis, R. P., 2020. Protein import into chloroplasts and its regulation by the ubiquitin-proteasome system.. *Biochemical Society Transactions,* 48(1), pp. 71-82..

Thor, K., 2019. Calcium—nutrient and messenger. *Frontiers in plant science,* Volume 10, p. 440.

Torres, M. A., Jones, J. D. G. & Dangl, J. L., 2006. Reactive oxygen species signaling in response to pathogens.. *Plant physiology,* 141(2), pp. 373-378.

Tozawa, Y. et al., 2007. Calcium-activated (p)ppGpp Synthetase in Chloroplasts of Land Plants. *Journal of Biological Chemistry,* 282(49), pp. 35536-35545.

Tracy, F. E. et al., 2008. NaCl-induced changes in cytosolic free Ca2+ in Arabidopsis thaliana are heterogeneous and modified by external ionic composition.. *Plant, Cell & Environment ,* 31(8), pp. 1063-1073.

Tuteja, N. & Mahajan, S., 2007. Calcium signaling network in plants: an overview. *Plant signaling & behavior ,* pp. 79-85.

Ullmann, A., Jacob, F. & Monod, J., 1967. Characterization by in vitro complementation of a peptide corresponding to an operator-proximal segment of the β-galactosidase structural gene of Escherichia coli.. *Journal of molecular biology ,* 24(2), pp. 339-343.

Ungar, I. A., 1996. Effect of salinity on seed germination, growth, and ion accumulation of Atriplex patula (Chenopodiaceae).. *American Journal of Botany,* 83(5), pp. 604-607.

Vadassery, J. & Oelmüller, R., 2009. Calcium signaling in pathogenic and beneficial plant microbe interactions: what can we learn from the interaction between Piriformospora indica and Arabidopsis thaliana.. *Plant signaling & behavior,* Issue 4.11, pp. 1024-1027.

Vainonen, J. P. et al., 2008. Light regulation of CaS, a novel phosphoprotein in the thylakoid membrane of Arabidopsis thaliana. *The FEBS journal,* 275(8), pp. 1767-1777.

von Heijne, G., Steppuhn, J. & Herrmann, R. G., 1989. Domain structure of mitochondrial and chloroplast targeting peptides. *European Journal of Biochemistry,* 180(3), pp. 535-545.

Vorasoot, N. et al., 2003. Effect of water stress on yield and agronomic characters of peanut (Arachis hypogaea L.). *Songklanakarin J. Sci. Technol,* 25(3), pp. 283-288.

Waldo, G. S., Standish, B. M., Berendzen, J. & Terwilliger, T. C., 1999. Rapid protein-folding assay using green fluorescent protein. *Nature biotechnology,* 17(7), pp. 691-695.

Walters, A. et al., 2007. Structural requirements of jasmonates and synthetic analogues as inducers of Ca2+ signals in the nucleus and the cytosol of plant cells. *Angewandte Chemie International Edition,* 46(25), pp. 4783-4785.

Wang, L. et al., 2016. Chloroplast-mediated regulation of CO2-concentratingmechanism by Ca2+-binding protein CAS in the greenalgaChlamydomonas reinhardtii. *Proceedings of the National Academy of Sciences ,* 113(44), pp. 12586-12591.

Wang, M., Zheng, Q., Shen, Q. & Guo, S., 2013. The Critical Role of Potassium in Plant Stress Response. *International Journal of Molecular Sciences,* 14(4), pp. 7370-7390.

Wang, W.-H.et al., 2012. Calcium-sensing receptor regulates stomatal closure through hydrogen peroxide and nitric oxide in response to extracellular calcium in Arabidopsis. *Journal of Experimental Botany,* 63(1), pp. 177-190.

Waszczak, C., Carmody, M. & Kangasjärvi, J., 2018. Reactive oxygen species in plant signaling. *Annual review of plant biology,* Volume 69, pp. 209-236.

Wehrman, T. et al., 2002. Protein–protein interactions monitored in mammalian cells via complementation of β-lactamase enzyme fragments. *Proceedings of the National Academy of Sciences,* 99(6), pp. 3469-3474.

Weinl, S. et al., 2008. A plastid protein crucial for Ca2+-regulated stomatal responses. *New Phytologist,* 179(3), pp. 675-686.

Wenjuan, L., Wang, M. & Ai, X., 2009. The role of calcium in regulating photosynthesis and related physiological indexes of cucumber seedlings under low light intensity and suboptimal temperature stress.. *Scientia Horticulturae,* Volume 123, pp. 34-38.

Westphal, S., Soll, J. & Vothknecht, U. C., 2001. A vesicle transport system inside chloroplasts. *FEBS letters,* 506(3), pp. 257-261.

Westphal, S., Soll, J. & Vothknecht, U. C., 2003. Evolution of chloroplast vesicle transport.. *Plant and cell physiology,* 44(2), pp. 217-222.

White, P. J., 2000. Calcium channels in higher plants. *Biochimica et Biophysica Acta (BBA)-Biomembranes,* 1465(1-2), pp. 171-189.

White, P. J. & Broadley, M. R., 2003. Calcium in Plants. *Annals of botany ,* pp. 487-511.

Wigley, W. C. et al., 2001. Protein solubility and folding monitored in vivo by structural complementation of a genetic marker protein.. *Nature biotechnology ,* 19(2), pp. 131-136.

Williamson, R. E. & Ashley, C. C., 1982. Free Ca 2+ and cytoplasmic streaming in the alga Chara. *Nature, 296(5858),* pp. 647-651.

Wise, R. R. & Hoober, J. K., 2007. The structure and function of plastids. In: *Springer Science & Business Media.* Dordrecht, The Netherlands: Springer.

Xie, X. et al., 2019. The Roles of Environmental Factors in Regulation of Oxidative Stress in Plant. *BioMed research international* .

Xu, F. et al., 2010. Antioxidant and antibacterial properties of the leaves and stems of Premna microphylla.. *Journal of Medicinal Plants Research,* 4(23), pp. 2544-2550.

Xu, L. et al., 2013. Acquisition, Conservation, and Loss of Dual-Targeted Proteins in Land Plants. *Plant physiology ,* 161(2), pp. 644-662.

Yamagishi, A., Satoh, K. & Katoh, S., 1981. The concentrations and thermodynamic activities of cations in intact Bryopsis chloroplasts.. *Biochimica et Biophysica Acta (BBA)-Bioenergetics 637.2,* pp. 252-263.

Yamamoto, H. & Shikanai, T., 2019. PGR5-dependent cyclic electron flow protects photosystem I under fluctuating light at donor and acceptor sides.. *Plant physiology,* 179(2), pp. 588-600.

Yamori, W. & Shikanai, T., 2016. Physiological functions of cyclic electron transport around photosystem I in sustaining photosynthesis and plant growth.. *Annual review of plant biology ,* Volume 67, pp. 81-106.

Yang, T. & Poovaiah, B., 2003. Calcium/calmodulin-mediated signal network in plants. *Trends in plant science,* 8(10), pp. 505-512.

Yang, T. & Poovaiah, B. W., 2000. Arabidopsis chloroplast chaperonin 10 is a calmodulin-binding protein.. *Biochemical and biophysical research communications,* 275(2), pp. 601-607.

Yang, Y.-J., Ding, X.-X. & Huang, W., 2019. Stimulation of cyclic electron flow around photosystem I upon a sudden transition from low to high light in two angiosperms Arabidopsis thaliana and Bletilla striata. *Plant Science,* Volume 287, pp. 110-166.

Yao, J. et al., 2018. Phenotyping of Arabidopsis Drought Stress Response Using Kinetic Chlorophyll Fluorescence and Multicolor Fluorescence Imaging. *Front. Plant Sci,* 9(603).

Yuan, F. et al., 2014. OSCA1 mediates osmotic-stress-evoked Ca 2+ increases vital for osmosensing in Arabidopsis. *Nature,* 514(7522), pp. 367-371.

Zelman, A. K., Dawe, A., Gehring, C. & Berkowitz, G. A., 2012. Evolutionary and structural perspectives of plant cyclic nucleotide-gated cation channels. *Frontiers in plant science,* Volume 3, p. 95.

Zhang, G. et al., 2014. Exogenous calcium alleviates low night temperature stress on the photosynthetic apparatus of tomato leaves.. *PLoS One,* 9(5), p. e97322.

Zhang, X. et al., 2006. Agrobacterium-mediated transformation of Arabidopsis thaliana using floral dip method.. *Nature Protocols,* 1(2), pp. 641-646.

Zhang, Y. et al., 2015. Aequorin-based luminescence imaging reveals differential calcium signalling responses to salt and reactive oxygen species in rice roots. *Journal of experimental botany ,* 66(9), pp. 2535-2545.

Zhu, J.-K., 2000. Genetic analysis of plant salt tolerance using Arabidopsis.. *Plant physiology,* 124(3), pp. 941-948.

Zhu, J.-K., 2002. Salt and drought stress signal transduction in plants.. *Annual review of plant biology,* 53(1), pp. 247-273.

Zhu, X. et al., 2013. Aequorin-based luminescence imaging reveals stimulus-and tissue-specific Ca2+ dynamics in Arabidopsis plants.". *Molecular plant,* 6(2), pp. 444-455.

Zielinski, R. E., 1998. Calmodulin and calmodulin-binding proteins in plants. *Annual review of plant biology ,* 49(1), pp. 697-725.

Zipfel, C. et al., 2004. Bacterial disease resistance in Arabidopsis through flagellin perception. *Nature,* 428(6984), pp. 764-767.

Eidesstattliche Erklärung

Ich erkläre hiermit, dass ich diese Dissertation selbstständig ohne Hilfe Dritter und ohne Benutzung anderer als der angegebenen Quellen und Hilfsmittel verfasst habe. Alle den benutzten Quellen wörtlich oder sinngemäß entnommenen Stellen sind als solche einzeln kenntlich gemacht.

Diese Arbeit ist bislang keiner anderen Prüfungsbehörde vorgelegt worden und auch nicht veröffentlicht worden.

Ich bin mir bewusst, dass eine falsche Erklärung rechtliche Folgen haben wird.

_____

Supplementary data

Table 19. List of ATG numbers of the proteins exported from the MS/MS analysis. The proteins are divided into PSI (light green), PSII (dark green), CYT*b6/f* (orange), LHC (pink), ATP synthesis (light blue), and PGR (red) groups.

AT5G23060.1	CAS calcium sensing receptor
AT1G31330.1	PSAF photosystem I subunit F
AT1G03130.1	PSAD-2, PSAD-1 photosystem I subunit D-1, D2
AT1G30380.1	PSAK photosystem I subunit K
AT1G52230.1	PSAH2, PSAH-2, PSI-H photosystem I subunit H2
AT1G55670.1	PSAG photosystem I subunit G
AT2G20260.1	PSAE-2 photosystem I subunit E-2
AT2G46820.2	PSAP, PSI-P photosystem I P subunit
AT3G16140.1	PSAH-1 photosystem I subunit
AT4G12800.1	PSAL photosystem I subunit l
AT4G28750.1	PSAE-1 Photosystem I reaction centre subunit IV / PsaE protein
ATCG00340.1	PSAB Photosystem I, PsaA/PsaB protein
ATCG00350.1	PSAA Photosystem I, PsaA/PsaB protein
ATCG00630.1	PSAJ
ATCG01060.1	PSAC iron-sulfur cluster binding
ATCG00020.1	PSBA photosystem II reaction center protein A
ATCG00270.1	PSBD photosystem II reaction center protein D
ATCG00280.1	PSBC photosystem II reaction center protein C
ATCG00560.1	PSBL photosystem II reaction center protein L
ATCG00580.2	PSBE photosystem II reaction center protein E
ATCG00680.1	PSBB photosystem II reaction center protein B
ATCG00710.1	PSBH photosystem II reaction center protein H
AT4G03280.2	PETC photosynthetic electron transfer C
ATCG00540.1	PETA photosynthetic electron transfer A
ATCG00600.1	PETG
ATCG00720.1	PETB photosynthetic electron transfer B
ATCG00730.1	PETD photosynthetic electron transfer D
AT1G20020.2	ATLFNR2 ferredoxin-NADP(+)-oxidoreductase 2
AT5G66190.1	ATLFNR1, FNR1 ferredoxin-NADP(+)-oxidoreductase 1
AT1G15820.1	LHCB6, CP24 light harvesting complex photosystem II subunit 6
AT1G29930.1	LHCB1.3 chlorophyll A/B binding protein
AT1G61520.2	LHCA3 photosystem I light harvesting complex gene 3
AT2G05070.1	LHCB2 photosystem II light harvesting complex gene
AT3G08940.2	LHCB4.2 light harvesting complex photosystem II

AT3G47470.1	LHCA4, CAB4 light-harvesting chlorophyll-protein complex I subunit
AT3G54890.4	LHCA1 photosystem I light harvesting complex gene 1
AT3G61470.1	LHCA2 photosystem I light harvesting complex gene 2
AT5G01530.1	LHCB4.1 light harvesting complex photosystem II
AT2G07698.1	ATP synthase subunit (ATP alpha)
AT4G04640.1	ATP synthase subunit (ATP gamma1)
AT4G32260.1	ATP synthase subunit (ATPG)
AT5G08690.1	ATP synthase subunit (ATP beta)
ATCG00120.1	ATP synthase subunit (ATP alpha)
ATCG00130.2	ATP synthase subunit (ATPF)
ATCG00140.1	ATPH ATP synthase subunit C family protein
ATCG00470.1	ATP synthase subunit (ATP epsilon)
ATCG00480.1	Beta subunit of ATP synthase
ATMG01190.E	ATP synthase subunit 1
AT4G22890.4	PGR5-LIKE A
AT4G03280.1	PGR1 photosynthetic electron transfer C

Acknowledgments

To begin with, I would like to express my sincere gratitude to Prof. Dr. Ute C. Vothknecht for providing me with the opportunity to be a part of her amazing team at the Plant Cell Biology Lab. I enhanced my knowledge and strengthened my skills through the opportunities she provided me to attend conferences and supervise several students and courses. This work results from her constant and meticulous supervision, which motivated and encouraged me to pursue my scientific interests. Working and studying under her leadership was an honor for me.

I want to extend my heartfelt appreciation to Dr. Fatima Chigri for her valuable advice, technical support, and generous guidance throughout my Ph.D., particularly when writing my thesis. She was accommodating in providing me with excellent instructions regarding the conduct of my experiments, and I am incredibly grateful to her for her assistance.

My special appreciation goes to my colleagues and friends, Maya Giridhar and Sakil Mahmud, who have supported me throughout this process. I am grateful to have worked with such loving, helpful, and knowledgeable colleagues whom I will cherish for the rest of my life.

Furthermore, I would like to express my gratitude to Prof. Dr. Dörmann for kindly accepting to be my second examiner, and Sabarna Bhattacharyya, who helped me with the Bioinformatics work and proof-reading parts of my thesis, Claudia Heym and Ursula Metbach, who provided technical support, and also Dr. Baluska, Gelareh and Sandra.

In addition, I would like to extend my thanks to Andras, Annelotte, Felipe, and Marianne, who have been great friends and supported me throughout my journey, and Matei, for not only being a great friend but also helped me with proof-reading of this work.

Next, I am truly blessed to have the never-ending support and love of my parents and my only brother, Amirhossein. Having you as a constant source of support is a great comfort, and your love raised me up again when I got weary.

I want to conclude by thanking my husband, Shayan. You have understood me best during this time, helping me get through this agonizing period in the most positive way, loving me, being my best friend, encouraging me, and supporting me in every way. This work would not have been possible without you next to me.